A THEORETICAL AND EXPERIMENTAL STUDY AT MACH 8 OF FLOW SEPARATION OF A FLAT PLATE WITH DEFLECTED TRAILING EDGE FLAP

By

Charles Borden Johnson

Thesis submitted to the Graduate Faculty of the
Virginia Polytechnic Institute
in candidacy for the degree of

MASTER OF SCIENCE

in

AEROSPACE ENGINEERING

August 1966

A THEORETICAL AND EXPERIMENTAL STUDY AT MACH 8 OF FLOW SEPARATION OF A FLAT PLATE WITH DEFLECTED TRAILING EDGE FLAP

By

Charles Borden Johnson

ABSTRACT

An experimental investigation was made into the effect of unit Reynolds number, flap angle, and wall temperature on the pressure distribution and flow field of a flat plate model with a trailing edge flap. The tests were conducted at a nominal Mach number of 8 and the nominal unit Reynolds number per foot was varied from 0.22×10^6 to 10.9×10^6. The results showed the unit Reynolds number and wall temperature effect on the extent of separation for both laminar and transitional separation. The pressure measurements at three wall temperature conditions are compared with the theory of Lees and Reeves for adiabatic and cool wall conditions.

A THEORETICAL AND EXPERIMENTAL STUDY AT MACH 8 OF FLOW SEPARATION OF A FLAT PLATE WITH DEFLECTED TRAILING EDGE FLAP

by

Charles Borden Johnson

Thesis submitted to the Graduate Faculty of the

Virginia Polytechnic Institute

in candidacy for the degree of

MASTER OF SCIENCE

in

AEROSPACE ENGINEERING

APPROVED:

Dr. James B. Eades

Dr. Fred R. DeJarnette

Dr. Robert K. Will

August 1966

Blacksburg, Virginia

II. TABLE OF CONTENTS

CHAPTER PAGE

III. LIST OF FIGURES

FIGURE PAGE

IV. INTRODUCTION

Flow separation is a common fluid mechanical phenomenon occurring on many configurations and over a range of conditions from subsonic to hypersonic flow. There have been a large number of investigations, both theoretical and experimental, of these configurations and the conditions causing flow separation. Recent reviews of flow separation research are given in references 1 through 3. The effect of flow separation in front of an upward deflected (that is, positive deflection angle) trailing-edge control surface can change considerably the performance of a hypersonic vehicle from that predicted by the idealized inviscid pressure distribution. In this thesis, only the geometry of a flat plate with an upward deflected flap will be considered. The experimental data are compared with predictions from the theory of Lees and Reeves (ref. 4) which is a shock-wave boundary-layer interaction theory.

As the free-stream Mach number increases into the hypersonic flow regime, laminar flow generally becomes more prevalent, therefore, increased attention has been focused on laminar separation and the associated laminar plateau pressure rise (see sketch 1). Typical examples of experimental investigations of flow separation on flat plates with trailing-edge flaps are found in references 5 to 24.

The purpose of this thesis is to present a detailed experimental and theoretical study of the effect of Reynolds number, flap angle, and wall temperature on the surface static pressure, the flow field, and the heat transfer for a flat plate (model) with a trailing-edge

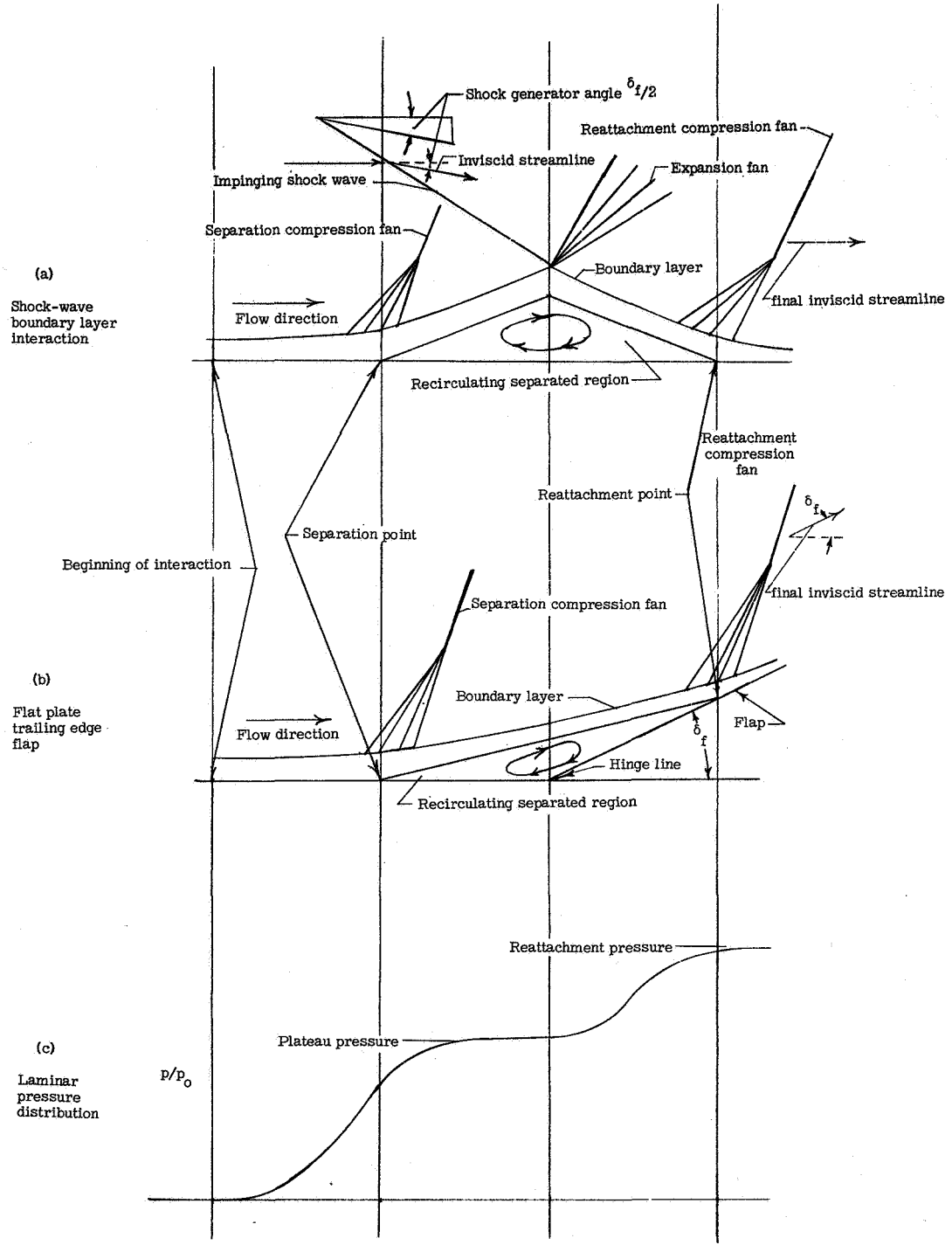

Sketch 1. Comparison of the basic flow models assumed for a shock wave boundary layer interaction and flat plate with a trailing edge flap and their associated laminar pressure distribution.

flap. The tests were conducted for wall to total temperature ratios of 0.14, 0.43, and 0.74, and flap angles of 10°, 20°, and 30°, for a unit Reynolds number range of $R = 0.22 \times 10^6$ to 4.3×10^6 per foot. Pressure and schlieren studies were made for all three wall-temperature ratios, while the heat-transfer studies were made only for a wall to total temperature ratio of 0.43. The separation point, the separation shock angle, and the separation flow deflection angle data were obtained from the schlieren studies. These angles and distances agreed qualitatively with the results indicated by the pressure studies. The pressure data for wall to total temperature ratios of 0.43 and 0.74 showed the extent of the interaction and separated region, the plateau pressure level and the flap pressures for a unit Reynolds number range of $R = 0.22 \times 10^6$ to 10.9×10^6 per foot.

Separation and reattachment points were also measured by oil-flow studies $\left(T_w/T_t = 0.43\right)$ for 10°, 20°, and 30° flap angles and unit Reynolds numbers ranging from 0.22×10^6 to 4.3×10^6 per foot. The trend in the movement of the separation point with a change in unit Reynolds number found from the oil-flow study clarifies the apparent contradictory results previously obtained for a much narrower range of Reynolds numbers (refs. 7 and 16). The effect on the movement of the interaction region when the separation goes from pure laminar type separation to a transitional type of separation, with an increase in unit Reynolds number, is shown. Reattachment pressures were determined from plots of the pressure distributions and the point of reattachment found from oil-flow studies.

The Lees and Reeves' theory was used to compute the pressure rise from the beginning of the interaction region to the end of the first pressure plateau region. The local similarity theory (ref. 25) was used to calculate the upstream boundary layer. The Lees and Reeves' solution was joined to the upstream boundary-layer solution by matching the value of the physical momentum thickness at the beginning of the Lees and Reeves' interaction region. Detailed results of these calculations are presented herein.

The Lees and Reeves' theory for the adiabatic wall $\left(T_w/T_t = 1.0\right)$ and cool wall $\left(T_w/T_t = 0.6\right)$ is compared to the experimental case of $T_w/T_t = 0.74$ and $T_w/T_t = 0.43$, respectively. The agreement between the pressure distribution, as predicted by the Lees and Reeves' theory, and the experimental pressure data is good over a large range of Reynolds numbers. The heat-transfer prediction, by a modified Lees and Reeves' method, shows a trend which agrees qualitatively with the experimental heat-transfer data.

V. LIST OF SYMBOLS

a speed of sound; also velocity profile parameter, $\left[\frac{\partial\left(\frac{\bar{u}}{\bar{u}_e}\right)}{\partial\left(\frac{\bar{Y}}{\delta_i}\right)}\right]_{\bar{Y}=0}$ for attached flow; $\left(\frac{\bar{Y}}{\delta_i}\right)_{f'=0}$ for separated flow

D defined by equation (A-14)

e enthalpy integral $\int_o^{\delta_i} S\, d\bar{Y}$

E integral, $\int_o^{\delta_i} \frac{\bar{u}}{\bar{u}_e} S\, d\bar{Y}$

f defined by equation (A-13), also stream function, equations (1) and (2)

h defined by equation (A-12), also enthalpy

H θ_i / δ_t^*

J θ^* / δ_t^*

L length of flat plate portion of the model, 10 inches

L' normalizing factor for the theoretical solution, equal to 1 foot

m defined by equation (A-6)

M Mach number

p pressure

P wall shear stress function, $\frac{\delta_t^*}{\bar{u}_e} \left(\frac{\partial \bar{u}}{\partial \bar{Y}}\right)_{\bar{Y}} = 0$

q heating rate

R dissipation function, $\frac{2\delta_t^*}{\bar{u}_e^2} \int_o^{\delta_i} \left(\frac{\partial \bar{u}}{\partial \bar{Y}}\right)^2 d\bar{Y}$

R	Reynolds number per foot (unit Reynolds number)
$R_{e\delta_t^*}$	Reynolds number, $\frac{a_\infty M_\infty \delta_t^*}{\nu_\infty}$
S	total enthalpy function, $\frac{h_t}{h_{t_e}} - 1$
T^*	enthalpy function, $E/S_w \delta_t^*$
T	temperature
u,v	velocity component parallel and normal to surface
$\bar{u}$	Stewartson's transformed velocity, equation (C-4)
x,y	coordinate parallel and normal to surface
$\bar{X}$, $\bar{Y}$	Stewartson's transformed coordinates, equation (C-2)
z	velocity integral, $\frac{1}{\delta_t^*} \int_o^{\delta_i} \frac{\bar{u}}{\bar{u}_e} d\bar{Y}$
α	defined by equation (3)
β	pressure gradient parameter
γ	ratio of specific heats, C_p/C_v
δ	boundary-layer thickness
δ_f	trailing-edge flap angle
δ_i	transformed boundary-layer thickness
δ_i^*	boundary-layer displacement thickness, $\int_o^{\delta_i} \left(1 - \frac{\bar{u}}{\bar{u}_e}\right) d\bar{Y}$
δ_t^*	transformed displacement thickness, $\delta_i^* + e$
ζ	stagnation enthalpy ratio, h_t/h_{t_e}
η	similarity variable, equation (C-5)

θ_i boundary-layer momentum thickness, $\int_o^{\delta_i} \frac{\bar{u}}{\bar{u}_e}\left(1 - \frac{\bar{u}}{\bar{u}_e}\right) d\bar{Y}$

θ_i^* mechanical "energy" thickness, $\int_o^{\delta_i} \frac{\bar{u}}{\bar{u}_e}\left(1 - \frac{\bar{u}^2}{\bar{u}_e^2}\right) d\bar{Y}$

Ⓗ local angle between streamline at $y = \delta$ and x-axis, $\tan^{-1}\left(v_e/u_e\right)$

μ viscosity

ν Prandtl-Meyer angle; also Kinematic viscosity, (μ/ρ)

ρ density

Subscripts

e local conditions external to the boundary layer

i transformed conditions

Pl plateau value

R reattachment value

t stagnation conditions

w wall conditions

x along the plate

o at the beginning of the interaction

∞ free-stream conditions

A prime indicates differentiation with respect to η

VI. APPARATUS AND TEST PROCEDURES

Description of the Models Used

The pressure model used for the tests at all three wall-temperature conditions is shown in figures 1 and 2. The instrumentation extends from 4.75 inches aft of the leading edge to 0.281 inch ahead of the trailing edge of the flap. The model had a sharp leading edge of about 0.001 inch thickness; the flat-plate portion of the model was 7.75 inches wide and 10.0 inches long. A 2.0-inch-long trailing-edge flap, which may be positioned at angles $\left(\delta_f\right)$ of 0°, 10°, 20°, and 30° (relative to the flat-plate portion of the model) extends across the back of the model. The model was also run with upper side plates which extended back from the leading edge at an angle of approximately 6° as indicated by the line labeled "side plates" in figure 1.

The heat-transfer model is shown in figures 3 and 4. The same leading edge piece, as used for the pressure model, was used on the heat-transfer model; the heat-transfer and pressure models were geometrically identical on the upper test surface.

Instrumentation

The pressure model was instrumented with 23 pressure orifices of 0.070 inch inside diameter as shown in figure 2. The pressures were measured with electrical hot-wire pressure gages (with a range of 0 to 20 millimeters of mercury) and electrical wire strain-gage pressure gages. The pressure range of the strain-gage type varied from 0 to 1

and 0 to 7.5 psia. The accuracy of the hot-wire pressure gage is considered to be ± 0.05 millimeter of mercury, while the accuracy of the strain-gage pressure transducer is considered to be 0.75 percent of full-scale deflection. The calibration of the hot-wire gage is extremely nonlinear, thus they must be calibrated with a high resolution (or a large number of points) in the lower pressure range. The strain-gage transducers are linear in calibration over their rated pressure range.

Pressure tests at $T_w\ T_t = 0.43$ and 0.15 were made with the electrical hot-wire type of pressure gages mounted inside the body of the model, as shown in figure 5. For pressure tests at $T_w\ T_t = 0.43$ the strain-gage transducers were used also; these were mounted inside the model vacuum chamber injection box below the tunnel test section as shown in figure 6. Stainless-steel tubing and plastic vacuum tubing were used for all pressure leads. For the pressure tests at $T_w\ T_t = 0.74$, both the electrical hot-wire and electrical wire strain-gage types were used. However, for tests at $T_w\ T_t = 0.74$ the gages were mounted outside of the tunnel, wrapped in a polyethalene bag, and immersed in an ice bath so that the gages could be kept at a constant temperature.

The instrumentation for the heat-transfer model (shown in fig. 4) consists of 30 gage (0.010 inch diameter) thermocouple wire mounted on an 0.029-inch-thick skin portion of the model. The thermocouple junctions were made by spot welding individual thermocouple wires on the inside surface of the model skin. The thin-skin portion was fabricated by milling a groove of 0.4-inch-wide in the 1-inch-thick

plate as indicated on figure 4. The flap was made from 0.030 inch stainless-steel plate. A cover was put on the back of the flap to shield it from any extraneous back-side heat inputs.

Test Apparatus and Procedures

The tests reported in this thesis were conducted in the Langley Mach 8 Variable Density Hypersonic Tunnel. This tunnel operates at a nominal Mach number of 8 over a Reynolds number (per foot) range of 0.20×10^6 to 12.0×10^6. A calibration of this facility can be found in reference 26 and a further description is given in reference 27. Throughout the tests the model was set at 0.5° angle of attack resulting in a range of local Mach number on the plate from about 7.4 to 7.8.

The pressure tests for $T_w/T_t = 0.43$ were made with the model at essentially room-temperature conditions since the data were taken at about 1/2 second after the model was positioned in the test section. When the gages were installed inside the model less than 1/2 second was required for the pressures to reach an equilibrium value over the range of test conditions. Equilibrium pressures were reached in approximately the same time lapse as for the higher pressure range, in this pressure range the size of the gages required that they be mounted outside the model (fig. 6).

Tests conducted at $T_w/T_t = 0.14$ were carried out with the model cooled by liquid nitrogen. The small hot-wire type gages were mounted inside the model - as shown in figure 5 - and were sprayed with liquid nitrogen. The leading-edge piece had two passages drilled through it

for liquid nitrogen cooling, as shown in figure 2. The pressure-gage cavity (fig. 5) and the flap also were sprayed with liquid nitrogen. When the model reached an isothermal temperature, of approximately 190° R, the model was injected into the tunnel and the pressure data were recorded 1/2 second after the model was positioned in the test section. The cold wall temperature of the model was measured by thermocouples mounted on the inside surface of the model at a point aft of the leading edge where the skin thickness was approximately 3/16 of an inch thick. A tight fitting cover was placed over the surface of the model during the cool-down period to prevent the formation of frost on the model surface. This cover was removed just prior to the injection of the model for a subsequent test.

For tests at $T_w/T_t = 0.74$, the model was heated, prior to its exposure to the supersonic stream, to approximately 1000° R by blowing heated air over it. The period of model heating was considered complete when the temperature of the model was close to the adiabatic wall temperature for a laminar-flow recovery factor. During an actual test, when the model was in the supersonic stream, the model temperature settled at an equilibrium value which gave a wall to total temperature ratio of approximately 0.74. The actual surface test temperature of the model ranged from 950° R to 1200° R, from the lowest to the highest Reynolds number tests, respectively. The same thermocouples as described above for the cold-wall tests were used to determine the surface temperature of the model for the hot-wall test. Data were recorded just prior to the time when there was a breakdown

of the supersonic flow in the tunnel. The length of a test run, up to flow breakdown, was approximately 60 seconds.

The heat-transfer tests were made with the model initially at room temperature. The model was injected into the tunnel test section from a vacuum chamber (fig. 6) which had been evacuated to test section stream static pressure. Approximately 0.05 second was required for the model to leave the chamber and enter the uniform test flow region, and the heat-transfer data were taken 1/2 second after the model was positioned in the test section.

VII. A REVIEW OF THEORETICAL LITERATURE

The problem of flow separation has been investigated theoretically since the time of Prandtl's early works, published in reference 28. In recent times one of the first efforts toward an analysis of supersonic separation was made by Chapman (ref. 21) in which the results of his mixing layer analysis (ref. 29) were used. Chapman's analysis represents a limiting case for separation with the assumption that the boundary-layer thickness is zero at the point of separation.

The Karman-Pohlhausen method was used by Gadd, Curle, and Savage, in references 30 to 32, respectively, without a great deal of success primarily because the assumed velocity profiles in the region of separation did not give the reverse flow found in experiment. Crocco and Lees (ref. 33) developed a semiempirical method which depends on the rate of entrainment of fluid from the external stream into the boundary layer. Results from the Crocco-Lees' method were only in qualitative agreement with experimental data. The Crocco-Lees' method, modified by Glick (ref. 34) predicted results that were in good agreement with pressure data as obtained from experiment. This method uses the concept of the dividing streamline; however, empirical data are required for its application. The Crocco-Lees' method was also used by Bray, Gadd, and Woodger (ref. 35) and met with reasonable success.

Tani, in reference 36, used an analysis similar to that of Wieghardt (ref. 37) and Walz (ref. 38) in that his solution for an attached flow with an adverse pressure gradient used the first moment

of momentum in addition to the zeroth moment and continuity equations. Tani used a quartic representation for the velocity profiles, however, the boundary condition which required that the momentum equation at the wall be satisfied was dropped. When this boundary condition was neglected the resulting one parameter, which characterizes the family of velocity profiles, was not directly related to the static-pressure distribution but was directly proportional to the shear stress at the wall. The one parameter describing the family of velocity profiles was obtained from the simultaneous solution of the zeroth moment of momentum and the first moment of momentum equations. The results of Tani's analysis have been found to be in good agreement with exact solutions of the boundary-layer equations. Poots, in reference 39, extended Tani's method by adding the energy equation to the continuity and two momentum equations.

Abbott, Holt, and Nielsen, in reference 40, studied the separated flow problem by using the continuity equation, the zeroth and the first moment of momentum equation, and the energy equation with a fourth degree polynomial expression for the velocity and temperature profiles and with one undetermined parameter per profile. The resulting separated flow pressure distributions did not have the correct trends primarily because of the use of polynomials for the velocity and temperature profiles. Lees and Reeves, in reference 4, developed a method for the shock-wave boundary-layer interaction problem where in the continuity equation, the momentum equation, and the first moment of momentum equation are solved simultaneously with

a one-parameter family of velocity and enthalpy profiles. Lees and Reeves used the Cohen and Reshotko profiles for the highly cooled wall cases and added the Stewartson profiles for the adiabatic wall cases, as found in references 41 and 42, respectively. This method gives good agreement with experimental pressure data for both adiabatic and cooled walls $T_w/T_t = 0.6$, however, for the highly cooled wall case $T_w/T_t = 0.2$ and for quantitative heat-transfer predictions the method is inadequate. The most promising method for predicting both pressure and heat transfer under highly cooled wall conditions is that of Holden (ref. 43) who adds the energy equation to the conservation of mass and the zeroth and first moment of momentum equations. Holden's method of solution is similar to that of Lees and Reeves in that he uses the velocity and enthalpy profiles from the upper and lower branches of the Cohen and Reshotko (ref. 41) solution. However, Holden's family of velocity and enthalpy profiles are determined by two parameters, one of which defines the velocity profile and the other defines the enthalpy profile. Both Holden and Lees and Reeves in their methods of solution uncouple the boundary-layer velocity profiles from the pressure-gradient parameter associated with the Cohen and Reshotko solution. For the Lees and Reeves' method of solution, once the velocity profile is determined there is only one enthalpy profile associated with the given velocity profile. On the other hand, in Holden's method the enthalpy profile is uncoupled from both the pressure-gradient parameter and the velocity profile and with inclusion of the energy equation the enthalpy profile

parameter can be determined. The results of Holden's method agree well with his "highly cooled" wall experimental heat transfer and pressure data (ref. 43).

VIII. THEORETICAL APPROACH

At the time the present experimental tests were conducted, the most promising theoretical approach to the flat-plate trailing-edge flap problem was the Lees and Reeves' theory of reference 4. Consequently, the method of Lees and Reeves' was programed, for use, on the IBM 7090 and approximately 120 case studies were calculated to check for agreement with experimental data. The first set of theoretical calculations were made for $T_w/T_t = 1.0$, which corresponded approximately to the $T_w/T_t = 0.74$ test conditions (appendix A). Additional boundary-layer parameters were calculated for the $T_w/T_t = 0.6$ case (appendix B) and the resulting predictions were compared with both the experimental pressure and heat-transfer data (appendix C).

The method of joining the Lees and Reeves' solution to the upstream boundary layer as used herein deviates slightly from the method indicated in reference 4. In order to apply the Lees and Reeves' theory the boundary layer upstream of the Lees and Reeves' interaction region was calculated. This upstream boundary-layer calculation took into account the favorable pressure gradient due to the induced boundary-layer effects. The value of momentum thickness, from the results of the upstream boundary-layer calculation, was matched to the Lees and Reeves' value of momentum thickness at the beginning of the interaction region; where this location for the start of the interaction region (from the upstream solution) was taken from experimental pressure data. The method of

matching the momentum thickness of the upstream solution to the Lees and Reeves' solution was used because the complete Lees and Reeves' solution, from the beginning of the interaction to the undisturbed flow downstream of the reattachment point, could not be matched to the physical size of the model. Specifically, the calculation from the hinge line through reattachment and downstream to a point where the solution reached a Blasius type of flow yielded a streamwise x-distance greater than the 2-inch-long flap of the model. The calculations made by using the Lees and Reeves' theory were done with the intention of predicting the initial shape of the pressure curve and the level of the plateau pressure. For the initial 120 cases for $T_w/T_t = 1.0$ and $T_w/T_t = 0.6$, only the region from the beginning of the interaction to the point of shock impingement was calculated. The details of the Lees and Reeves' calculations are given in appendixes A and B.

Upstream Boundary-Layer Calculation

The locally similar solutions of Beckwith and Cohen (ref. 25) were used to calculate this upstream boundary layer with a pressure gradient. The boundary-layer equations, in the similarity coordinates, with the simplifying assumptions of constant c_p and $\rho\mu$ and with $p_r = 1.0$, reduce to

$$f''' + ff'' + \beta\left(\zeta - f'^2\right) = 0 \tag{1}$$

and

$$\zeta'' + f\zeta' = 0 \tag{2}$$

where the notation is that of reference 25.

The local external flow properties for the upstream boundary-layer solutions were calculated from the induced pressure effects for the case of weak interaction from the theory of Bertram and Blackstock found in reference 44. The equation for the induced pressure (at $\gamma = 1.40$) is

$$\frac{P}{P_\infty} = 1 + \frac{\alpha}{\sqrt{1 + \alpha}} \left[1 + \frac{\alpha}{2(1 + \alpha)} \right] + \frac{0.4285\ \alpha^2}{(1 + \alpha)} \left[1 + \frac{\alpha}{2(1 + \alpha)} \right]^2 \tag{3}$$

where

$$\alpha = 0.7\ G\bar{X},$$

$$G = 0.34416 \left(T_w/T_t - 0.3859 \right)$$

and

$$\bar{X} = \frac{M_\infty^{\ 3} \sqrt{C}}{\sqrt{R_{\infty,x}}},$$

where

$$C = \frac{\mu_w\ T_\infty}{\mu_\infty\ T_w}$$

The local values of Mach number, temperature, velocity, and local Reynolds number per foot at the edge of the boundary layer were computed from

$$M_e = \sqrt{\left[\left(P/P_\infty\right)^{-2/7}\left(5 + M_\infty{}^2\right)\right] - 5.0} \tag{4}$$

$$T_e/T_\infty = \frac{5 + M_\infty{}^2}{5 + M_e{}^2} \tag{5}$$

$$u_e = M_e\, 49.1 \sqrt{T_e} \tag{6}$$

and

$$R/ft = \frac{1.812 \times 10^8 \left(T_e + 201.6\right) M_e\, P_e}{T_e{}^2} \tag{7}$$

for $\gamma = 1.40$. Thus, with local conditions external to the boundary layer calculated from equations (3) to (7), the upstream boundary layer was obtained from a numerical solution of equations (1) and (2) at 35 points along the flat plate.

The Lees and Reeves' solution between the beginning of the interaction region and the shock impingement point depends only on the separation point value of the transformed displacement thickness, assumed local conditions at the edge of the boundary layer, and the previous upstream history of the boundary layer. Therefore, the Lees and Reeves' solution, as calculated for a shock-wave boundary-layer interaction, may be readily applied to a flat plate with a trailing-edge flap, from the beginning of the interaction region to the vicinity of the hinge line.

The regions from the shock impingement point to beyond the reattachment point, for the case of a shock-wave boundary-layer interaction, are analogous to certain regions for a trailing-edge flap configuration if the wedge angle of the shock generator is half the flap angle since the final total compression angle of the inviscid flow then would be the same for the two configurations. The corresponding assumed flow models for the shock-wave boundary-layer interaction and for the flat plate with trailing-edge flap are shown in sketch 1. For the shock-wave boundary-layer interaction a fluid element external to the boundary layer and moving parallel to the plate surface turns through an angle of $\delta_f/2$ as it passes through the impinging shock wave. The same fluid element external to the boundary layer is turned again by an angle of $\delta_f/2$ as it passes through the reattachment compression fan and then moves downstream, parallel to the plate surface. For the flat plate with a trailing-edge flap the fluid element external to the boundary layer is turned by an angle of δ_f as it passes over the flap and through the reattachment compression fan. Thus if the shock generator angle is taken as half of the flap angle the external flow for both conditions will experience the same total compression angle and will have a similar static-pressure history, over the surface, as is shown in part c of sketch 1. In the flow models assumed for both configurations, the increase in entropy along the edge of the boundary layer is neglected; that is, the compression is assumed to occur through a series of weak waves rather than by one strong shock wave.

Procedure Used for Application of the Lees and Reeves' Theory

In figure 7 the experimental values of the beginning of the interaction region, as taken from measured pressure distributions, are shown for three different wall to total temperature conditions. The beginning of the interaction region, $(X/L)_o$, is selected as the point where the pressure begins to rise above the undisturbed upstream values due to the adverse pressure gradient feeding forward from the flap. At this $(X/L)_o$ location the Lees and Reeves' solution is joined to the upstream boundary-layer solution. The upstream boundary-layer momentum thickness is shown in figures 8 and 9 for a plate 10 inches long at values of $T_w/T_t = 1.0$ and $T_w/T_t = 0.6$, respectively. The calculations for figures 8 and 9 were made for a unit Reynolds number range of 0.22×10^6 to 4.3×10^6 per foot. (The Mach number and unit Reynolds number actually varied slightly along the plate according to the weak interaction equations.) The value of the momentum thickness at the beginning of the interaction, θ_o, from the Lees and Reeves' solution and for the various test Reynolds numbers, is plotted against the assumed local Mach number at the point of separation, $(Me)_s$, as shown in figures 10 and 11. Specific cases were calculated using the Lees and Reeves' theory for unit Reynolds numbers of 0.22×10^6 to 4.3×10^6 per foot, and local Mach numbers at separation from 6.5 to 7.5 at 0.1 intervals in $(Me)_s$. The undisturbed flat-plate Mach number was varied from 7.4 to 7.8 to correspond to the change in the test-section Mach number with the

change in free-stream unit Reynolds number. Typical plots of pressure against x from the beginning of the interaction region are shown in figure 12 for various values of unit Reynolds number and for $T_w/T_t = 1.0$ and 0.6.

The first step in the application of the Lees and Reeves' theory, as used in this thesis, was to obtain, from figure 7, for a given T_w/T_t and unit Reynolds number, the $(X/L)_o$ value for the beginning of the interaction. This value of $(X/L)_o$ is then used to find the value of the momentum thickness at the beginning of the interaction, θ_o, for the upstream solution, from figures 8 and 9. This value of θ_o is then used to enter figure 11 or 12, at the given T_w/T_t and R values, to obtain the corresponding value of $(Me)_s$ which, in turn, is used to specify the particular Lees and Reeves' solution and pressure distribution for the given test conditions.

The technique for selecting the particular solution to be used is best illustrated by following the dashed line in figure 11. In this instance the flat-plate value of momentum thickness is 0.20×10^{-3} ft and the unit Reynolds number is 0.65×10^{6} per foot; this gives a value of $(Me)_s = 6.641$. Rather than calculate a new solution for this value of $(Me)_s$ the solution used for a comparison with the experimental data was selected to correspond to $(Me)_s = 6.6$, that is, to the left of where the dashed line in figure 12 strikes the abscissa.

It can be seen in figure 12, for all values of unit Reynolds number, that as the Mach number at separation increases, the rate of

the pressure increase (with distance) decreases, for a sizable (X/L') distance, before the pressure begins to climb toward a plateau value. This slow rate of increase in pressure occurs in the region between $p/p_o = 1.00$ and $p/p_o = 1.10$; this makes it difficult to determine the beginning of the interaction region. For the purpose of comparing theory with experimental data, this difficulty was overcome by linearly extrapolating the slope of the curve at $p/p_o = 1.10$ to the abscissa as is shown (typically) by the dash-dot line in figure 12 for $R = 0.22 \times 10^6$ per foot and $(Me)_s = 6.8$. The point where the extrapolated lines crossed the X/L' axis was considered to be the theoretical point for the beginning of the interaction region; this was matched to the experimental value of the beginning of the interaction region. Thus the theoretical and experimental techniques of determining the beginning of the interaction region were consistent, in that both methods used a sudden pressure rise to define the beginning of the interaction region. (The experimental technique for determining the beginning of the interaction region has been previously discussed with figure 7.)

It should be noted in figure 12 that at the separation point - for the $T_w/T_t = 0.6$ case - the pressure ratio curves have a distinct discontinuity in slope. When the theoretical curves were compared with the experimental data the discontinuities in slope were faired to give a smooth pressure rise. The reason for the discontinuity in the slope of the pressure curves at the point of separation is

believed to be due to the change in slope of the separated and attached profile parameters (see appendix B) upstream and downstream of the point of separation.

In figure 13 a comparison is shown between the growth of the momentum and displacement thicknesses for the upstream similar solution boundary layer, and for the downstream Lees and Reeves' solution, at a unit Reynolds number of 0.22×10^6 per foot. The upstream boundary layer is joined to the Lees and Reeves' calculation at an X/L value of 0.515. It can be seen that both the momentum thickness and the displacement thickness match at the point where the two solutions are joined. The results of the typical calculation, shown in figure 13, indicate that the momentum thickness changes less than the displacement thickness in the presence of an adverse pressure gradient for the interaction and separated regions.

Plots of local Mach number at separation versus the plateau pressure, as obtained from the Lees and Reeves' theory, for unit Reynolds numbers from 0.22×10^6 to 4.3×10^6 per foot, are shown for $T_w/T_t = 0.6$ and 1.0 in figures 14 and 15, respectively. The Lees and Reeves value of the plateau pressure was taken from theoretical $T_w/T_t = 0.6$ and $T_w/T_t = 1.0$ curves of figure 12. The dashed lines represent the theoretical values of plateau pressure, based on the experimental value of the beginning of the interaction as found in figure 7. In addition to figure 7, figures 8 through 11 were used to obtain the proper value of the local Mach number at separation (as discussed previously) for the dashed lines of figures

14 and 15. The predicted values of plateau pressures in figures 14 and 15 are confined to a narrow band which decreases steadily with an increase in unit Reynolds number.

IX. TEST RESULTS

Transition Point Data

Transition can affect the extent of separation as well as the pressure levels associated with separation; therefore, the location of transition on the model was studied in order to determine at what unit Reynolds numbers transition begins, and the location of its beginning.

The location of the transition point was determined from heat-transfer data obtained by setting the flap at a zero angle of deflection and testing the heat-transfer model as if it were a flat plate. These heat-transfer data were plotted along the length of the model in terms of the Stanton number times the square root of the local Reynolds number ($St \sqrt{Re_x}$). It is known that the value for the undisturbed laminar boundary layer over a flat plate of $St \sqrt{Re_x}$ is approximately 0.400. The point at which this flat-plate heat-transfer data began to rise above the 0.40 value of $St \sqrt{Re_x}$ was taken as the location for the beginning of transition. A summary of these flat-plate transition data is shown in table I.

TABLE I.- FLAT-PLATE TRANSITION POINT DATA

Unit Reynolds number (per foot)	Distance from leading edge to the transition point (in)	Local transition Reynolds number (Re_x)
2.65×10^6	9.0	1.99×10^6
3.45×10^6	8.0	2.30×10^6
4.3×10^6	7.5	2.69×10^6
10.9×10^6	5.5	5.28×10^6

The effect of flap deflection is to increase the local Reynolds number slightly in the separated region and to a larger extent on the flap. For example, at a unit Reynolds number of 1.46×10^6 per foot the heat-transfer data for $\delta_f = 0^\circ$ indicate no transition on the plate. For the test at the same unit Reynolds number ($R = 1.46 \times 10^6$ per foot) with a 30° flap deflection ($\delta_f = 30^\circ$) the pressure will increase over the entire flap, with a peak increase of a factor of 4, over the flat-plate value, occurring near the trailing edge of the flap. This increase in pressure on the flap should give a high enough unit Reynolds number to cause transition to occur in the separated region in the neighborhood of the point of reattachment. In addition to the pressure disturbance that the flap causes, the very nature of the separated shear layer would also increase the possibility of transition. Becker and Korycinski (ref. 22) found that in the presence of extensive separation that the transition Reynolds number (based on free-stream conditions and distance to transition point) was less by a factor of approximately 4 than the transition Reynolds number for which there was no separation. Futhermore, the separated shear layer could be considered analogous to a wake flow which is inherently unstable and will give earlier transition than would be expected for a given unit Reynolds number. Thus it can be seen that even though transition first occurs on the flat plate at a unit Reynolds number of 2.65×10^6 per foot that when there is extensive flow separation transition can occur in the separated layer at a lower unit Reynolds number.

The effect of the deflection of the flap on the location of the point of transition is shown by a comparison of the apparent location of transition (for a unit Reynolds number of 2.65×10^6 per foot) for the $\delta_f = 0^\circ$ and $\delta_f = 30^\circ$ cases. The $\delta_f = 0^\circ$ case shows, from Table I, that transition is 9 inches from the leading edge; while the $\delta_f = 30^\circ$ case shows, from heat-transfer data, that transition in the separated region has moved forward to 7.75 inches from the leading edge. The local Reynolds number at transition based on these X lengths for the $\delta_f = 0^\circ$ and $\delta_f = 30^\circ$ configurations are 1.99×10^6 and 2.148×10^6, respectively. The Reynolds number for the $\delta_f = 30^\circ$ case was based on a measured pressure in the region of separation.

The determination of the exact point of transition on the flat-plate model with a trailing-edge flap deflected is quite difficult due to the complex flow field which is present. If transition occurs on the flap of the model it is very difficult to determine where transition occurs, from the heat-transfer data, due to the rapid rise in the heating rate on the flap. If transition occurs upstream of the hinge line, in the separated flow region, the location of the actual point is further complicated by the low heating rate and the reverse flow in the separated region. In general, the trend, by all test methods (oil flow, pressure, and heat transfer), is that the flap deflection will increase the local Reynolds number and will, in turn, move the transition point upstream.

Room-Temperature Wall-Pressure Tests

The pressure tests with the wall at room temperature were run with the model shown in figures 1 and 2. The results of the pressure tests, for $T_w/T_t = 0.43$ at flap angles of 10°, 20°, and 30° are shown in figures 16(a), 16(b), and 16(c) for a Reynolds number per foot ranging from 0.22×10^6 to 4.3×10^6. The results from tests run with side plates are shown in figure 16(d), for flap angles of 10°, 20°, and 30°, and Reynolds numbers per foot of 1.06×10^6 and 2.65×10^6. The pressures, from figure 16, have been ratioed to the measured pressure at the beginning of the interaction region. All the pressure data in figure 16 are compared to the Lees and Reeves' theory (ref. 4) for a $T_w/T_t = 0.6$, and with the beginning of the interaction region determined as described in the Theoretical Approach section. The agreement between experiment and the Lees and Reeves' theory is, in general, good for the range of unit Reynolds numbers of 0.22×10^6 per foot and 1.46×10^6 per foot. The test in this Reynolds number range are in a flow regime where the separation plateau pressure level is not strongly affected by transitional effects, as was noted in the previous section in which transition on the flat plate model did not occur until a unit Reynolds number of 2.65×10^6 per foot. It was also pointed out in the previous section that undoubtedly transition was occurring in the separated shear layer at unit Reynolds numbers lower than 2.65×10^6 per foot due to the flap disturbance and the inherent instability of the separated shear layer. Even though transition is undoubtedly occurring in the shear layer for

tests run at unit Reynolds numbers less than 2.65×10^6 per foot the point of transition is far enough downstream (over the flap) that it will not affect the laminar plateau pressure distribution but will have an effect on the extent of the separation. When the transitional effects become more pronounced at unit Reynolds numbers of 2.65×10^6 per foot and 4.3×10^6 per foot (see previous section) the Lees and Reeves' theory tends to underpredict the level of pressure due to a rise in the pressure above the laminar plateau value in the area of transition. The rise in pressure when transition occurs in the separated region was previously noted by Chapman, Kuehn, and Larson in reference 21. The location of the point of transition on a flat plate has been previously stated to be at 9.0 and 7.5 inches from the leading edge for unit Reynolds numbers of 2.65×10^6 per foot and 4.3×10^6 per foot. For the tests at a unit Reynolds number of 2.65×10^6 per foot, in figures 16(a) through 16(d), the rise in pressure above the laminar plateau value occurs at approximately 9.0 inches from the leading edge, with higher flap angles (particularly 30°) having the pressure rise above plateau value start at a more upstream position than the lower flap angles. For the tests at a unit Reynolds number of 4.3×10^6 per foot in figures 16(a) through 16(c) the separation is all turbulent because the transition point is upstream of the point of separation, thus no agreement would be expected at $R = 4.3 \times 10^6$ per foot with the laminar theory of Lees and Reeves. The side plate data in figure 16(d) at a unit Reynolds number of 1.06×10^6 per foot show that as the flap angle increases the

level of plateau pressure also increases and the Lees and Reeves' theory tends to slightly underpredict for the 20° and 30° flap angles, as was the case with no side plates. A comparison between the $\delta_f = 30^{\circ}$, $R = 2.65 \times 10^6$ per foot cases in 16(c) and 16(d) shows that the extent of separation is greater for the side-plate tests. In general, the addition of side plates increases the extent of separation for all flap angles and flow conditions. The pressures measured upstream of the separation interaction in figures 16(a) to 16(d) agree well with the viscous interaction theory of Bertram and Blackstock (ref. 44). The theoretical viscous interaction curves shown are ratioed to the theoretical pressure level at the beginning of the interaction.

Figure 17 shows the schlieren photographs for tests at a $T_w/T_t = 0.43$, at flap angles of 10°, 20°, and 30°, over a Reynolds number per foot ranging from 0.22×10^6 to 10.9×10^6. These pictures were used to determine the angle of the leading-edge shocks, the separated layer shock, and the deflection angle of the separated boundary layer. In addition, the pictures were used to determine the separation point - based on the location where the separation shock wave intersects the boundary layer. These measurements of the separation point were found to be in good agreement with oil-flow separation point data.

Figure 18 shows the room-temperature wall-pressure distribution (ratioed to the plate static pressure) as calculated for the inviscid flat plate model set at $1/2^{\circ}$ positive angle of attack. The pressure

ratios are shown in figures 18(a), 18(b), and 18(c) for flap angles of 30°, 20°, and 10°, respectively, and for Reynolds numbers per foot varying from 0.22×10^6 to 10.9×10^6. The side plates pressure data are also shown in figures 18(d) and 18(e) for flap angles of 30°, 20°, and 10°. The separated layer oblique shock theory in figure 18 was calculated from the apparent measured flow deflection angle above the separated layer (fig. 17) and based on the value of Mach number ahead of the interaction region. The value of Mach number ahead of the interaction region was calculated from the measured value of the leading-edge shock angle, above the interaction region, and the free-stream Mach number. All oblique shock parameters were taken from reference 45. Also plotted in figure 18 are the values of the beginning of the interaction, X_o; the separation point X_s; and the reattachment point, X_R. The values of the separation point and the reattachment point (fig. 18) were taken from oil-flow studies. The beginning of the interaction region is taken from the expanded plots of pressures - in the area of the plateau and interaction region - as has been previously discussed in the Theoretical Approach section. The separated layer oblique shock values of pressure agree, for the most part, with the measured pressure plateau values with the exception of a few of the lower unit Reynolds numbers where the shock pressures tend to slightly overpredict the measured values.

The peak pressure ratio in figure 18(a) for the 30° flap at $R = 10.9 \times 10^6$ per foot, is 29.6 compared to the inviscid flap oblique shock value of 28.4. For $R = 4.3 \times 10^6$ per foot the peak

value is 41.8 compared to the inviscid value of 28.3; and for $R = 2.65 \times 10^6$ per foot the peak value is 44.8 which is an increase of approximately 58 percent over the inviscid value. The reason that the measured peak pressure exceeds the inviscid shock pressure is because of the quasi-isentropic compression which occurs through a series of waves rather than through a single shock. In figure 18(b) a similar trend can be seen where for the 20° flap, with the highest unit Reynolds number of 10.9×10^6 per foot, the value approaches the inviscid value of 14.2; while at the Reynolds numbers per foot of 4.3×10^6 and 2.65×10^6 the peak pressure rise increases to a level above the inviscid value with a decrease in unit Reynolds number. The reason for this phenomenon is again a quasi-isentropic compression through a series of waves rather than a single shock. In figure 18(c) for the 10° flap, the peak pressure rise has a similar trend as that exhibited in figures 18(a) and 18(b), for the 30° and 20° flap, only to a much lesser degree.

The tests made with side plates are shown in figures 18(d) and 18(e) and are compared with similar runs made with no side plates. The tests for the 30° flap, with side plates, (fig. 18(d)) show that the pressure ratio in the plateau region is higher for the runs with side plates; and also, that the extent of separation is greater with the side plates as compared to the runs with no side plates. The side-plate data in figure 18(d), in general, indicate a slower rise to the peak pressure value on the flap. This lag in pressure rise, on the flap with side plates, is due primarily to the thicker separated boundary layer; this in turn causes a lag in the turning of the flow

in a direction parallel to the flap. The side-plate data for the 20° and 10° flap angles (fig. 18(e)) again exhibit a greater extent of separation than the no-side-plate data and, in general, lags the no-side-plate data in the rise on the flap to the peak pressure value.

In figure 19 the measured values of flow deflection angle ψ from the plate surface, due to the flow separation, and the resulting oblique shock angle θ_2 are plotted against unit Reynolds number. The angles were measured from the schlieren pictures of figure 17 (see sketch 2 for a description).

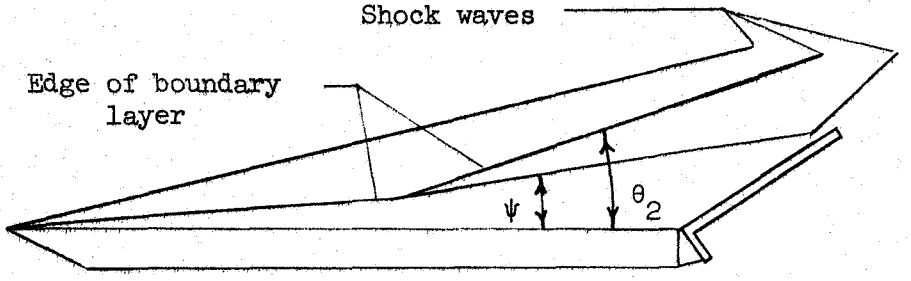

Sketch 2

From figure 19 it can be seen that for a given free-stream unit Reynolds number the flow deflection angle, and the corresponding shock-wave angle, decrease as the flap angle decreases. Figure 19 also shows that as the unit Reynolds number decreases the flow deflection and the corresponding shock angle increase. The reason for this increase in flow deflection angle, with a decrease in unit Reynolds number, is due to the increase of the rate of growth of the displacement thickness with a decrease in unit Reynolds number. For example, from the Lees and Reeves' calculations, at unit Reynolds numbers of

0.22×10^6, 1.06×10^6, and 4.3×10^6 per foot, the linear rate of growth of the displacement thickness ($d\delta^*/dx$) over the separated region is 0.1194, 0.065, and 0.0414, respectively. Thus it can be seen that the results shown in figure 19 are consistent with computed boundary-layer growth from the separated flow analysis of Lees and Reeves.

A comparison of the plateau pressure obtained from oblique shock theory applied to data of figure 17, the Lees and Reeves' theory, and measured static pressure values (for no side plates) is shown in figure 20. The comparison is made for flap angles 10°, 20°, and 30° and for unit Reynolds numbers varying from 0.22×10^6 to 4.3×10^6 per foot. The oblique shock curves in figure 20 are faired curves taken from another plot of the individual data points. These faired oblique shock curves deviate approximately 2 percent from the individual data points. The oblique shock plateau pressures were calculated from the flow deflection angles (figure 19) and the local value of Mach number just upstream of the interaction point. The local Mach number was calculated from the leading-edge shock-wave inclination and the free-stream Mach number. The Lees and Reeves' prediction for the plateau pressure ratio for flap angles of 10°, 20°, and 30° was taken from figure 14 for the various unit Reynolds numbers. The measured plateau pressures for flap angles of 20° and 30° were taken from the plotted data of figure 16. No experimental plateau pressures for a 10° flap angle are presented since the short length of separated flow region was so short in length that a pressure plateau could not form.

The plateau pressures of figure 16 have been ratioed to the pressure at the beginning of the interaction to describe a $(p/p_o)_{pl}$ value. In general, the oblique shock value of plateau pressure is higher than the measured value and the Lees and Reeves' value is slightly lower. The difference in the Lees and Reeves' value of plateau pressure between figure 16 and figure 20 lies in the fact that the plateau pressures for figure 20 are taken from figure 14 for an exact value of $(Me)_s$, while the plateau pressure in figure 16 was taken from figure 12 for a nominal value of $(Me)_s$ based on the method discussed in the Theoretical Approach section.

Surface Oil-Flow Studies

The pressure model (fig. 1) was used for the oil-flow studies and was tested with and without side plates. Prior to making an oil-flow test a pattern of drops, consisting of an oil-lamp black mixture, was placed on the surface of the plate as shown on the left in figure 21. The viscosity of the oil was increased with increasing unit Reynolds number in order that a flow pattern could be established in approximately the same length of time for all runs. The model was rapidly injected into the wind tunnel's airstream; as soon as the rearward movement of the oil drops stopped the model was retracted from the stream. The temperature of the model in the area of separation varied from approximately 90° F to 100° F for all the oil-flow tests. This temperature was measured with a thermocouple located 8 inches downstream from the leading edge, on the inside surface of the model, at an area where the skin is approximately 3/16 of an inch

thick. The oil drops were placed on the model just prior to the run; a picture was taken of the oil dots in the undisturbed position, and then immediately after the run a second picture was taken of the oil-flow pattern. These pictures were used as a means for determining the location of the separation point. A typical oil-flow pattern is shown in figure 21, for a free-stream unit Reynolds number of 4.3×10^6 per foot and a flap angle of 20°. It can be seen from these oil-flow photographs that the surface streamlines are parallel to the inviscid flow before the interaction region; however, in the reverse flow region the surface oil flow shows the streamlines diverge (outward) indicating that the surface flow is three dimensional in nature. The use of the side plates considerably reduced the divergence of the flow in the separated region.

The viscosity of the oil for each Reynolds number and flap angle could not be chosen so as to insure a clear and distinct pattern of oil flow in the separated region for each run. For the majority of runs the oil droplets in the reverse flow region were displaced to some extent toward the separation point due to surface shear. Any movement of the oil drops could be detected by superimposing the negatives taken before and after the run. The use of this oil-flow evaluation technique was extremely helpful in determining the location of the point of separation. In figure 21 this point is indicated by arrows.

A comparison between the separation point location, as indicated by the oil-flow pattern and as obtained from schlieren photographs,

shows good agreement when the schlieren separation point is chosen at the intersection of the shock wave from the separated layer and the apparent outer edge of the boundary layer. The difference between the oil flow and the schleiren separation-point locations, for the 30° flap and over the Reynolds number range, was a most 1/8 inch. Similar agreement was found for the 20° and 10° flap angles for Reynolds numbers above 0.4×10^6 per foot and 1.0×10^6 per foot, respectively.

The types of flow separation are classified in reference 21 into three distinct regimes: (1) "laminar," in which transition occurs downstream of reattachment, (2) "transitional," in which transition occurs between separation and reattachment, and (3) "turbulent," in which transition occurs upstream of separation. In an effort to show theoretically the effect on the movement of the point of separation with an increase in unit Reynolds number in a regime where the separation is purely laminar, calculations were made using the laminar separation theory of Lees and Reeves (ref. 4). The calculations (table II) using the Lees and Reeves' theory, were made for a constant local Mach number at the point of separation and the unit Reynolds number was varied from 0.22×10^6 per foot to 2.65×10^6 per foot.

TABLE II.- EFFECT OF UNIT REYNOLDS NUMBER ON THE EXTENT OF THEORETICAL LAMINAR SEPARATION

(Constant $(Me)_{sep}$, Lees and Reeves' Solution)

Reynolds number per foot	Distance from leading edge to beginning of interaction region (inches)
0.22×10^6 (0.72×10^6/m)	9.5 (.2411 m)
0.29×10^6 (0.95×10^6/m)	5.75 (.1460 m)
0.42×10^6 (1.38×10^6/m)	3.35 (.08508 m)
0.65×10^6 (2.13×10^6/m)	1.65 (.04190 m)
1.06×10^6 (3.48×10^6/m)	1.00 (.0254 m)
1.46×10^6 (4.79×10^6/m)	0.55 (.01396 m)
2.65×10^6 (8.69×10^6/m)	0.25 (.00635 m)

The distance from the leading edge to the beginning of the interaction region in table II was determined by matching the value of displacement thickness from a flat-plate local similarity solution to the value of displacement thickness at the beginning of the Lees and Reeves' solution. The results of the laminar theory in table II show that as the unit Reynolds number increases, the interaction region and, in turn, the separation point move upstream. The results from an experimental investigation by Miller, Hijman, and Childs (ref. 16), in which all the data presented were for pure laminar separation, showed that as the Reynolds number increased (up to a value of approximately 1×10^6 per foot) the separation point moved upstream. Thus both theoretical and experimental evidence show that for pure laminar separation the point of separation moves upstream

with an increase in unit Reynolds number. On the other hand, the experimental data of Chapman, Kuehn, and Larson (ref. 21) showed that at Mach numbers from 2.7 to 3.5, when the separation went from a pure laminar separation to transition separation, the point of separation moved downstream. Chapman, Kuehn, and Larson's data also showed that a further increase in the unit Reynolds number caused the separation to become turbulent and the separation point moved further downstream. Becker and Korycinski (ref. 22) showed the same effect on the movement of the point of separation with a change in unit Reynolds number for laminar, transition, and turbulent separation as was found in this thesis and as was found in the work of Miller, Hijman, and Childs (ref. 16) and Chapman, Kuehn, and Larson (ref. 21). From the above experimental evidence it appears that for transitional separation the separation point moves downstream with an increase in unit Reynolds number and for laminar separation the movement is in the upstream direction for an increase in unit Reynolds number.

The distance from the leading edge to the point of separation, as obtained from oil-flow data, is shown in figure 22 for free-stream unit Reynolds numbers from 0.22×10^6 to 4.3×10^6 per foot for flap angles of 10°, 20°, and 30°, and for the studies with and without side plates. The results show that the separation point moves forward appreciably as the flap angle is increased and generally moves forward as the unit Reynolds increases - up to a value of approximately 0.8×10^6 per foot. At the lower Reynolds numbers (up to $R = 0.4 \times 10^6$ per foot), for the 10° and 20° flap angles, the rearward

movement of the separation point with increasing Reynolds number is attributed to the fact that the thick shear layer at the edge of the separated flow passes well above the uppermost portion of the (2-inch-long) deflected flap. An examination of the schlieren photographs (fig. 17) showed that when the shear layer was deflected upward by the flap, the separation point began to move forward (for laminar separation) on the plate with increasing Reynolds number, as was noted for the 30° deflected flap. The laminar separation data in reference 16, at free-stream Mach numbers of 13 and 16, clearly indicate a forward movement of the separation point with an increase in unit Reynolds number as discussed in the previous paragraph. It can be seen in figure 22 that for all three flap angles the separation point begins to move to the rear of the plate at a unit Reynolds number of approximately 1.0×10^6 per foot. This reversal in the trend of separation point movement is attributed to the effect of boundary-layer transition from laminar to turbulent flow occurring in the region of separated flow. For these data it is apparent that separation, up to a unit Reynolds number of approximately 1.0×10^6 per foot, gives laminar separation; and for a unit Reynolds number above approximately 1.0×10^6 per foot the separation is transitional - independent of the extent of separation and flap angle. A similar rearward movement of the separation point due to a transition to turbulent flow in the separated region was found in reference 21 at a Mach number of 2.7, as discussed in the previous paragraph. In figure 23 the results of an oil-flow study to determine the

reattachment point on the flap are shown. The reattachment point clearly moves toward the hinge line as the Reynolds number increases. The location of reattachment on the flap, for a given unit Reynolds number, varies only slightly with a change in flap angle. It is only at a unit Reynolds number of 1.06×10^6 per foot that there is any appreciable change in the point of reattachment with a change in flap angle. This change in the point of reattachment - at a unit Reynolds number of 1.06×10^6 - is attributed to a delay in the transitional effects with a decrease in flap angle. The solid lines in figure 23 are the predicted reattachment points as obtained from a linear extension of the dividing streamline from the point of separation (fig. 22) to the flap at an angle equal to the flow deflection angle of figure 19. The experimental data points are further downstream from the hinge line at the lower unit Reynolds numbers than the values based on the linear extension of the initial flow deflection angle. This indicates that the dividing streamline curves upward as it moves downstream from the point of separation.

In figure 24 the pressure ratios, at the reattachment point on the flap, are plotted against Reynolds number per foot. For a given unit Reynolds number the level of pressure increases with an increase in flap angle, as would be expected; however, the reattachment pressure levels are considerably lower than the oblique shock inviscid pressure levels. The reason that these reattachment pressure levels are so much smaller than the inviscid oblique shock values is that at

the point of reattachment the inviscid stream has not yet turned parallel to the flap and the compression process is just starting.

Chapman's analysis for the reattachment pressure rise - as set forth in reference 21 - gives a constant value of $(p/p_o)_R$ of approximately 7.0 for the nominal Mach number of these tests. These data show that the reattachment pressure ratio is a strong function of Reynolds number and flap angle.

Wall-Temperature Effects

In order to determine the wall-temperature effect on separation, experimental tests were conducted at wall to total temperature ratios of 0.14, 0.43, and 0.76. Figure 25 shows the measured flat-plate static pressure, 5 inches aft of the leading edge, ratioed to the theoretical inviscid flat-plate static pressure at $1/2^\circ$ positive angle of attack, and the theoretical viscous interaction pressure effects of Bertram and Blackstock (ref. 44) for T_w/T_t = 0.14, 0.43, and 0.74. The results in figure 25 show that the T_w/T_t = 0.43 and 0.74 pressure ratios decrease with an increase in unit Reynolds number and most of the measured pressure ratios tend to underpredict the theory by approximately 10 percent. The pressure data at T_w/T_t = 0.14 at the two lowest units Reynolds numbers ($R = 0.29 \times 10^6$ and 0.42×10^6 per foot) considerably underpredict the theory while the remaining values of pressure ratio at the higher Reynolds numbers still underpredict the theory but only by approximately 10 percent or less. The large discrepancy between data and theory, for

$T_w/T_t = 0.14$, at the two lowest unit Reynolds numbers may be caused by a shift in the gage calibration due to a temperature effect on the "hot-wire" gage. In spite of the possibility of a shift in calibration, which would cause an error in the absolute value of the measured pressure, the pressure-ratio (p/p_o) distribution over the model should be reasonably accurate.

The experimental pressure tests, conducted at $T_w/T_t = 0.14$, 0.43, and 0.74, are shown in figures 26 through 31. The measured pressures for the three wall temperatures have been ratioed to the measured pressure at the beginning of the interaction region. The pressure data in figures 26 to 31, for the temperature ratios of 0.43 and 0.74, are compared to calculations based on Lees and Reeves' theory for wall conditions of $T_w/T_t = 0.6$ and $T_w/T_t = 1.0$, respectively. In addition, pressure distributions, based on the flat-plate viscous interaction theory of Bertram and Blackstock (ref. 44), are calculated (and plotted) for wall to total temperature ratios of 0.43 and 0.74.

The wall-temperature effects at $\delta_f = 10^o$, in figure 26, show good agreement with the Lees and Reeves' theory for unit Reynolds numbers of 0.42×10^6 to 1.46×10^6 per foot. The effect of increased wall cooling tends to increase the pressure ratio over the flap, particularly for $T_w/T_t = 0.14$, and to reduce the extent of separation. At unit Reynolds numbers of 1.46×10^6 and 2.65×10^6 per foot the effect of increased wall cooling is to considerably decrease the extent of separation.

The decrease in the extent of separation at the higher Reynolds numbers is caused by the flow going from a laminar type of separation to a transitional type of separation, as was previously pointed out in the section on oil-flow studies. The additional effects of wall cooling at the higher Reynolds numbers is to further reduce the extent of separation, as shown in reference 46, for a cone-cylinder flare at Mach 5 at a similar unit Reynolds number range. Thus the combined effects of transitional separation and wall cooling tend to reduce significantly the extent of separation with the increase in unit Reynolds number (above 1.46×10^6 per foot).

The results shown in figures 27(a) and (b) for the 20° flap indicate that for unit Reynolds numbers of 0.29×10^6 and 0.42×10^6 per foot conditions at $T_w/T_t \approx 0.15$ have a greater extent of separation and a higher plateau pressure value than either the $T_w/T_t = 0.43$ or the $T_w/T_t = 0.74$ case. The $T_w/T_t = 0.74$, for figures 27(a) and (b), falls between the $T_w/T_t = 0.15$ and 0.43 cases in both the extent of separation and the level of plateau pressure. For unit Reynolds numbers from 0.65×10^6 to 1.46×10^6 per foot in figures 27(c), (d), and (e) indicate only a small influence due to wall temperature in the plateau pressure region, but indicate a decrease in flap pressure ratio with an increase in wall-temperature ratio. The higher unit Reynolds numbers of 2.65×10^6 and 4.3×10^6 per foot, in figures 27(f) and (g), indicate a marked decrease in the extent of separation with a decrease in the wall-temperature ratio,

and also show a decrease in the flap pressure ratio with an increase in the wall to total temperature ratio.

For the 30° flap angle the results of the wall-temperature effect on the pressure data (in figures 28(a) and 28(b)) for a unit Reynolds number of 0.29×10^6 and 0.42×10^6 per foot show a higher plateau pressure level and greater extent of separation for the $T_w/T_t = 0.15$ ratio than either for $T_w/T_t = 0.43$ or 0.74 cases. The $T_w/T_t = 0.71$ case, in figure 28(a), falls between the 0.11 and 0.48 temperature ratios in both the level of pressure ratio and the extent of separation. At a unit Reynolds number of 0.42×10^6 per foot, in figure 28(b), the pressures measured at $T_w/T_t = 0.43$ and 0.74 are in reasonably close agreement and are below the pressure level for $T_w/T_t = 0.14$. The results in figures 28(c), 28(d), and 28(e), for unit Reynolds numbers from 0.65×10^6 to 1.46×10^6 per foot, show only a small effect in the interaction and plateau region due to wall temperature; however, the flap pressure ratios show a decrease with an increase in the wall to total temperature ratio. Again, as in the 20° flap tests, for unit Reynolds number of 2.65×10^6 and 4.3×10^6 per foot, the effect of wall cooling significantly reduces the extent of separation, as shown in figures 28(f) and 28(g). This decrease in the extent of separation at the two highest unit Reynolds numbers, with a decrease in wall temperature, is attributed to the combined effect of wall cooling and transition in the separated region; this has been discussed previously. In figures 28(f) and 28(g) - as in

the previous high Reynolds number figures - the pressure ratio on the flap decreased with an increase in wall to total temperature ratio.

The tests in figures 29, 30, and 31 were made with side plates (see fig. 1) at unit Reynolds numbers of 1.06×10^6 and 2.65×10^6 per foot for flap deflection angles of 10°, 20°, and 30°. In general, the results of figures 29, 30, and 31 show a slight decrease in the extent of separation with wall cooling at a unit Reynolds number of 1.06×10^6 per foot, and a marked decrease in the extent of separation with wall cooling at a unit Reynolds number of 2.65×10^6 per foot. Figures 29 to 31 also show a decrease in flap pressure ratio with an increase in the wall to total temperature ratio for both unit Reynolds numbers.

In general, the comparison between experimental and theoretical data in figures 26 to 31 shows good agreement with the Lees and Reeves' theory (ref. 4) and with the Bertram and Blackstock viscous interaction theory (ref. 44). An inspection of the experimental data of figure 26 shows that as the wall to total temperature ratio decreases the pressure gradient from the beginning of the interaction region to approximately the hinge line becomes slightly steeper. Calculations by the Lees and Reeves' theory show that the $T_w/T_t = 0.6$ wall condition had a steeper pressure gradient from the beginning of the interaction to the pressure plateau (value) than did the $T_w/T_t = 1.0$ wall condition. Curle and Gadd (refs. 31 and 47) theoretically predicted that the pressure gradient at separation should be inversely proportional to the wall temperature. This prediction agrees with the

results of calculations by the Lees and Reeves' theory at wall temperature ratios of $T_w/T_t = 1.0$ and 0.6; Gadd experimentally showed this effect of the wall temperature on the pressure gradient, and reported it in reference 48. For the majority of the cases calculated by the Lees and Reeves' theory, and compared to experimental data, the plateau value for the hot-wall case $(T_w/T_t = 1.0)$ was slightly higher than the cool-wall case $(T_w/T_t = 0.6)$ when the extent of separation was long enough to allow the hot-wall case $(T_w/T_t = 1.0)$ to reach a plateau value. The fact that the $T_w/T_t = 1.0$ calculations, using the theory of Lees and Reeves, give a higher plateau pressure can also be seen from figure 31, and by a comparison of figures 14 and 15.

It should be noted that the absolute value of experimental plateau pressure for hot-wall cases $(T_w/T_t = 0.74)$ is higher than the cool-wall cases $(T_w/T_t = 0.43)$. However, when the absolute values of plateau pressure are ratioed to the value of the pressure at the beginning of the interaction region, values of the plateau pressure ratios at $T_w/T_t = 0.43$ and $T_w/T_t = 0.74$ are brought fairly close together. This can be seen from an inspection of figure 25 and the results of figures 26 to 31.

The schlieren photographs at wall to total temperature ratios of 0.14, 0.43, and 0.74, and for flap angles of 20° and 30°, are shown in figure 32. These photographs were used to determine the wall-temperature effect upon the flow deflection angles, the shock-wave angles, and the separation points over a unit Reynolds number range

of 0.22×10^6 to 4.3×10^6 per foot. The results of the schlieren analysis show that the flow deflection angle (fig. 33) and the shock-wave angle, measured from the point of separation, decrease continuously with increasing unit Reynolds number for all three wall-temperature ratios. The effect of wall temperature on flow deflection and shock angle is not large; however, it should be noted that the highly cooled wall ($T_w/T_t = 0.14$) and the hot-wall condition ($T_w/T_t = 0.74$) have slightly higher values of deflection and shock-wave angle than does the room-temperature wall condition ($T_w/T_t = 0.43$). This fact was reflected in the measured pressures and has been brought out in the discussion of figure 25 and figures 26 to 31.

It should be noted, from figures 18(a), 18(b), and 18(c), that the pressure rise on the flap only approached a peak value of pressure for a unit Reynolds number greater than 1.46×10^6 per foot. The reason that the pressures did not reach a peak value on the flap, for unit Reynolds numbers of 1.46×10^6 per foot and below, was because the length of flap was so short that it did not allow the flow to attain undisturbed flat-plate conditions. The short length of flap undoubtedly had some effect on the length of separation; however, to what degree the flap length affected the extent of separation would require a separate investigation. In general, it was determined from the results of the separation point data (figs. 22 and 34), and the reattachment point data (fig. 23), that above a unit Reynolds number of 1×10^6 per foot the short length of flap had a small effect on the extent of separation. It was observed experimentally that for

$T_w/T_t = 0.43$ an increase in unit Reynolds number, up to a value of approximately 1.0×10^6 per foot will move the separation point forward. A departure from this experimental trend, found for unit Reynolds numbers below 1×10^6 per foot, is attributed to the flap length being too short.

The separation-point data, taken from schlieren pictures of figure 32, are shown in figure 34. These separation point data for $T_w/T_t = 0.43$ in figure 34, are in reasonable agreement with the surface oil-flow technique, for separation point data, at room-temperature wall condition ($T_w/T_t = 0.43$), as discussed for figure 22. As stated previously for the room-temperature wall conditions it is felt that separation, up to a unit Reynolds number of approximately 1.0×10^6 per foot, yields a laminar separation; but for unit Reynolds numbers above $1.0 = 10^6$ per foot the separation is of a transitional type. For the 30° flap angle, the results in figure 34 for the room-temperature wall ($T_w/T_t = 0.43$), and the hot wall ($T_w/T_t = 0.74$), show that the separation point moves forward on the plate with increasing unit Reynolds number up to a value of approximately 1.0×10^6 per foot. From this point, an increase in the unit Reynolds number for $T_w/T_t = 0.43$ and $T_w/T_t = 0.74$ rapidly moves the separation point toward the hinge line. For a flap angle of 30° the wall-temperature effects for the laminar separation show that the highly cooled wall ($T_w/T_t = 0.14$) has the greatest extent of separation, while the $T_w/T_t = 0.43$ and 0.74 cases have nearly equal extent of separation. When the effects of transition become significant, at a

unit Reynolds number of approximately 1.0×10^6 per foot, the effect of wall cooling for a given unit Reynolds number tends to decrease the extent of separation significantly. The wall-temperature effect, shown in figure 34 for $\delta_f = 20^\circ$, is quite similar to the 30° flap plot with the extent of laminar separation being greatest for the highly cooled wall condition $(T_w/T_t = 0.15)$, the hot-wall condition $(T_w/T_t = 0.74)$ extent of separation being next to the greatest; and the room-temperature wall condition $(T_w/T_t = 0.43)$ having the smallest extent of separation. Again, for the 20° flap deflection, when the transitional effects become predominant at a unit Reynolds number above approximately 1.0×10^6 per foot the wall cooling, for a given unit Reynolds number, consistently tends to decrease the extent of separation.

In figure 35 the values of plateau pressure ratios for $T_w/T_t = 0.14$, 0.43, and 0.74, at flap angles of 20° and 30° are shown; these were taken from the plots of figures 26 to 31. It can be seen (fig. 35) that the level of plateau pressure decreases with an increase in the unit Reynolds number for all three wall-temperature ratios and both flap angles. The highly cooled wall $(T_w/T_t = 0.14)$ and the hot wall $(T_w/T_t = 0.74)$ give higher values of plateau pressure than the room-temperature wall condition $(T_w/T_t = 0.43)$, up to a unit Reynolds number of 1.0×10^6 per foot. At a unit Reynolds number of about 1.0×10^6 per foot the transitional effects become significant and the plateau pressure level, for a given unit Reynolds number, decreases with an increase in wall cooling.

Figure 36 shows a correlation of plateau pressure coefficients in terms of the local Reynolds number and local Mach number at the beginning of the interaction region. The data points are for a range of unit Reynolds numbers from 0.22×10^6 to 2.65×10^6 per foot, and wall to total temperature ratios of 0.14, 0.43, and 0.74. The local flow properties were evaluated from the measured wall pressures, shock angles, and the oblique shock relations. The beginning of the interaction region was determined, from expanded plots of the pressure data, figures 15 and 26 to 31, as the point where the pressure began to rise above the flat-plate value. These data show reasonable agreement with the expression given by Hakkinen, Greber, and Trilling (ref. 49), but falls slightly above the theory of Erdos and Pallone (ref. 50). The lower Mach number data of Chapman, Kuehn, and Larson (ref. 21) and the data of Miller, Hijman, and Childs (ref. 16) also are higher than the values for $\left(C_p\right)_{Pl} \left(Re_{x_o}\right)^{1/4}$ due to Erdos and Pallone (ref. 50).

Heat-Transfer Results

The heat-transfer results that are to be presented in this thesis are preliminary in nature. These data were taken as "typical results" from approximately 50 heat-transfer tests in which the flap angle and unit Reynolds number were varied. A complete presentation of the heat-transfer tests will be forthcoming in a future paper, where the experimental data will be compared with Holden's theory (ref. 43).

Three typical comparisons, of the heat-transfer theory with experimental data, are shown in figure 37. The information in figure 37 is presented only for the region upstream of the hinge line. It can be seen (fig. 37) that the heat-transfer theory, described in detail in appendix C, predicts the general downward trend but does not follow the heating ratio exactly. In the reduction of the data the measured values of q were divided by the theoretical flat-plate value of q at the beginning of the interaction region. The flat-plate value of q was calculated from the local similarity solutions of Beckwith and Cohen (ref. 25); the local similarity values of $St\sqrt{Re_x}$ for a unit Reynolds number range of 0.22×10^6 to 4.3×10^6 per foot varied from 0.393 to 0.405 due to changes in the local flow conditions. The flat-plate values of q were evaluated at the X/L location corresponding to the beginning of the interaction region found in figure 7. There was good agreement between the measured and calculated value of q in the area of flow upstream of the interaction region.

One reason for the lack of better agreement between the heat-transfer theory and experiment is believed to be due to the limitation in the Lees and Reeves' method of a one-parameter family of velocity and enthalpy profiles. In a recent paper by Holden (ref. 43) for the solution of the shock-wave boundary-layer interaction, the energy equation was added to the three basic equations which were used in the Lees and Reeves' method. Holden's method of solution is quite

similar to that of Lees and Reeves; however, his use of the energy equation, and the use of the two-parameter method for describing the velocity and enthalpy profiles, has enabled him to obtain good theoretical agreement with the measured heat-transfer data.

X. CONCLUDING REMARKS

The Lees and Reeves' (ref. 4) theory, for a shock-wave boundary-layer interaction, has been applied to the case of a flat plate with a relatively short (20 percent chord) trailing-edge flap. Calculations, by this theory, were carried out from the beginning of the interaction region to downstream of reattachment on the flap; however, only the calculation for the region from the beginning of the interaction region to the maximum extent of the laminar plateau region was used. The results for the flow over the flap were not used because the extent of the theoretical flow over the flap was found to be considerably longer than the actual extent of the 2-inch-long flap. The Lees and Reeves' solutions were joined to the upstream boundary layer by matching the momentum thickness of the two flow regions at the experimentally determined point for the beginning of the interaction region. Agreement between the separation pressure data and the Lees and Reeves' theory was found to be good. Lees and Reeves' upper and lower branch boundary-layer parameters, for a wall to total temperature ratio of 0.6, were calculated from local similarity boundary-layer solutions and then polynomials were curve fit to the parameter for use in the separated flow solution. The working plots of flat-plate momentum thickness, momentum thickness at the beginning of the Lees and Reeves' solution, and pressure distributions, used to predict the pressure, are contained herein.

The range of free-stream Mach number, and unit Reynolds number, for the working plots is 7.4 to 7.8, and 0.22×10^6 to 4.3×10^6 per foot, respectively.

The results of an extensive surface oil-flow study, conducted at room-temperature wall conditions, showed that for pure laminar separation an increase in unit Reynolds number will move the separation point upstream; however, when the boundary layer becomes transitional an increase in unit Reynolds number will move the separation point toward the hinge line. It was also found that the use of side plates and an increase in the size of the flap angle increased the extent of separation. The flap-angle reattachment point, according to the oil-flow study, showed that for a given unit Reynolds number the point of reattachment changed very little with a change in flap angle from 10° to 30°.

The pressures measured on the 30° flap at a unit Reynolds number of 2.65×10^6 per foot indicated a pressure rise of approximately 58 percent over the oblique shock reattachment value. The reason for this rise in pressure is believed to be due to a quasi-isentropic compression occurring through a series of waves rather than a single shock. Similar pressure rises, only to a lesser degree, are noted for the 20° flap angles for unit Reynolds numbers from 2.65×10^6 to 4.3×10^6 per foot.

The measured separation flow-deflection angles and shock-wave angles, for wall to total temperature ratios of 0.14, 0.43, and 0.74 - which were taken from a schlieren study - indicate qualitative

agreement with the measured pressures and the theoretical calculations made using the Lees and Reeves' theory. The schlieren photographs, used for these measurements, are contained herein. The measured values of plateau pressure are, for the most part, slightly less than the separated layer oblique shock values and slightly more than the values predicted by the Lees and Reeves' theory (for plateau pressure).

The wall-temperature effects at wall to total temperature ratios of 0.14, 0.43, and 0.74 indicated the following:

(1) For a flap angle of 10° the wall-temperature effects, for $T_w/T_t = 0.43$ and 0.74, on the pressure rise to the plateau, were negligible for unit Reynolds numbers from 0.29×10^6 to 2.65×10^6 per foot, and agreed well with the theory of Lees and Reeves' for $T_w/T_t = 1.0$ and $T_w/T_t = 0.6$.

(2) For flap angles of 20° and 30° at unit Reynolds numbers of 0.29×10^6 per foot and 0.42×10^6 per foot the tests at $T_w/T_t = 0.15$ had the highest plateau pressure level, the $T_w/T_t = 0.74$ the next highest level, and the $T_w/T_t = 0.43$ the lowest level. The $T_w/T_t = 0.43$ data showed the closest agreement to the Lees and Reeves' theory for $T_w/T_t = 0.6$ and $T_w/T_t = 1.0$.

(3) For flap angles of 20° and 30°, at unit Reynolds numbers of 0.65×10^6 and 1.46×10^6 per foot, the plateau pressure, for all three wall-temperature ratios, was nearly the same and is in close agreement with the Lees and Reeves' theory for $T_w/T_t = 1.0$ and $T_w/T_t = 0.6$.

(4) For flap angles of 10°, 20°, and 30°, at unit Reynolds numbers of 2.65×10^{6} per foot and 4.3×10^{6} per foot, the effect of wall cooling tends to significantly reduce the extent of separation.

(5) For a unit Reynolds number range of 0.22×10^{6} per foot to 1.0×10^{6} per foot the point of separation, for a 20° flap, shows: (a) that the highly cooled wall $\left(T_w/T_t = 0.14\right)$ has the greatest extent of separation; (b) the hot wall $\left(T_w/T_t = 0.74\right)$ has the next greatest extent; and (c) the room-temperature wall $\left(T_w/T_t = 0.43\right)$ has the least extent of separation. These results were taken from a study of the schlieren photographs.

(6) For a unit Reynolds number from 1.0×10^{6} to 4.3×10^{6} per foot an increase in wall cooling markedly decreased the extent of separation and also reduced the level of the plateau pressure.

The viscous interaction theory of Bertram and Blackstock in reference 44 agreed well with the experimental flat-plate data for $T_w/T_t = 0.43$ and 0.74.

A correlation of the plateau pressure with the local Mach number and Reynolds number at the beginning of the interaction showed reasonable agreement with the theory of Hakkinen, Greber, and Trilling.

The effect of side plates on the model as compared to the results with no side plates showed: (1) a reduction in the three dimensionality of the flow in the separated region, (2) a slight increase in the plateau pressure level, and (3) a considerable increase in the

extent of separation. The variation of the extent of separation with a change in unit Reynolds number was the same for the condition with and without side plates.

XI. SUMMARY

An experimental investigation was made of the flow separation on a flat-plate model with a trailing-edge flap deflected at angles of 10°, 20°, and 30° relative to the plate surface. These tests were conducted at a nominal Mach number of 8 and a nominal unit Reynolds number (per foot) ranging from 0.22×10^{6} to 10.9×10^{6}. Pressure measurements and schlieren studies were made for wall to total temperature ratios of 0.14, 0.43, and 0.74. Surface oil-flow studies were conducted at a wall to total temperature ratio of 0.43. Local similarity boundary-layer calculations were made upstream of the interaction region. Properties of the interaction and separated flow region were calculated using the Lees and Reeves' shock-wave boundary-layer interaction theory. The two theories were joined at the beginning of the interaction region by matching their boundary-layer momentum thicknesses.

The results showed good agreement between the experimental and calculated pressures for adiabatic and room-temperature wall conditions. The oil-flow study showed the variation in the extent of separation, with a change in unit Reynolds number, for both laminar separation and transitional separation. The effect of wall cooling, for transitional separation, showed a reduction in the extent of separation. The peak pressure rise, on the flap, for conditions where the separated shock impinged on the flap, were as high as 58 percent above the inviscid flap pressure.

XII. ACKNOWLEDGMENTS

The author wishes to express his appreciation to the National Aeronautics and Space Administration for permitting material obtained from a research project conducted at the Langley Research Center to be used in this thesis.

The author also wishes to thank Dr. James B. Eades, Head of the Aerospace Engineering Department, for his assistance and patience while this thesis was being prepared.

Finally, the author wishes to express his gratitude to his wife, Kay, for her encouragement and understanding during the period of his residency at Virginia Polytechnic Institute and in the preparation of this thesis.

XIII. REFERENCES

1. Wuerer, J. E.; and Clayton, F. I.: Flow Separation in High Speed Flight, A Review of the State-of-the-Art. Douglas Aircraft Company, Inc., Report No. SM-46429, April 1965.

2. Kaufman, L. G.; Hartofilis, S. A.; Evans, W. J.; Omas, R. A.; Meckler, L. H.; and Weiss, D.: A Review of Hypersonic Flow Separation and Control Characteristics. Gruman Aircraft Engineering Corp., Report No. ASD TDR 62-168, March 1962.

3. Nielsen, Jack N.; and Goodwin, Frederick K.: Investigation of Hypersonic Flow Separation and Its Effect on Aerodynamic Control Characteristics. VIDYA Report No. 63, January 1962.

4. Lees, Lester; and Reeves, Barry L.: Supersonic Separated and Reattaching Laminar Flows: I. General Theory and Application to Adiabatic Boundary Layer-Shock Wave Interactions, AIAA, Vol. 2, No. 11, Nov. 1964, pp. 1907-1920.

5. Putnam, Lawrence E.: Investigation of Effects of Ramp Span and Deflection Angle on Laminar Boundary-Layer Separation at Mach 10.03. NASA TN D-2833, May 1965.

6. Kaufman, L. G.; Meckley, L. H.; Hartofilis, S. A.; and Weiss, D.: An Investigation of Hypersonic Flow Separation and Control Characteristics. Grumman Aircraft Engineering Corporation, Report No. AFFDL-TR-64-174, January 1965.

7. Gray, J. D.: Laminar Boundary-Layer Separation on Flared Bodies at Supersonic and Hypersonic Speeds. Von Karman Gas Dynamics Facility, ARO, Inc., Report No. AEDC-TDR-64-277, January 1965.

8. Holden, Michael: Separated Flow Studies at Hypersonic Speeds, Part II, Two-Dimensional Wedge Separated Flow Studies. Cornell Aeronautical Laboratory, Inc., CAL Report No. AF-1285-A-13 (2), December 1964.

9. Holden, Michael: Separated Flow Studies at Hypersonic Speeds, Part I, Separated Flows over Axisymetric Spiked Bodies. Cornell Aeronautical Laboratory, Inc., CAL Report No. AF-1285-A-13 (1), December 1964.

10. Ginoux, J. J.: Laminar Separation in Supersonic Flow. Von Karman Institute for Fluid Dynamics, Report No. AF EOAR 64-7, October 1964.

11. Sterrett, James R.; and Holloway, Paul F.: On the Effect of Transition on Parameters Within a Separation Region at Hypersonic Speeds - With Emphasis on Heat Transfer. Presented at the ASME Hydraulic Division Conference Symposium on Fully Separated Flow, Philadelphia, Pennsylvania, May 18-21, 1964.

12. Pate, S. R.: Investigation of Flow Separation on a Two-Dimensional Flat Plate Having a Variable-Span Trailing-Edge Flap at M = 3 and 5. Von Karman Gas Dynamics Facility, ARO, Inc., Report No. AEDC-TDR-64-14, March 1964.

13. Burchfield, C. G.; Hube, F. K.; and Burdette, J. E.: An Experimental Heat-Transfer Investigation in Regions of Flow Separation at Mach Number 8. Von Karman Gas Dynamics Facility, ARO, Inc., Report No. AEDC-TDR-64-30, February 1964.

14. Pressure and Heat Transfer Measurements for Hypersonic Flows over Expansion Corners and Ahead of Ramps. Gruman Aircraft Engineering Corporation, Report No. RSD-TDR-63-679, December 1963.

15. Naer, A. L.: An Investigation of Separated Flows on Two-Dimensional Models at Mach Numbers 5 and 8. Von Karman Gas Dynamics Facility. ARO, Inc., Report No. AEDC-TDR-63-200, October 1963.

16. Miller, D. S.; Hijman, R.; and Childs, M. E.: Mach 8 to 22 Studies of Flow Separations Due to Deflected Control Surfaces. AIAA Summer Meeting, Los Angeles, California, June 17-20, 1963, Preprint 63-173.

17. Bogdonoff, S. S.; and Vas I. E.: Some Experiments on Hypersonic Separated Flows. ARS Journal, Vol. 32, No. 10, October 1962.

18. Sterrett, James R.; and Emery, James C.: Experimental Separation Studies for Two-Dimensional Wedges and Curved Surfaces at Mach Numbers of 4.8 to 6.2. NASA TN D-1014, February 1962.

19. Eminton, E.: Simple Theoretical and Experimental Studies of the Flow Through a Three-Shock System in a Corner. Royal Aircraft Establishment, (Farnborough), Report No. AERO 2784, September 1961.

20. Sterrett, James R.; and Emery, James C.: Extension of Boundary Layer Separation Criteria to a Mach Number of 6.5 by Utilizing Flat Plates with Forward-Facing Steps. NASA TN D-618, December 1960

21. Chapman, D. R.; Kuehn, D. M.; and Larson, H. K.: Investigation of Separated Flows in Supersonic and Subsonic Streams with Emphasis on the Effect of Transition. National Advisory Committee for Aeronautics, Report 1356, 1958.

22. Becker, John V.; and Korycinski, Peter F.: Heat Transfer and Pressure Distribution at a Mach Number of 6.8 on Bodies with Conical Flares and Extensive Flow Separation. NASA TN D-1260, 1962.

23. Love, Eugene S.: Pressure Rise Associated with Shock-Induced Boundary Layer Separation. NACA TN 3601, 1955.

24. Townsend, James C.: Effect of Leading Edge Bluntness and Deflection Angle on Laminar Boundary Layer Separation in Hypersonic Flow. NASA TN D-3290, 1966.

25. Beckwith, Ivan E.; and Cohen, Nathaniel B.: Application of Similar Solutions to Calculations of Laminar Heat Transfer on Bodies with Yaw and Large Pressure Gradient in High Speed Flow. NASA TN D-625, 1961.

26. Stainback, P. Calvin: Heat Transfer Measurements at a Mach Number of 8 in the Vicinity of a 90° Interior Corner Alined with the Free-Stream Velocity. NASA TN D-2417, 1964.

27. Schaefer, William T., Jr.: Characteristics of Major Active Wind Tunnels at the Langley Research Center. NASA TM X-1130, 1965.

28. Prandtl, L.: Note on the Calculations of Boundary Layers. NACA TM 959, 1940.

29. Chapman, Dean R.: Laminar Mixing of a Compressible Fluid. NACA Report 958, 1950.

30. Gadd, G. E.: Boundary Layer Separation in the Presence of Heat Transfer. AGARD Report No. 280, April 1960.

31. Curle, N.: The Effects of Heat Transfer on Laminar-Boundary-Layer Separation in Supersonic Flow. The Aeronautical Quarterly, Vol. XII, pp. 309-336, November 1961.

32. Savage, S. B.: The Effect of Heat Transfer on Separation of Laminar Compressible Boundary Layers. CALCIT Separated Flows Project, Technical Report No. 2, June 1, 1962.

33. Crocco, L.; and Lees, L.: A Mixing Theory for the Interaction Between Dissipative Flows and Nearly Isentropic Streams. Journal of the Aerospace Sciences, Vol. 19, No. 10, pp. 649-676, Oct. 1952.

34. Glick, Herbert S.: Modified Crocco-Lees Mixing Theory for Supersonic Separated and Reattaching Flows. GALCIT Hypersonic Research Project Memorandum No. 53, May 2, 1960.

35. Bray, K. N. C.; Gadd, G. E.; and Woodger, M.: Some Calculations by the Crocco-Lees and Other Methods of Interactions Between Shock Waves and Laminar Boundary Layers, Including Effects of Heat Transfer and Suction. Aeronautical Research Council Report 21,834, FM 2937, April 1960.

36. Tani, Itiro: On the Approximate Solution of the Laminar Boundary Layer Equations. Journal of the Aerospace Sciences, Vol. 21, No. 7, pp. 487-504, July 1954.

37. Wieghardt, K.: Uber einen Energiesatz Zur Berechnung Laminarer Grenzschicten. Ingenieur-Archiv, Vol. 16, Nos. 3 and 4, pp. 231-242, 1948.

38. Walz, A.: Anwendung des Energiesatzes Von Weighardt auf einparametrige Gesch windig Keitsprofile in laminaren Grenzschichten. Ingenieur-Archiv, Vol. 16, pp. 243-248, 1948.

39. Poots, G.: A Solution of the Compressible Laminar Boundary Layer Equation with Heat Transfer and Adverse Pressure Gradient. Quarterly Journal of Mechanics and Applied Mathematics, Vol. 13, 1960.

40. Abbott, Douglas E.; Holt, Maurice; and Nielsen, Jack N.: Investigation of Hypersonic Flow Separation and its Effect on Aerodynamic Control Characteristics, ASD-TDR-62-963, Nov. 1962.

41. Cohen, Clarence B.; and Reshotko, Eli: Similar Solutions for the Compressible Laminar Boundary Layer with Heat Transfer and Pressure Gradient. NACA Report 1293, 1956.

42. Stewartson, K.: Further Solutions of the Falkner-Skan Equation. Proceedings of the Cambridge Philosophical Society, Vol. 50, part 3, pp. 454-465, July 1964.

43. Holden, M. S.: An Analytical Study of Separated Flows Induced by Shock Wave-Boundary Layer Interaction. CAL Report No. AI-1972-A-3, Dec. 1965.

44. Bertram, Mitchel H.; and Blackstock, Thomas A.: Some Simple Solutions to the Problem of Predicting Boundary-Layer Self-Induced Pressures. NASA TN D-798, 1961.

45. Dennard, John S.; and Spencer, Patricia B.: Ideal-Gas Tables for Oblique-Shock Flow Parameters in Air at Mach Numbers from 1.05 to 12.0. NASA TN D-2221, 1964.

46. Schaefer, John W.; and Ferguson, Harold: Investigation of Separation and the Associated Heat Transfer and Pressure Distributions on Cone-Cylinder-Flare Configurations. ARS paper, Space Flight Report to the Nation. New York, Oct. 9-15, 1961.

47. Gadd, G. E.: A Theoretical Investigation of the Effects of Mach Number, Reynolds Number, Wall Temperature and Surface Curvature on Laminar Separation in Supersonic Flow. Aeronautical Research Council, FM 2415, June 1956.

48. Gadd, G. E.: An Experimental Investigation of Heat Transfer Effects on Boundary Layer Separation in Supersonic Flow. Aeronautical Research Council. FM 2395, April 1956.

49. Hakkinen, R. J.; Greber, I.; Trilling and Abarbanel, S. S.: The Interaction of an Oblique Shock Wave with a Laminar Boundary Layer, NASA Memo 2-18-59-W, 1959.

50. Erdos, John; and Pallone, Adrian: Shock-Boundary Layer Interaction and Flow Separation. RAD TR-61-23, 1961.

XIV. BIBLIOGRAPHY

1. Kutscherenter, Paul H. Jr.: Investigation of Hypersonic Inlet Boundary Layer. Interaction Technical Report AFFDL-TR-65-36 Air Force Flight Dynamics Laboratory, March 1965.

2. Sanders, F.; and Crabtree, L. F.: A Preliminary Study of Large Regions of Separated Flow In a Compression Corner. TN No. Aero. 2751.

3. Chapman, Dean R.: Laminar Mixing of a Compressible Fluid. NACA Rept. 950, 1950.

4. Bray, K.N.C.; Gadd, G. E.; and Woodger, M.: Some Calculations by the Crocco-Lees and Other Methods of Interactions Between Shock-Waves and Laminar Boundary Layers. A.R.C. No. 21834, April 1960.

5. Chuan, Raymond L.: An Investigation of Shock Wave Boundary Layer Interaction. USCEC Report 40-201, August 1955.

6. Cheng, Sin-I: Laminar Separated Flow Within Rejoining or Reattaching Boundary Layers. AFOSR - 64-1596, July 1964.

7. Crocco, Luigi; and Probstien, Ronald F.: The Peak Pressure Rise Across An Oblique Shock Emerging From a Turbulent Boundary Layer Over a Plane Surface. Report 254, Princeton University Gas Dynamics Laboratory, March 1954.

8. Mueller, T. J.; Korst, H. H.; and Chew, W. L.: On the Separation, Reattachment and Redevelopment of Incompressible Turbulent Shear Flow. ASME Journal of Basic Engineering, June 1964.

9. Savage, Stuart B.: The Effect of Heat Transfer on Separation of Laminar Compressible Boundary Layers. Separated Flows Project, TR No. 2 (GALCIT) June 1, 1962.

10. Seban, R. A.: Heat Transfer and Flow with Separated and Reattached Boundary Layers as Produced by Surface Irregularities. WADC TR-56-217, May 15, 1965.

11. Thwaites, B.: Approximate Calculation of the Laminar Boundary Layer. The Aeronautical Quarterly, Vol. I, November 1949.

12. Crocco, Luigi; and Lees, Lester: A Mixing Theory for the Interaction Between Dissipative Flows and Nearly Isentropic Streams. J.A.S. Vol. 19 No. 10, October 1952, pp. 649-676.

13. Smith, A.M.O.: Rapid Laminar Boundary-Layer Calculations by Piecewise Application of Similar Solutions. J.A.S. Vol. 23, No. 10, Oct. 1956, pp. 901-912.

14. Massey, B. S.; and Clayton, B. R.: Laminar Boundary Layers and Their Separation From Curved Surfaces. A.S.M.E. Paper No. 64-WA/FE-5, January 1965.

15. Kistler, A. L.: Fluctuating Wall Pressure Under a Separated Supersonic Flow. J.P:L. TR No. 32-505, March 1964.

16. Liepmann, Hans Wolfgang: The Interaction Between Boundary Layer and Shock Waves in Transonic Flow. J.A.S. Vol. 13, No. 12, Dec. 1946, pp. 623-638.

17. Tani, Itiro: On the Approximate Solution of the Laminar Boundary Layer Equations. J.A.S. Vol. 21, No. 7, July 1954, pp. 487-504.

18. Honda, M.: A Theoretical Investigation of the Interaction Between Shock Waves and Boundary Layers. J.A.S. Vol. 25, No. 11, Nov. 1958, pp. 667-678.

19. Crocco, Luigi: Considerations on the Shock-Boundary Layer Interaction. Presented at Conference of High-Speed Aeronautics. Jan. 1955.

20. Illingworth, C. R.: The Effect of Heat Transfer on the Separation a Compressible Laminar Boundary Layer. Quarterly Journal of Mechanics and Applied Mathematics. Vol. VII, Pt. 1 (1954).

21. Ackert, J.; Feldmann, F.; and Rott, N.: Investigation of Compression Shocks and Boundary Layers in Gases Moving at High Speed. NACA TM 1113, January 1947.

22. Oswatitsch, K.; and Wieghart, K.: Theoretical Analysis of Stationary Potential Flows and Boundary Layers at High Speed. NACA TM 1189, April 1948.

23. Romeo, David J.; and Sterrett, James R.: Aerodynamic Interaction Effects Ahead of a Sonic Jet Exhausting Perpendicularly from a Flat Plate Into a Mach Number 6 Free Stream. NASA TN-D 743, April 1961.

24. Pinckney, S. Z.: Boundary-Layer Changes Across An Incident Reflecting Shock. AIAA-ASME Hypersonic Ramjet Conference, April 23-25, 1963.

25. Reshotko, Eli; and Tucker, Maurice: Effect of a Discontinuity on Turbulent Boundary-Layer Thickness Parameters with Application to Shock-Induced Separation, NACA TN 3454, May 1955.

26. Temple, G.: Note on the Conditions at a Separation Point. A.R.C. FM 2583, Sept. 10, 1957.

27. Lochtenberg, B. H.: Some Studies of Transition in a Laminar Boundary Layer After Separation. A.R.C. FM 2319, October 29, 1955.

28. Kelley, Lawrence R.: Wind Tunnel Tests at Supersonic Mach Numbers to Determine Heat-Transfer Coefficients in the Shock Wave Boundary Layer Interaction Region on a Plane Surface. USCEC Report 65-41, December 27, 1963.

29. Nicoll, Kenneth M.: A Study of Laminar Hypersonic Cavity Flows. AIAA preprint No. 64-47, AIAA Meeting Jan. 20-22, 1964.

30. Cheng, Sin-I; and Bray, K.N.C.: On the Mixing Theory of Crocco and Lees and its Application to the Interaction of Shock Wave and Laminar Boundary Layer

Part I Generals and Formulation

Part II Results and Discussion

Princeton Gas Dynamics Laboratory, Report No. 376, November 1957.

31. Lam, S. H.: Heat Transfer Through a Region of Closed Streamline. Princeton University Report 469, May 1959.

32. Maskell, E. C.: Flow Separation in Three Dimensions. R.A.E. Report No. Aero 2565, November 1955.

33. Picken, J.: Free-Flight Measurements of Pressure and Heat Transfer in Regions of Separated and Reattached Flow at Mach Numbers up to 4. A.R.C., CP No. 706, September 1960.

34. Greber, Isaac: Interaction of Oblique Shock Waves With Laminar Boundary Layers. M.I.T. Technical Report 59-2, April 28, 1959.

35. Curle, N.: Laminar Boundary Layer Equations for Flows Having a Stagnation Point and Separation. A.R.C., R and M. No. 3164, December 1958.

36. Bray, K. N. C.: Some Notes on Shock-Wave Boundary-Layer Interactions, and on the Effect of Suction on the Separation of Laminar Boundary Layers. A.R.C. Technical Report C.P. No. 332, August 24, 1956.

37. Gadd, G. E.: Interactions Between Shock Waves and Boundary Layer Presented at Conference of Boundary Layer Research, August 26-29, 1957.

38. Stratford, B. S.: Flow in the Laminar Boundary Layer near Separation. A.R.C. R and M No. 3002, November 1954.

39. Gadd, G. E.: The Effects of Convex Surface Curvature on Boundary Layer Separation in Supersonic Flow. A.R.C. Technical Report C.P. No. 289, November 26, 1955.

40. Korst, H. H.: Dynamics and Thermodynamics of Separated Flows. Presented at Symposium of Rutgers Engineering Centennial, 1965.

XV. VITA

Charles Borden Johnson was born on June 17, 1931, in Boston, Massachusetts. He received his elementary education at Lawrence Elementary School, Brookline, Massachusetts, and secondary education at Hanover, New Hampshire High School, graduating from high school in June 1949. In September 1949 he enrolled in the University of North Carolina and received a Bachelor of Arts in Political Science degree in June 1953. Following graduation he served three years in the U.S. Navy and was released from active duty in May 1956. In July 1956 he enrolled in North Carolina State College and received a Bachelor of Science degree in Mechanical Engineering with an Aeronautical Option in June 1959. Following graduation he came to work at the Langley Research Center of the National Aeronautics and Space Administration in the Aero Physics Division. In September 1962 he enrolled in the Aerospace Engineering Department at Virginia Polytechnic Institute as a graduate student. Currently he is in the Hypersonic Fluid Mechanics Section at the Langley Research Center and is completing his degree requirements for the Master of Science degree in Aerospace Engineering.

Charles B Johnson

XVI. APPENDIXES

APPENDIX A

LEES AND REEVES' SOLUTION FOR THE LAMINAR SEPARATED BOUNDARY LAYER

The Lees and Reeves' theory (ref. 4) gives the solution for the laminar boundary layer in which a pressure disturbance is propagated upstream through a supersonic flow. A pressure disturbance may be generated by a shock wave impinging on the boundary layer or it may be caused by a trailing-edge flap - the Lees and Reeves' theory may be applied to either of the two types of disturbances. The theory, and its calculations as used in this thesis, applies at the beginning of the interaction region and is used to the point of the shock impingement (the hinge line) for the cases where the temperature ratio is $T_w/T_t = 0.6$ and $T_w/T_t = 1.0$. The flow field on the flap was determined by this theory for a few cases but it was found that the extent of the calculated region over the flap was considerably longer than the actual size of the flap on the model.

The Lees and Reeves' method requires a solution of the first moment of momentum, the zeroth moment of momentum, and the conservation of mass equations coupled with an inviscid streamline and Prandtl-Meyer solution. The method gives the solution for the boundary layer and the flow external to the boundary layer within the framework of a single parameter family of velocity profiles. This one parameter determines the velocity and enthalpy profile for

specified regions of attached and separated flows; yet it is not directly related to the local static pressure gradient. The local pressure gradient is determined from the local inviscid flow inclination and the Prandtl-Meyer solution.

For the $T_w/T_t = 1.0$ conditions the Stewartson (ref. 42) and the Cohen and Reshotko (ref. 41) boundary-layer solutions were used to evaluate the integral parameters used in the Lees and Reeves' solution. For the case with heat transfer, $T_w/T_t = 0.6$, the boundary-layer profiles were calculated from the local similarity solutions with $Pr = 1.0$, C_p = constant and $\rho\mu$ = constant. These boundary-layer solutions were used to calculate the integral parameters (see appendix B). These integral parameters were then curve fitted (by a polynominal expression) as a function of the single parameter, a, used to describe the entire family of velocity profiles for both attached and separated flows. The fitted curves, of the integral parameters, for $T_w/T_t = 0.6$ are tabulated in appendix B. The local similarity solutions reduce to a solution which is the same as that of Cohen and Reshotko (ref. 42) when a Prandtl number of unity and a constant heat capacity are used.

The Lees and Reeves' method of calculation starts at the point of separation and moves upstream until a flat-plate (Blasius type) solution is reached at the upstream "end" of the interaction. The value of local Mach number and unit Reynolds number are fixed at the point of separation and the value of transformed displacement thickness at the point of separation is iterated for until the proper

upstream solution is found at the beginning of the interaction region. The conditions needed to satisfy the two-point boundary-value problem are (1) the rate of change with respect to the transformed $\bar{X}$ distance of the local Mach number and (2) the shape parameter approach zero as the parameter describing the family of velocity profiles approaches the zero pressure gradient value for attached flow. After the correct value of the displacement thickness, at the point of separation, is found the solution moves downstream into the separated flow region. The basic equations used in the method are noted below. Equations A 1 to A 4 were integrated by a fourth-order Runge-Kutta integration procedure which extrapolates to a zero interval size as a correction factor. All equations were integrated using δ_t^* as the independent variable; they are

$$\frac{da}{d\delta_t^*} = \dot{a} = \left(\frac{1}{\delta_t^*}\right)\left(\frac{N2}{N3}\right)\left(\frac{1}{\frac{dH}{da}}\right), \tag{A-1}$$

$$\frac{dM_e}{d\delta_t^*} = \dot{M}_e = \left(\frac{N1}{N3}\right)\left(\frac{M_e}{\delta_t^*}\right), \tag{A-2}$$

$$\frac{d\bar{X}}{d\delta_t^*} = \dot{\bar{X}} = \left(\frac{a_\infty}{\nu_\infty}\right)\left(\frac{M_e \delta_t^*}{R}\right)\left[\delta_t^*\left(\frac{dH}{da}\right)\left(\frac{dJ}{dH}\right)\dot{a} + J + \left(3J + 2S_w T^*\right)\left(\frac{\delta_t^*}{M_e}\right)\dot{M}_e\right], \tag{A-3}$$

and

$$\frac{dX}{d\delta_t^*} = \dot{X} = \left[\frac{(1 + m_e)}{(1 + m_\infty)}\right]^{\frac{3\gamma-1}{2(\gamma-1)}} \left(\frac{a_\infty}{\nu_\infty}\right) \left(\frac{M_e \delta_t^*}{R}\right) \left[\delta_t^* \left(\frac{dH}{da}\right) \left(\frac{dJ}{dH}\right) \dot{a} + J\right.$$

$$\left. + \left(3J + 2S_w T^*\right) \left(\frac{\delta_t^*}{M_e}\right) \dot{M}_e\right]; \qquad \text{(A-4)}$$

where

$$\frac{a_\infty}{\nu_\infty} = \frac{1.812 \times 10^8 \left(T_\infty + 201.6\right) P_\infty}{T_\infty^2}, \qquad \text{(A-5)}$$

$$m_e = \frac{\gamma - 1}{2} M_e^2, \qquad \text{(A-6)}$$

$$\tilde{R}_{e_{\delta_t^*}} = M_e \delta_t^* \left(1.812 \times 10^8\right) \left(T_\infty + 201.6\right) \frac{P_\infty}{T_\infty 2}, \qquad \text{(A-7)}$$

$$\nu\left(M_e\right) = \sqrt{\frac{\gamma + 1}{\gamma - 1}} \tan^{-1}\left\{\sqrt{\frac{\gamma - 1}{\gamma + 1}} \sqrt{M_e^2 - 1}\right\} - \tan^{-1}\left(\sqrt{M_e^2 - 1}\right) \qquad \text{(A-8)}$$

$$\nu\left(M_\infty\right) = \sqrt{\frac{\gamma + 1}{\gamma - 1}} \tan^{-1}\left\{\sqrt{\frac{\gamma - 1}{\gamma + 1}} \sqrt{M_\infty^2 - 1}\right\} - \tan^{-1}\left(\sqrt{M_\infty^2 - 1}\right) \qquad \text{(A-9)}$$

$$\text{Tan } \textcircled{H} \cong \textcircled{H}, \qquad \text{(A-10)}$$

$$\textcircled{H} = \nu\left(M_\infty\right) - \nu\left(M_e\right), \qquad \text{(A-11)}$$

$$h = - \tilde{R}_{e_{\delta_t^*}} \frac{(1 + m_e) \tan (H)}{m_e \left(1 + m_\infty\right)}, \qquad \text{(A-12)}$$

$$f = 2H + \left[\frac{(3\gamma - 1)}{(\gamma - 1)}\right] + \left[\frac{(\gamma + 1)}{(\gamma - 1)}\right]\left[\frac{m_e}{1 + m_e}\right] H + \left\{\frac{\left(M_e^2 - 1\right)}{\left(m_e\left(1 + m_e\right)\right)}\right\} z, \quad \text{(A-13)}$$

$$D = \left[\frac{(1 + m_e)}{m_e}\right] \left[\left(3J + 2S_w T^*\right) - (2H + 1)\left(\frac{dJ}{dH}\right)\right]$$

$$+ \left[(2H + 1) - f\right] \left[J - H\left(\frac{dJ}{dH}\right)\right], \quad \text{(A-14)}$$

$$N_1 = \left[\frac{(1 + m_e)}{m_e}\right]\left[R - P\left(\frac{dJ}{dH}\right)\right] + (P + h)\left[J - H\left(\frac{dJ}{dH}\right)\right], \quad \text{(A-15)}$$

$$N_2 = \left[\frac{(1 + m_e)}{m_e}\right]\left[\left(3J + 2S_w T^*\right) P - R(2H + 1)\right]$$

$$+ (P + h) \left[H\left(3J + 2S_w T^*\right) - fJ\right] + (RH + Jh)$$

$$\times \left[f - (2H + 1)\right], \quad \text{(A-16)}$$

and

$$N_3 = (P + h)\left[f\left(\frac{dJ}{dH}\right) - \left(3J + 2S_w T^*\right)\right] - \left[f - (2H + 1)\right]\left[R + h\left(\frac{dJ}{dH}\right)\right]. \quad \text{(A-17)}$$

These additional equations are used in the solution:

$$\frac{P_e}{P_o} = \left[\frac{\left(1 + m_{e_{x_o}}\right)}{\left(1 + m_e\right)}\right]^{\gamma/\gamma-1} \qquad \text{(A-18)}$$

$$\delta^* = \delta_t^* \left[\frac{\left(1 + m_e\right)}{\left(1 + m_\infty\right)}\right]^{\gamma+1/2(\gamma-1)} \left[\left(1 + m_e\right) + m_e H\right], \qquad \text{(A-19)}$$

and

$$\theta = \left\{\left[\frac{1 + m_e}{1 + m_\infty}\right]^{\frac{\gamma + 1}{2(\gamma - 1)}}\right\} \theta_i. \qquad \text{(A-20)}$$

APPENDIX B

LEES AND REEVES' BOUNDARY-LAYER PARAMETERS FOR $T_w/T_t = 0.6$

The curve fit parameters, for the boundary-layer integral parameters, for $T_w/T_t = 0.6$, that were used in the Lees and Reeves' calculation are listed in tables 1-A and 1-B for attached and separated flow parameters, respectively. These parameters were calculated from local similarity solutions using a Prandtl number of unity and constant heat capacity. The integral parameters, in the notation of reference 2, are:

$$H = \frac{\int_o^\delta f' \, (1 - f') \, d\eta}{\int_o^\delta (\zeta - f') \, d\eta} \tag{B-1}$$

$$J = \frac{\int_o^\delta f' \, (1 - f'^2) \, d\eta}{\int_o^\delta (\zeta - f') \, d\eta} \tag{B-2}$$

$$P = f''_w \int_o^\delta (\zeta - f') \, d\eta \tag{B-3}$$

$$R = 2 \int_o^\delta (\zeta - f') \, d\eta \int_o^\delta (f'')^2 \, d\eta \tag{B-4}$$

$$T^* = \frac{\int_0^\delta f' \, (\zeta - 1) \, d\eta}{\left(t_w - 1\right) \int_0^\delta (\zeta - f') \, d\eta} \tag{B-5}$$

and

$$Z = \frac{f\big|_\delta}{\int_0^\delta (\zeta - f') \, d\eta} \tag{B-6}$$

The value of f', at the edge of the boundary layer, was taken as 0.9995 for all calculations. The parameters (B-1) to (B-6) were fitted to various order polynomials by the method of least squares, as a function of the "a" parameter defined by the Lees and Reeves' method. The Parameters H, J, P, R, T*, and Z, listed in tables 1-A and 1-B, are defined in (B-1) to (B-6) (above) while ζ'_w and m_β are defined in appendix C.

The polynomials, listed in tables 1-A and 1-B, occur in the general form

$$H = A + Ba + Ca^2 + Da^3 + Ea^4 + Fa^5 + Ga^6 + Ha^7$$

and vary from 4th order for the attached flow parameter to as high as 7th order for separated flow.

TABLE I-A COEFFICIENTS FOR ATTACHED FLOW (T_w/T_t = .6)

Parameter	A	B	C	D	E
H	+.3321009	+.13986596	+.01179970	-.00946576	+.00275081
J	+.50348534	+.19925458	+.02442816	+.00089497	-.00135237
R	+.9388926	-.41635211	+.19676828	-.06663378	+.01160929
P (If a > 0.4)*	+.00432494	+.28136774	-.04773970	-.01147897	+.00336312
Z	+1.894155	+.79107769	+.18536477	-.00701481	+.007183026
T*	+.17239089	+.13440415	+.01340911	+.01577639	-.00074312
ζ'_w	+.12409628	+.05559569	-.03955804	+.02479668	-.00555449
m_β	-.1094301	-.01730765	+.05114864	+.02927415	+.01006094

* If $0 \leq a \leq .4$
  $P = .2715\,a$

TABLE I-B COEFFICIENTS FOR SEPARATED FLOW (T_w/T_t = .6)

Parameter	A	B	C	D	E	F	G	H
H	+.3318532	-.52778371	+.2626242	-3.0420035	+4.3360826			
J	+.50378811	-.99282899	+5.100377	-52.405373	+251.93463	-630.63668	+788.67751	-384.52197
R(If a > .06)*	+.92651705	+3.5312703	-48.027304	+502.05092	-2393.2702	+6017.3521	-7518.2889	+3648.4459
P(If a > .05)**	-.00302374	-.5727471	-7.2003253	+53.081567	-263.80331	+669.6665	-745.74645	+286.17898
Z	+1.8961545	-2.5925828	-6.8986577	+55.663569	-186.92544	+281.81194	-155.92	
T*	+.17241606	-.40731561	-.11445041	+.8055802	-1.1635996	+1.1703974		
ζ'_w(If a > .05)†	+.12554626	-.16814151	+1.4798979	-19.391634	+105.05788	-293.36703	+401.23095	-210.28584
m_β	-.10887434	-.10113126	+2.5761168	-17.154012	+59.001127	-89.996992	+48.966367	

* If $(0 \leq a \leq .06)$, $R = 0.9388926 + 1.806118a$
** If $(0 \leq a \leq .05)$, $P = -.889a$
† If $(0 \leq a \leq .05)$, $\zeta'_w = .12409628 + .1022052a$

APPENDIX C

HEAT TRANSFER IN THE SEPARATED REGION

The Lees and Reeves' method has been extended, to obtain heat transfer, by using the slope of the enthalpy profile at the wall (ζ'_w) - corresponding to a given velocity and enthalpy profile which are defined in terms of the single parameter "a". The enthalpy and velocity profiles were calculated from local similarity solutions for an $T_w/T_t = 0.6$, $Pr = 1$, $\rho\mu$, and C_p = constant. A polynomial for ζ'_w as a function of the single parameter "a" is given in appendix B for both separated and attached flows.

The heat-transfer expression is derived from the basic definition of the heat transfer through a boundary layer to a wall; that is,

$$q_w = K_w \left(\frac{\partial T}{\partial y} \right)_w \tag{C-1}$$

Then, by using the Stewartson transformation,

$$d\bar{X} = \frac{P_e \, a_e}{P_\infty \, a_\infty} dx, \quad d\bar{Y} = \frac{a_e \, \rho}{a_\infty \, \rho_\infty} dy \tag{C-2}$$

with the definition of the enthalpy function

$$S_w = \frac{\left(h_t\right)_w}{\left(h_t\right)_\infty} - 1 \tag{C-3}$$

and a longitudinal velocity description of

$$\bar{u} = \frac{a_\infty}{a_e} u \tag{C-4}$$

along with the definition

$$\eta = \underline{Y}\sqrt{\frac{m+1}{2}\frac{\overline{u}_e}{\nu_o \underline{X}}} \tag{C-5}$$

where

$$m = \frac{\beta}{2-\beta}$$

results in the heat-transfer expression

$$q_w = \frac{K_w P_e}{\rho_\infty R}\sqrt{\frac{m+1}{2}\, u_e\left(\frac{T_e}{T_\infty}\right)^{1/2}\frac{\rho_t}{\mu_t}\frac{1}{\underline{X}}}\left(\frac{\zeta'_w}{S_w+1}\right) \tag{C-6}$$

The parameters, ζ'_w and m, which are substituted into equation (C-6), are plotted in figures 38 and 39 as a function of the Lees and Reeves' parameter "a". The transformed upstream flow (fig. 40) was used to join the upstream $\underline{X}$ history with the value of $\overline{X}$ from the Lees and Reeves' solution. The value of $\underline{X}$, from figure 40, was selected at the X/L position corresponding to the beginning of the interaction region, obtained from figure 7 for a given flap angle and unit Reynolds number. The transformed value of $\underline{X}$ at the beginning of the interaction region was added to the calculated value of $\overline{X}$ from the Lees and Reeves' solution at each point of calculation. The sum of these two values (of $\underline{X}$) was then used as the value of $\overline{X}$ in equation (C-6).

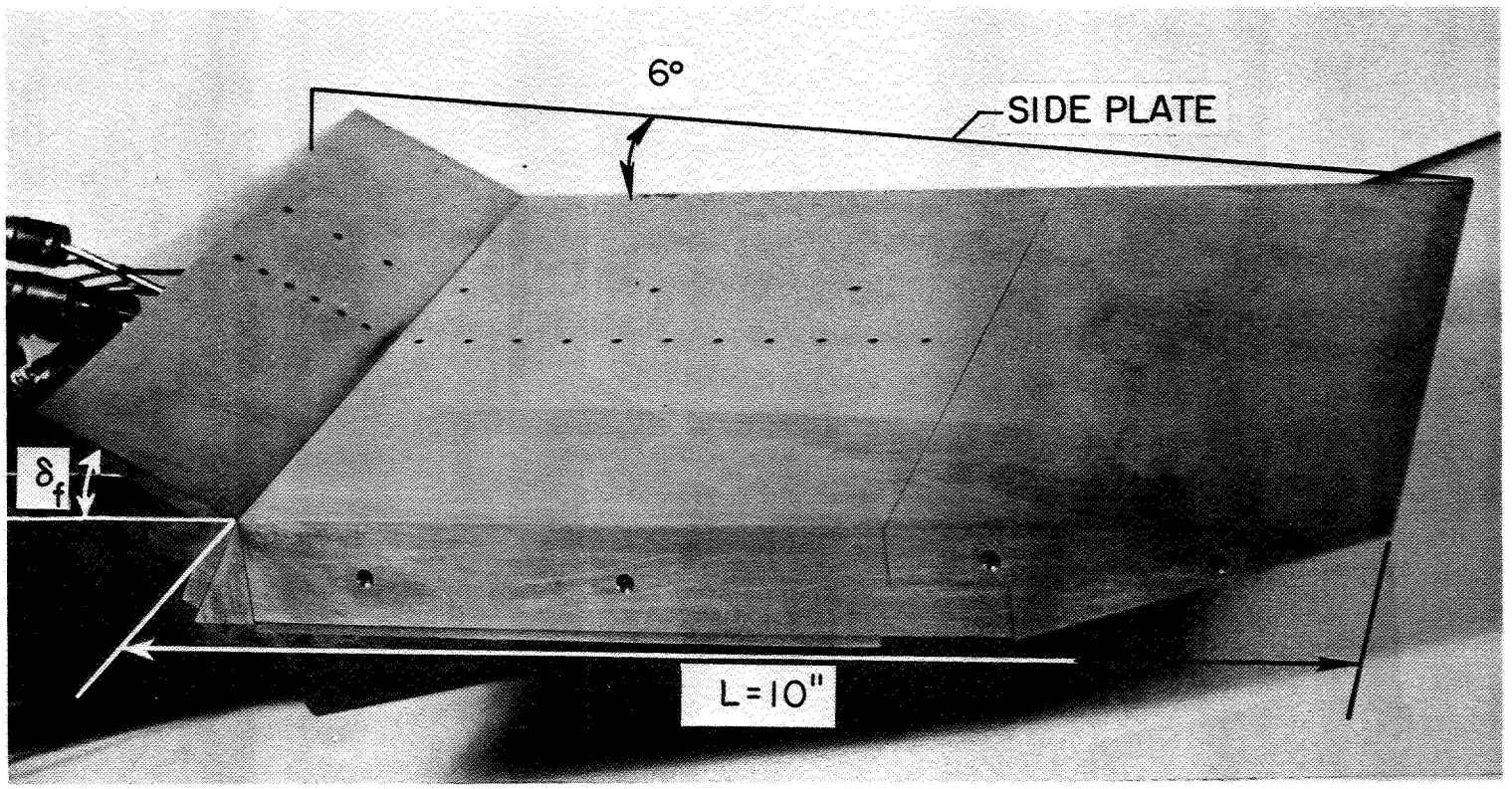

Figure 1.- Photograph of pressure model.

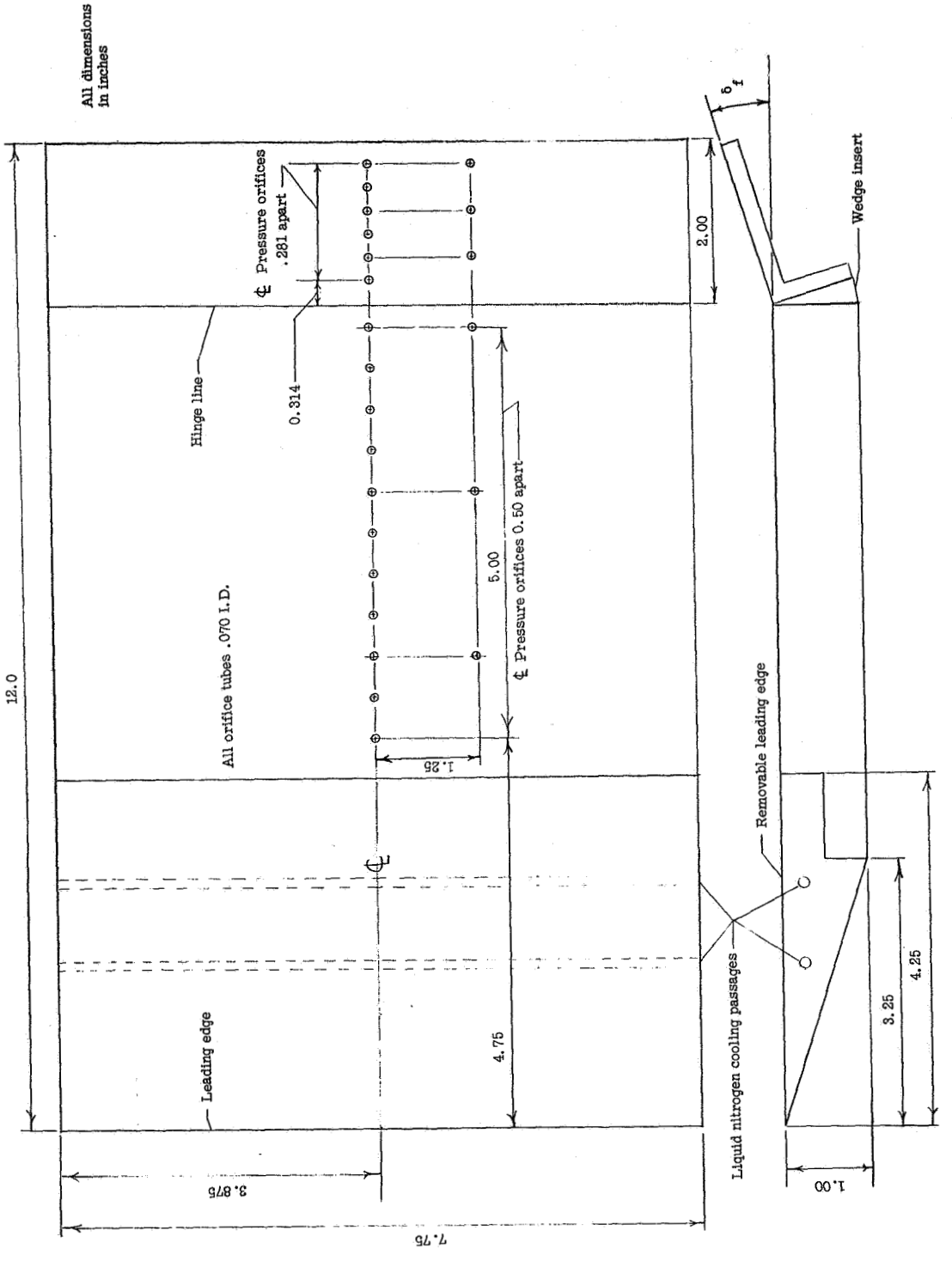

Figure 2.- Schematic of the pressure model.

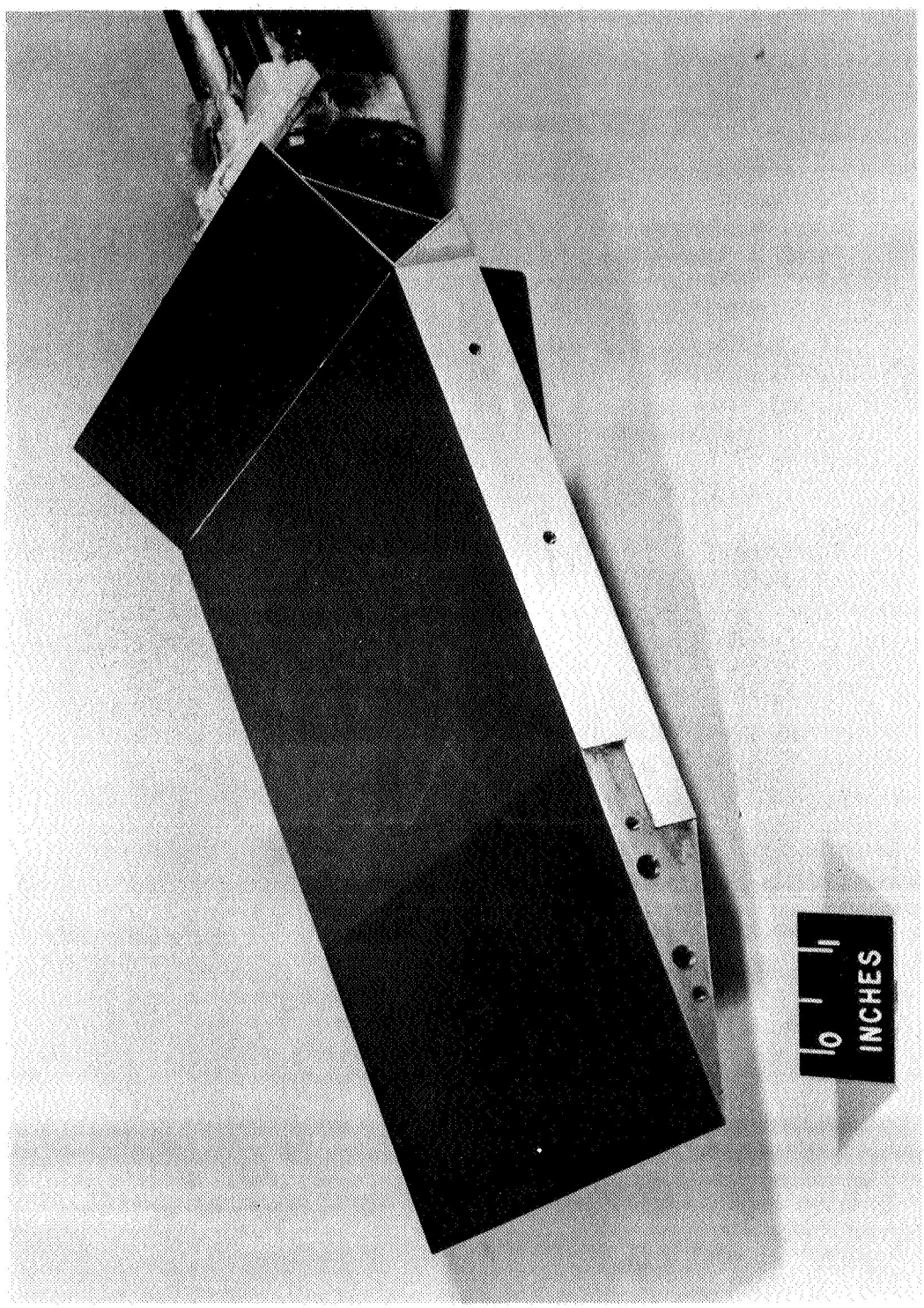

Figure 3.- Photograph of heat-transfer model.

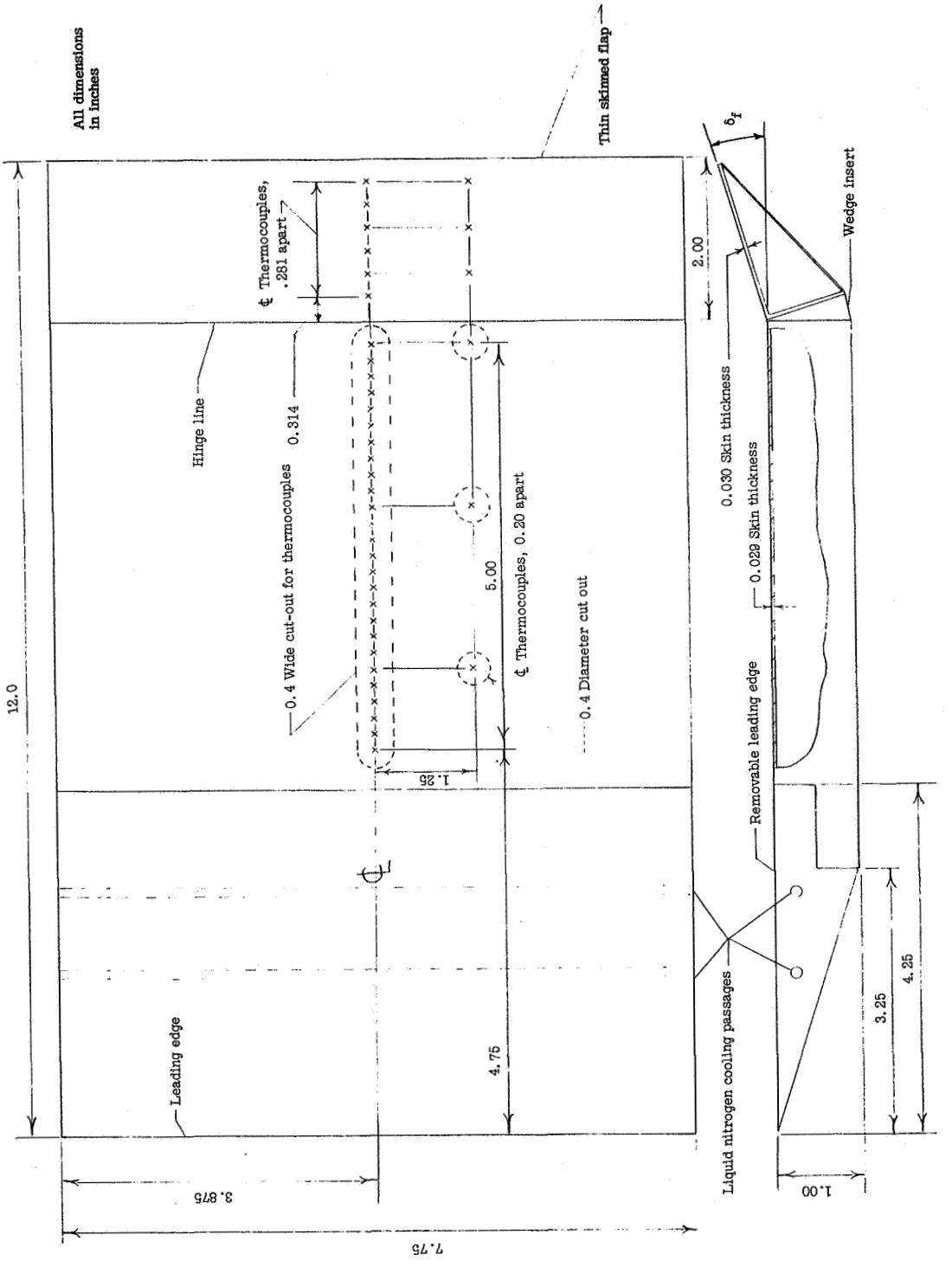

Figure 4.- Schematic of the heat transfer model.

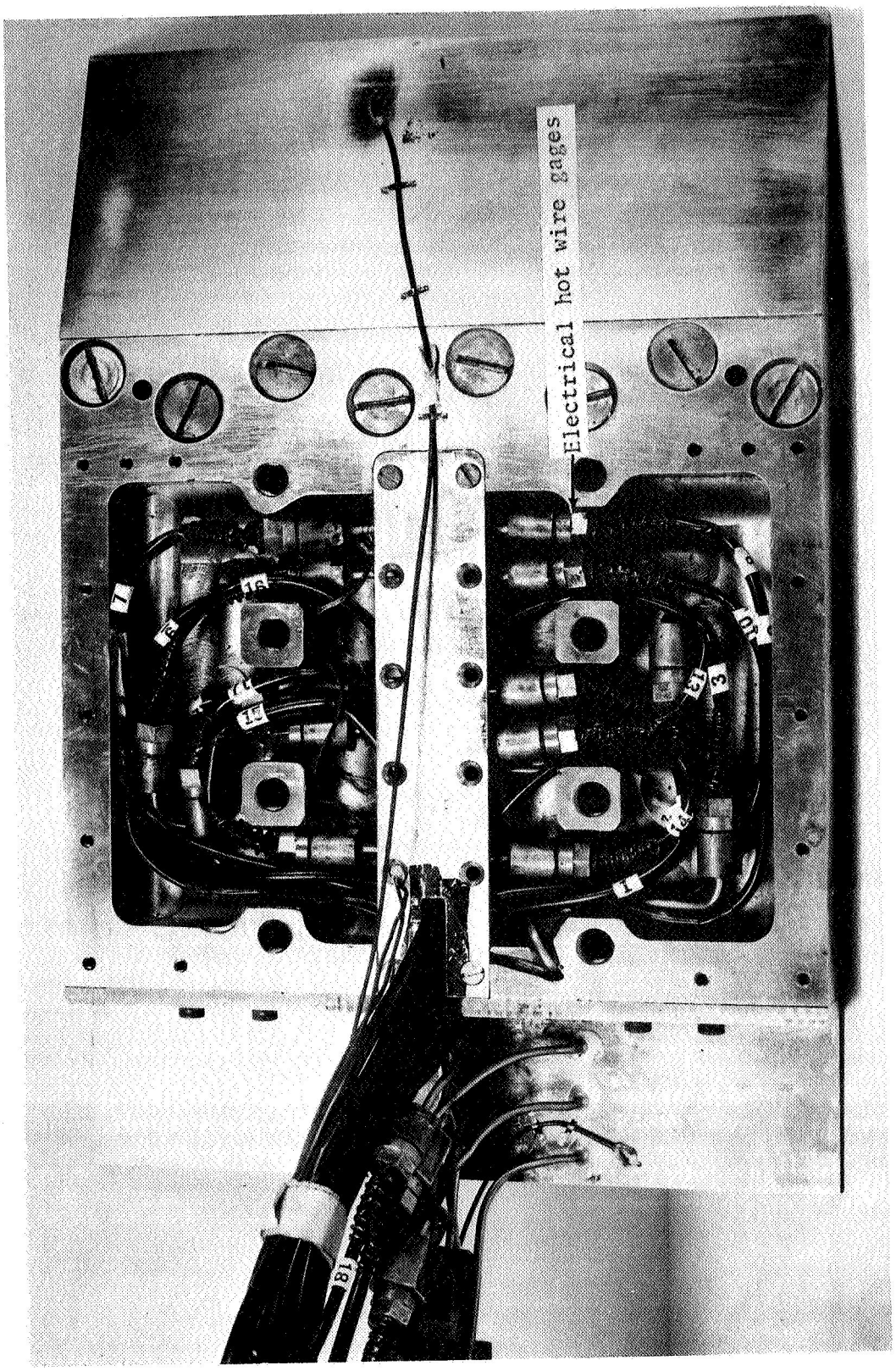

Figure 5.- View from below the pressure model showing pressure-gage installation.

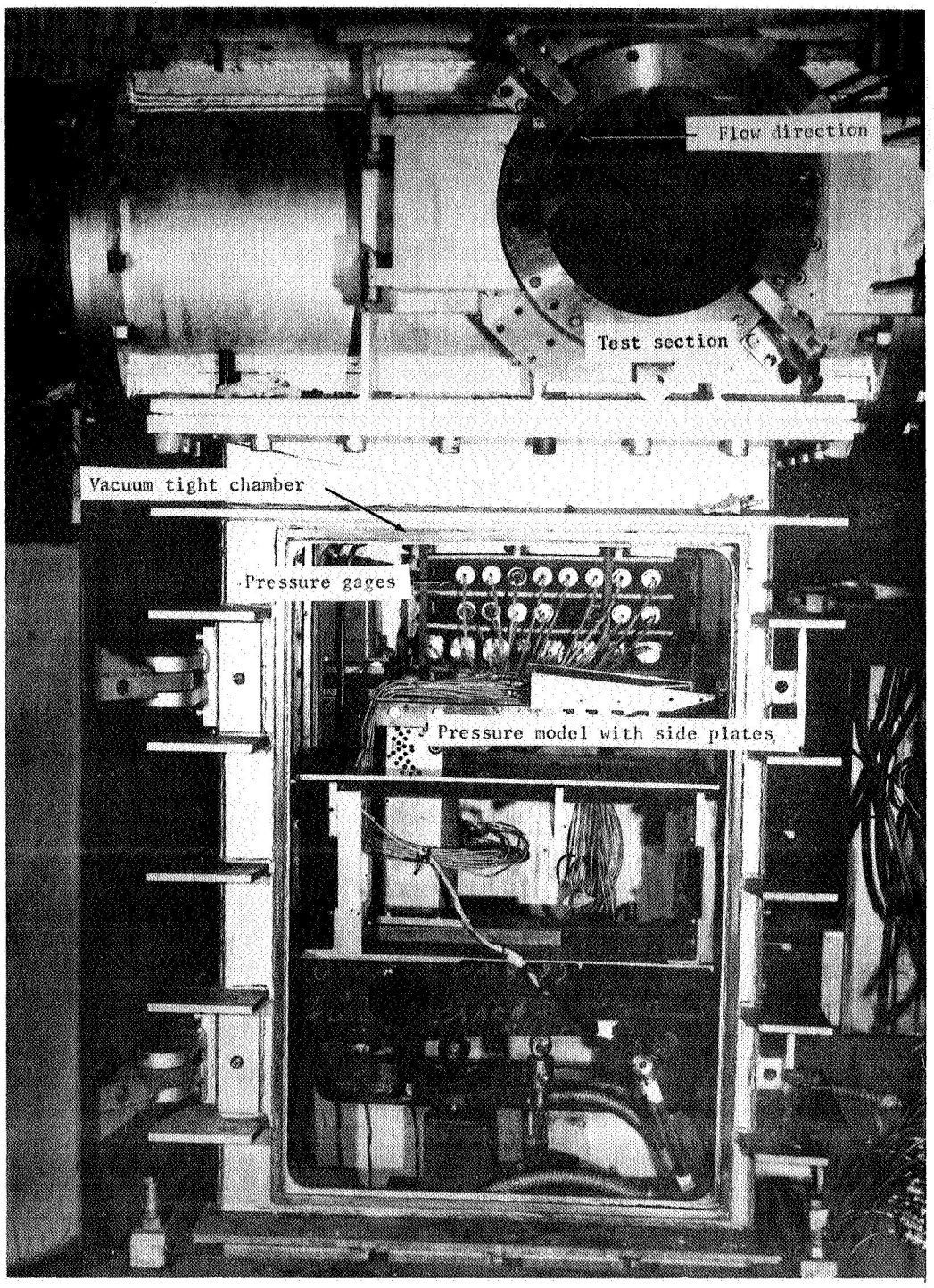

Figure 6.- Mach 8 tunnel apparatus, showing pressure model with upper side plates.

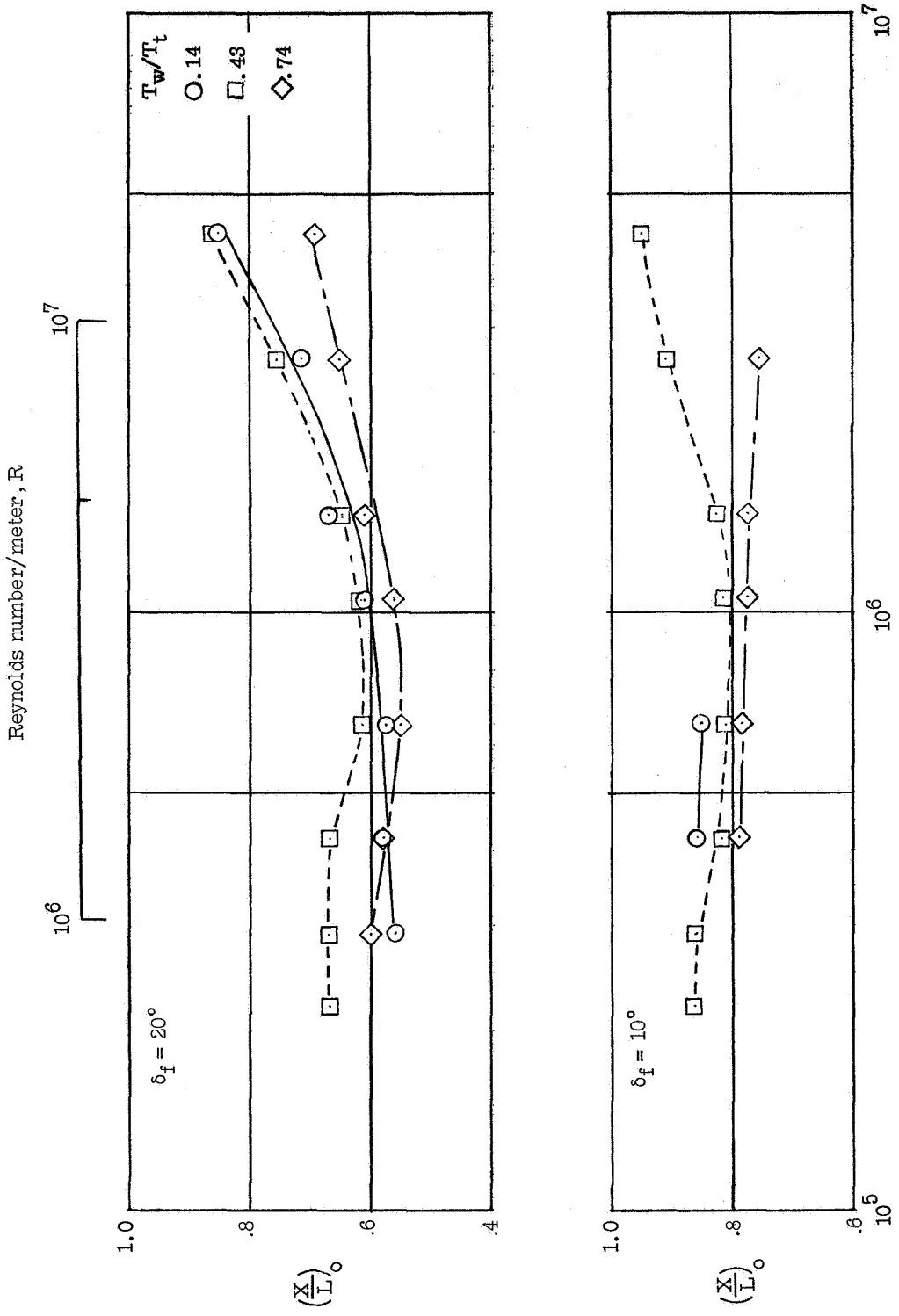

Figure 7.- The variation in the location of the beginning of the interaction region for two flap angles and three wall conditions at various unit Reynolds numbers.

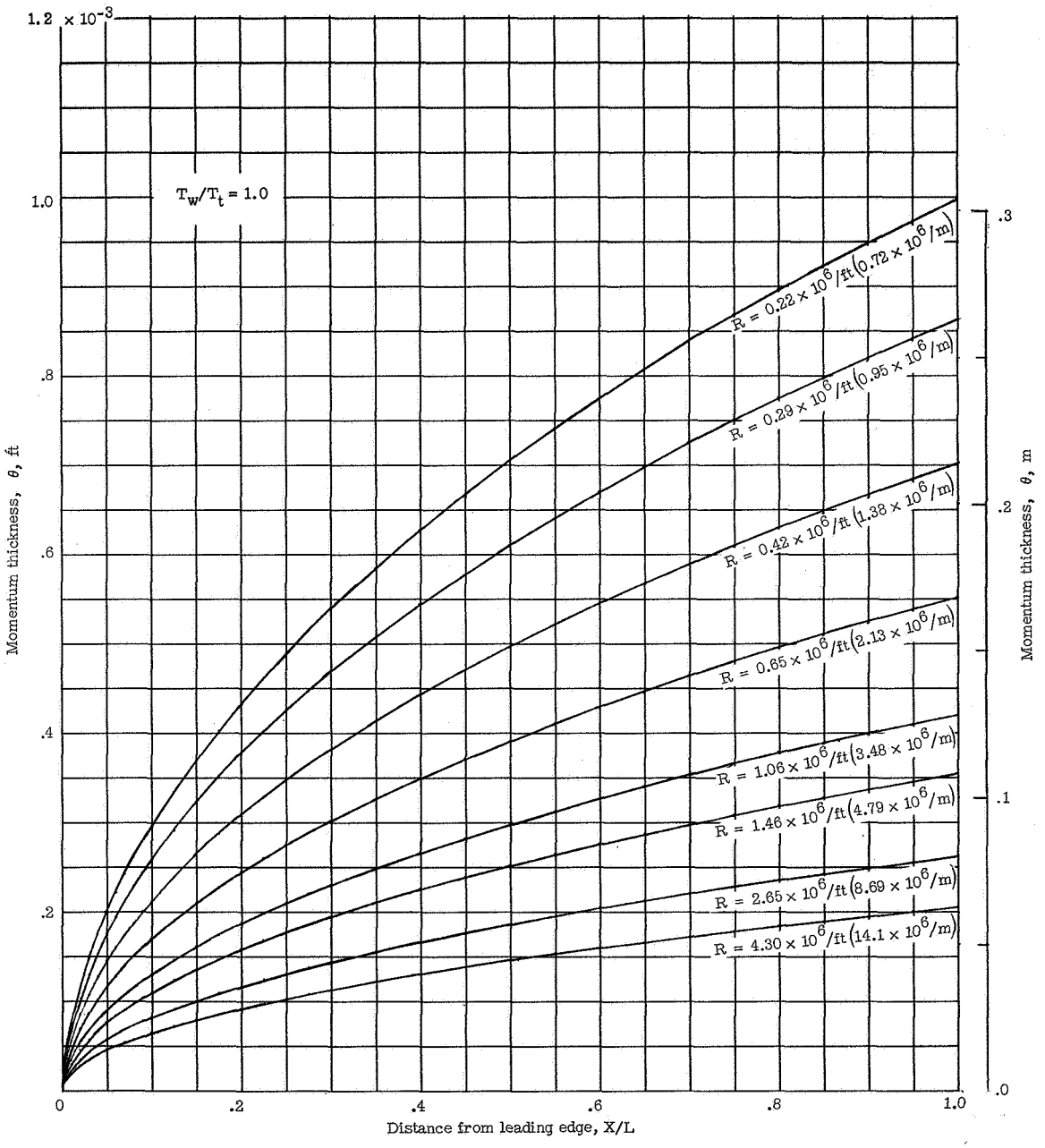

Figure 8.- The momentum thickness along a flat plate at a nominal Mach number of 8 for adiabatic wall conditions at various unit Reynolds numbers.

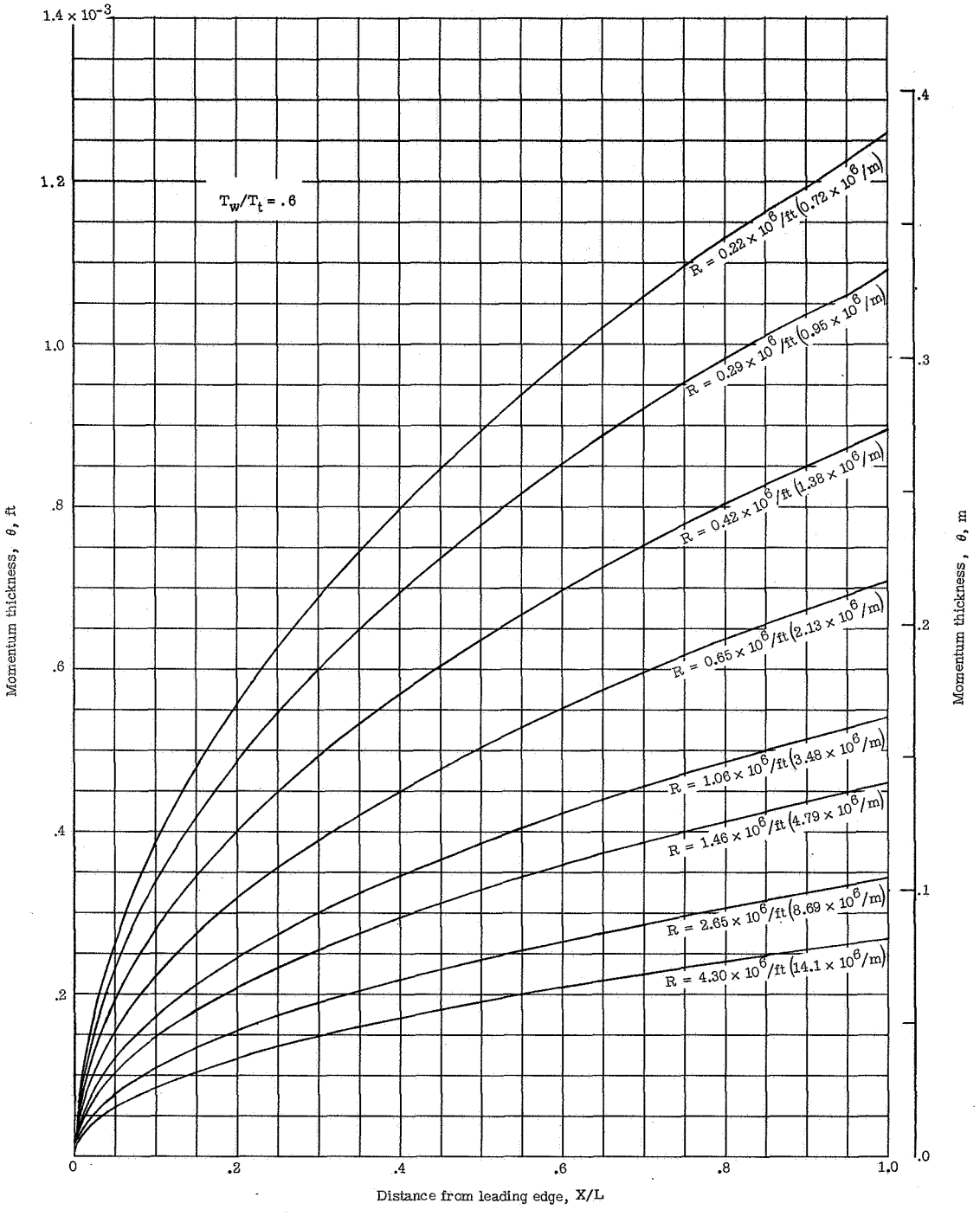

Figure 9.- The momentum thickness along a flat plate at a nominal Mach number of 8 for cool-wall conditions at various unit Reynolds numbers.

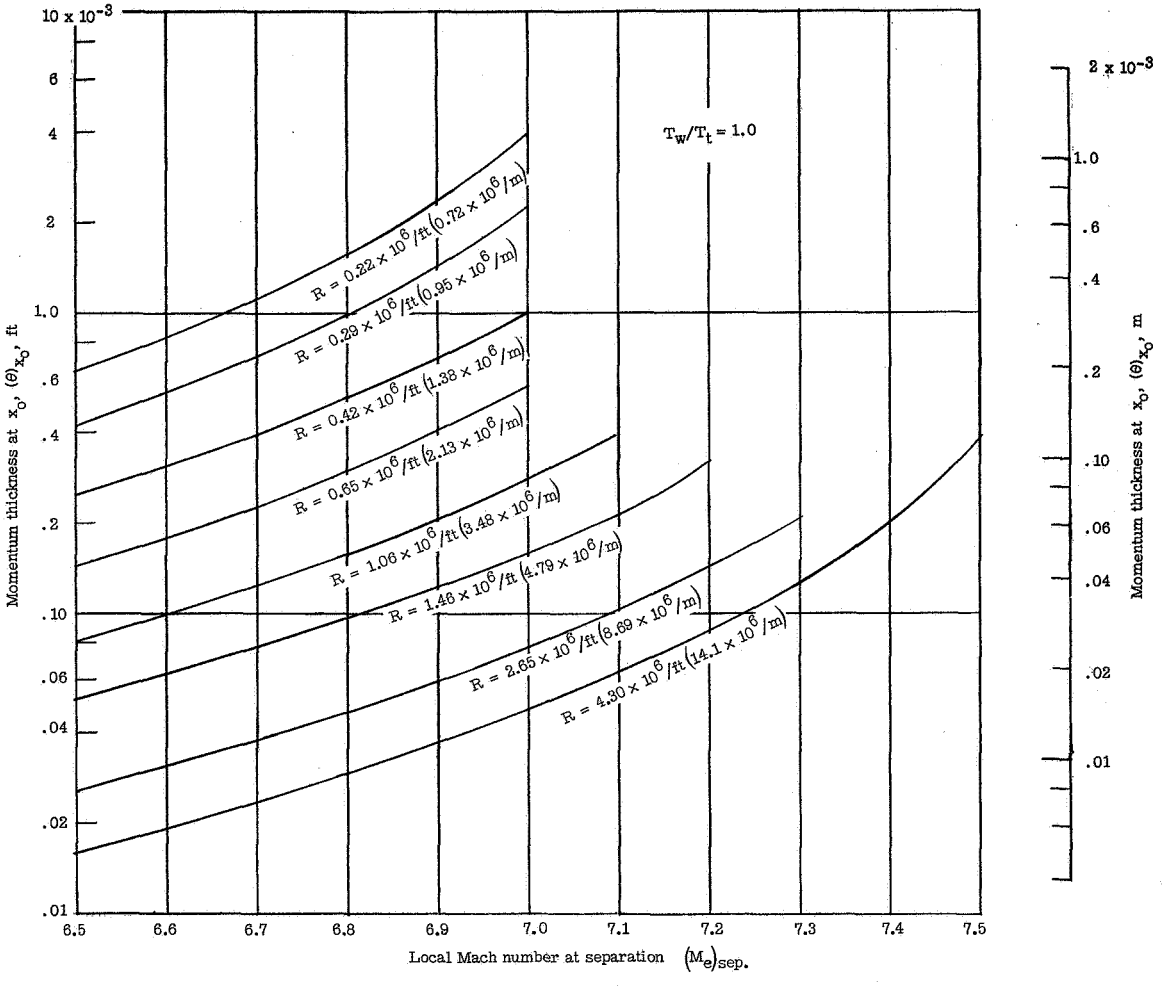

Figure 10.- The momentum thickness at the beginning of the interaction region versus the local Mach number at separation for adiabatic wall conditions at various unit Reynolds numbers.

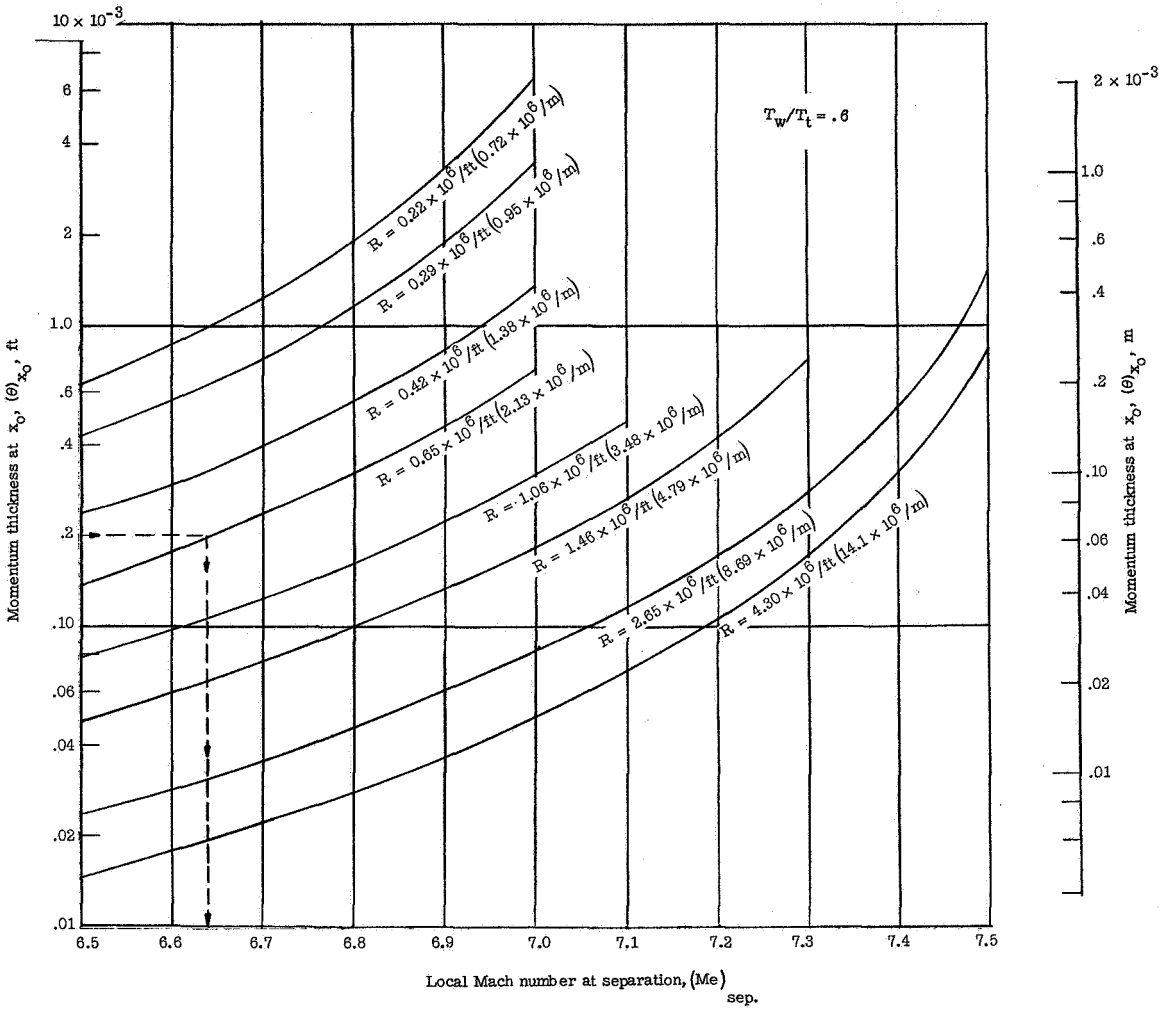

Figure 11.- The momentum thickness at the beginning of the interaction region versus the local Mach number at separation for cool-wall conditions at various unit Reynolds numbers.

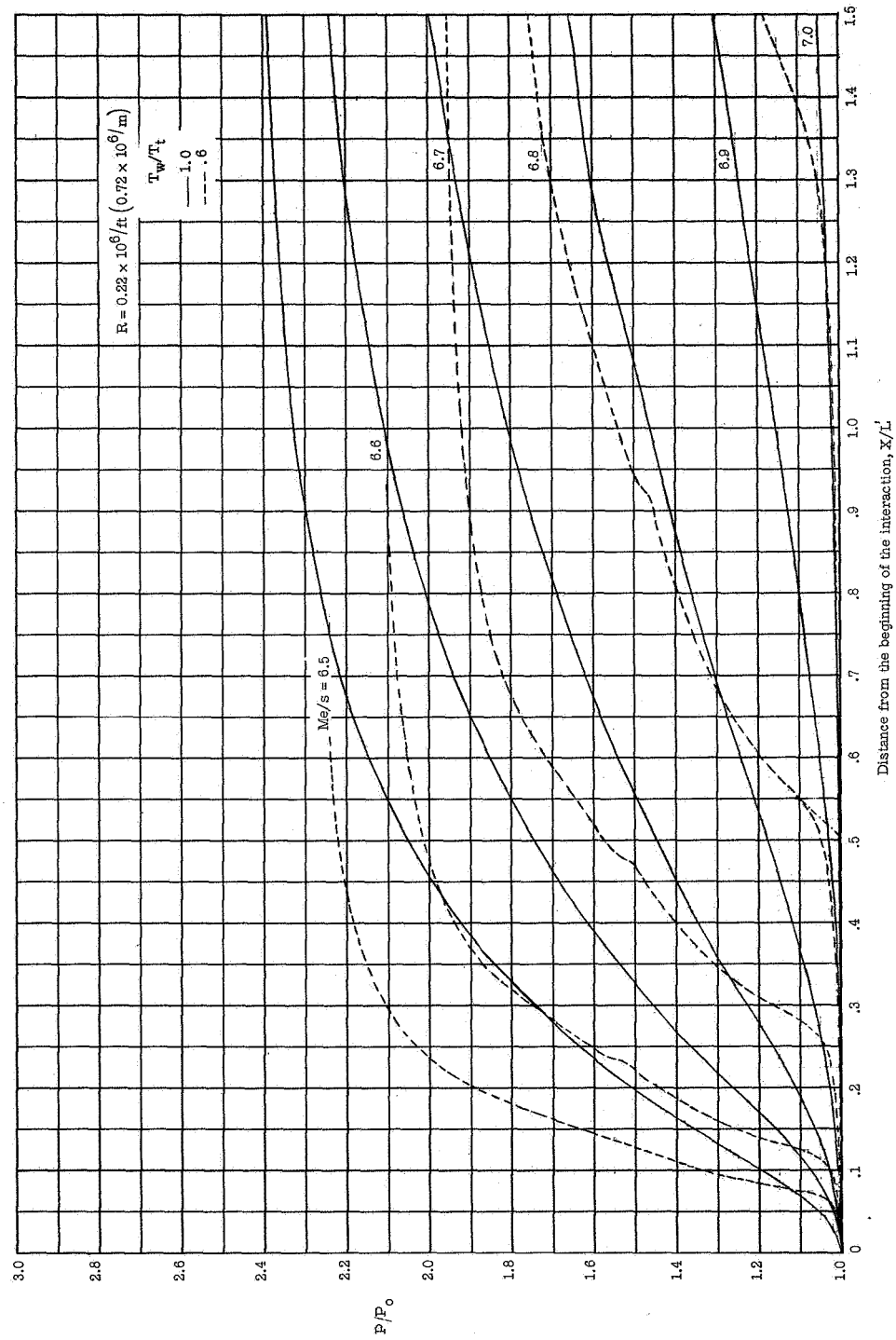

(a) R = 0.22 × 10^6/ft (0.72 × 10^6/m).

Figure 12.- The theoretical pressure rise due to separation for various local Mach numbers, at separation, for cool and adiabatic wall conditions at various unit Reynolds numbers.

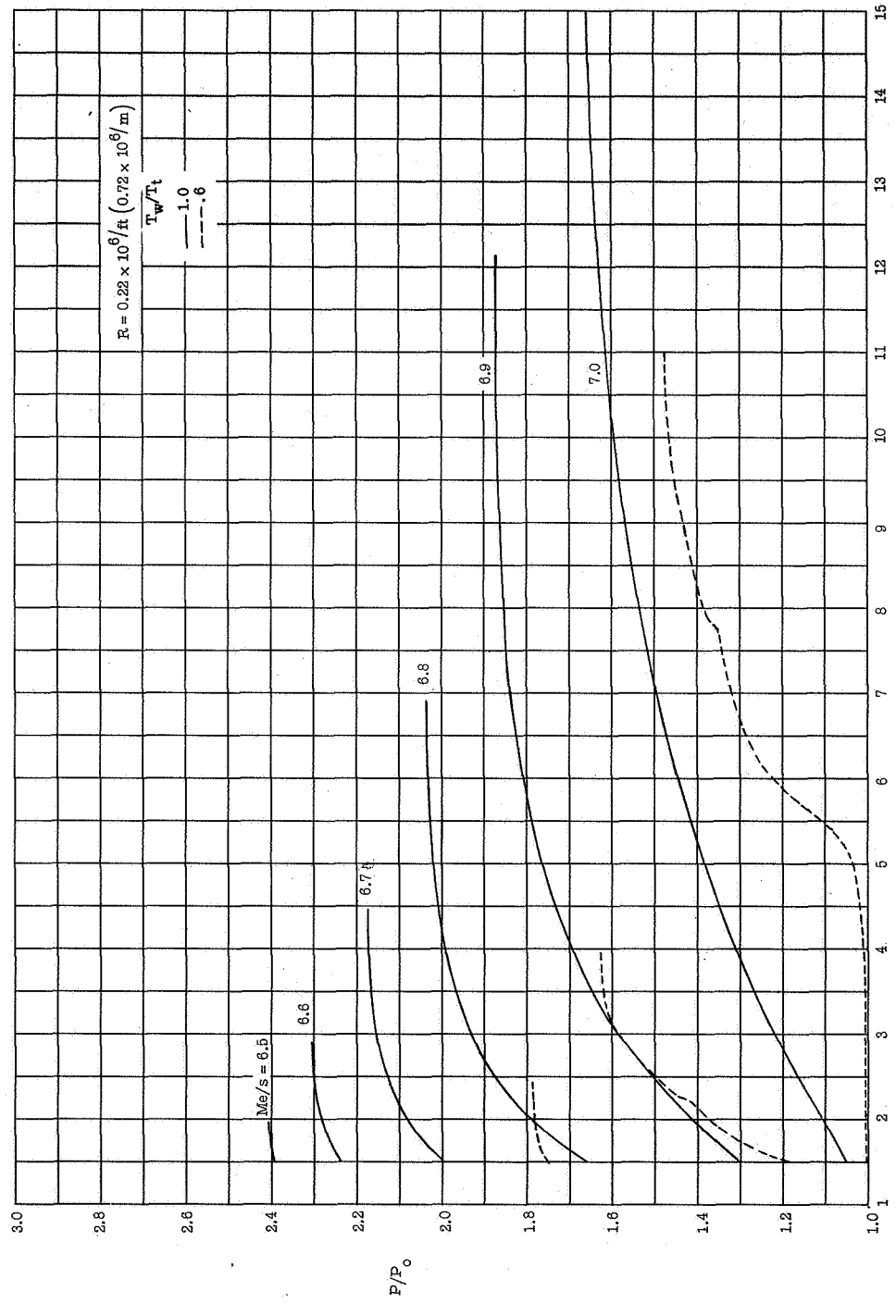

(b) R = 0.22×10^6/ft (0.72×10^6/m).

Figure 12.- Continued.

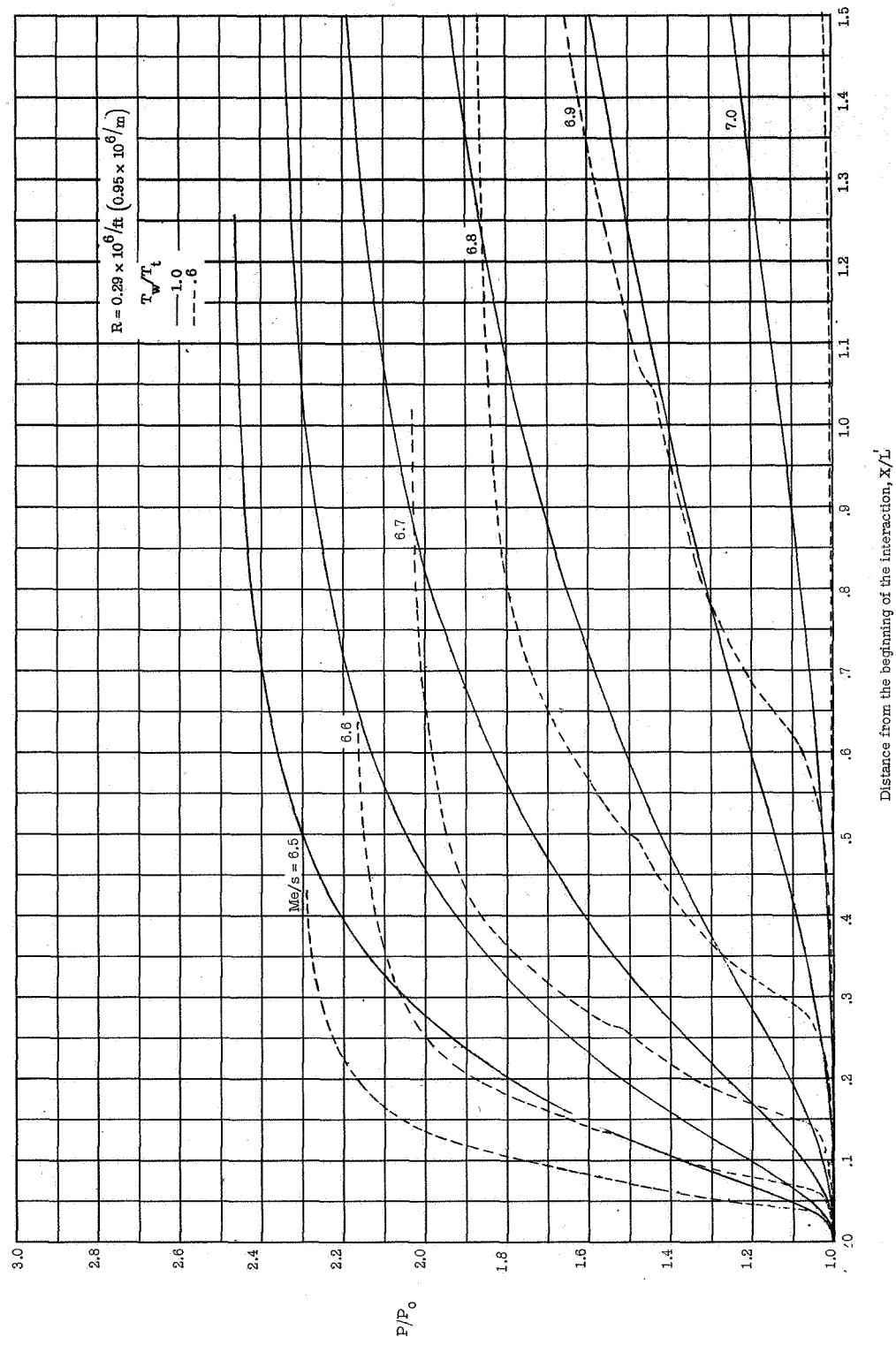

(c) R = 0.29 × 10^6/ft (0.95 × 10^6/m).

Figure 12.- Continued.

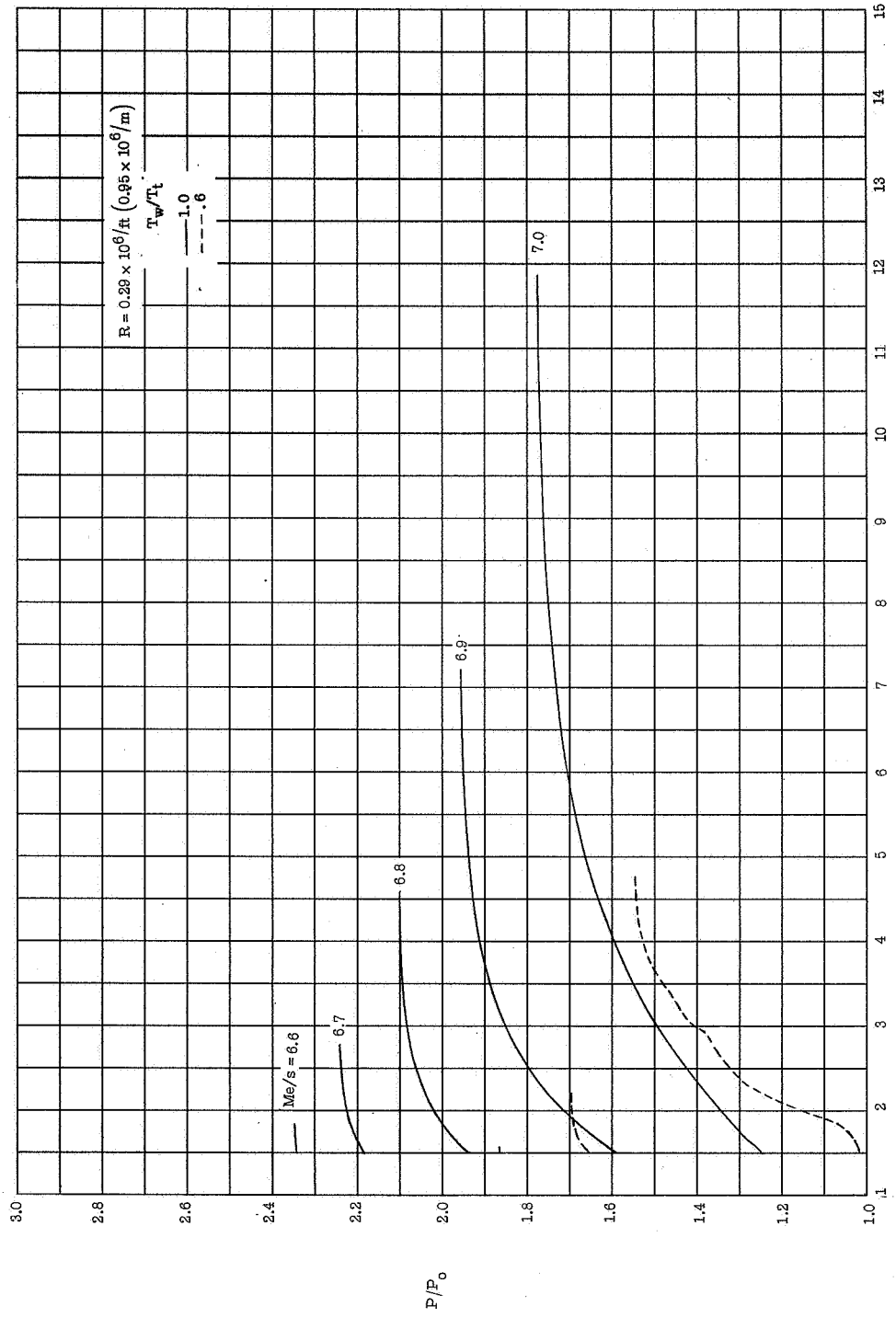

(d) R = 0.29×10^6/ft (0.95×10^6/m).

Figure 12.- Continued.

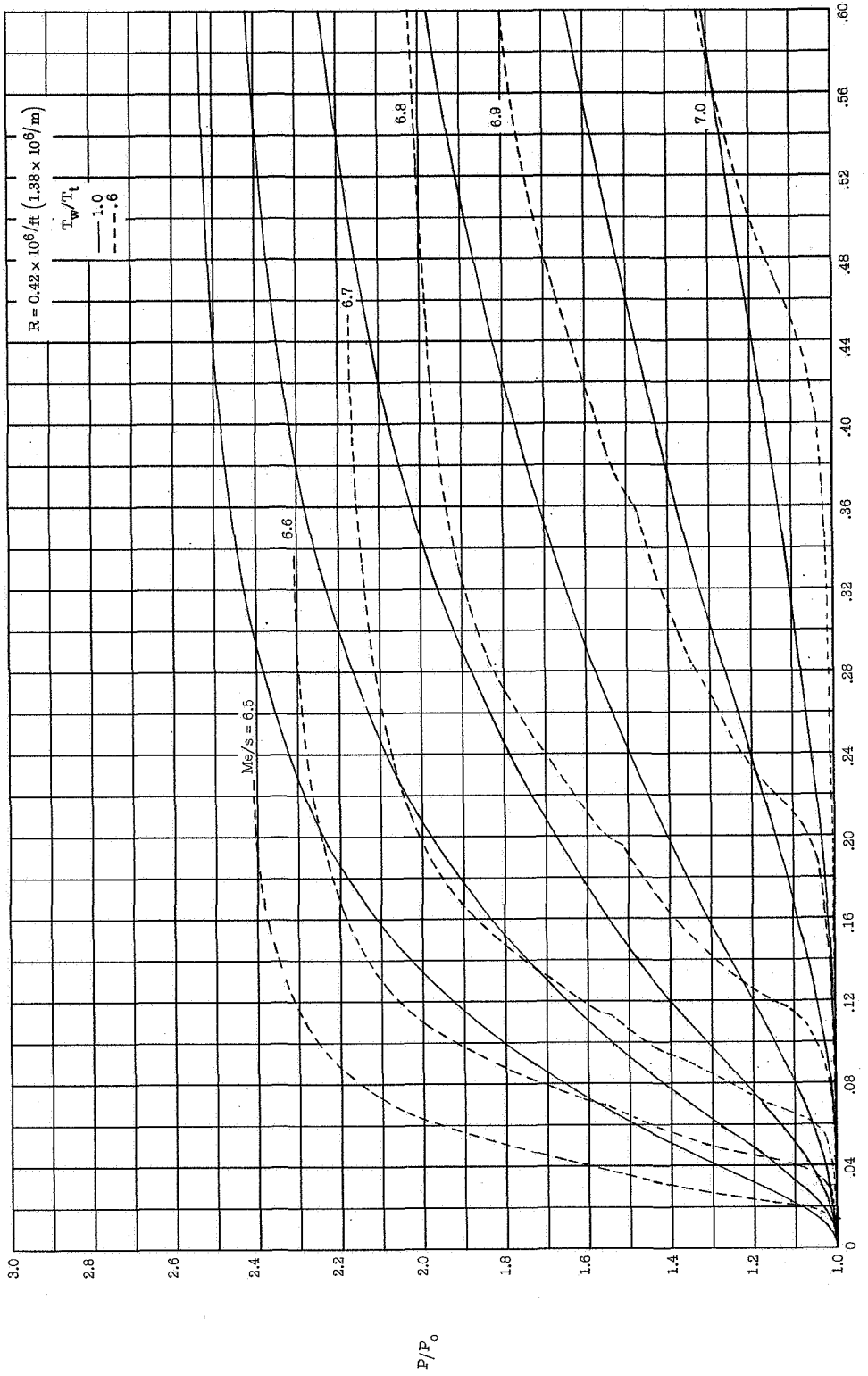

(e) R = 0.42×10^6/ft (1.38×10^6/m).

Figure 12.- Continued.

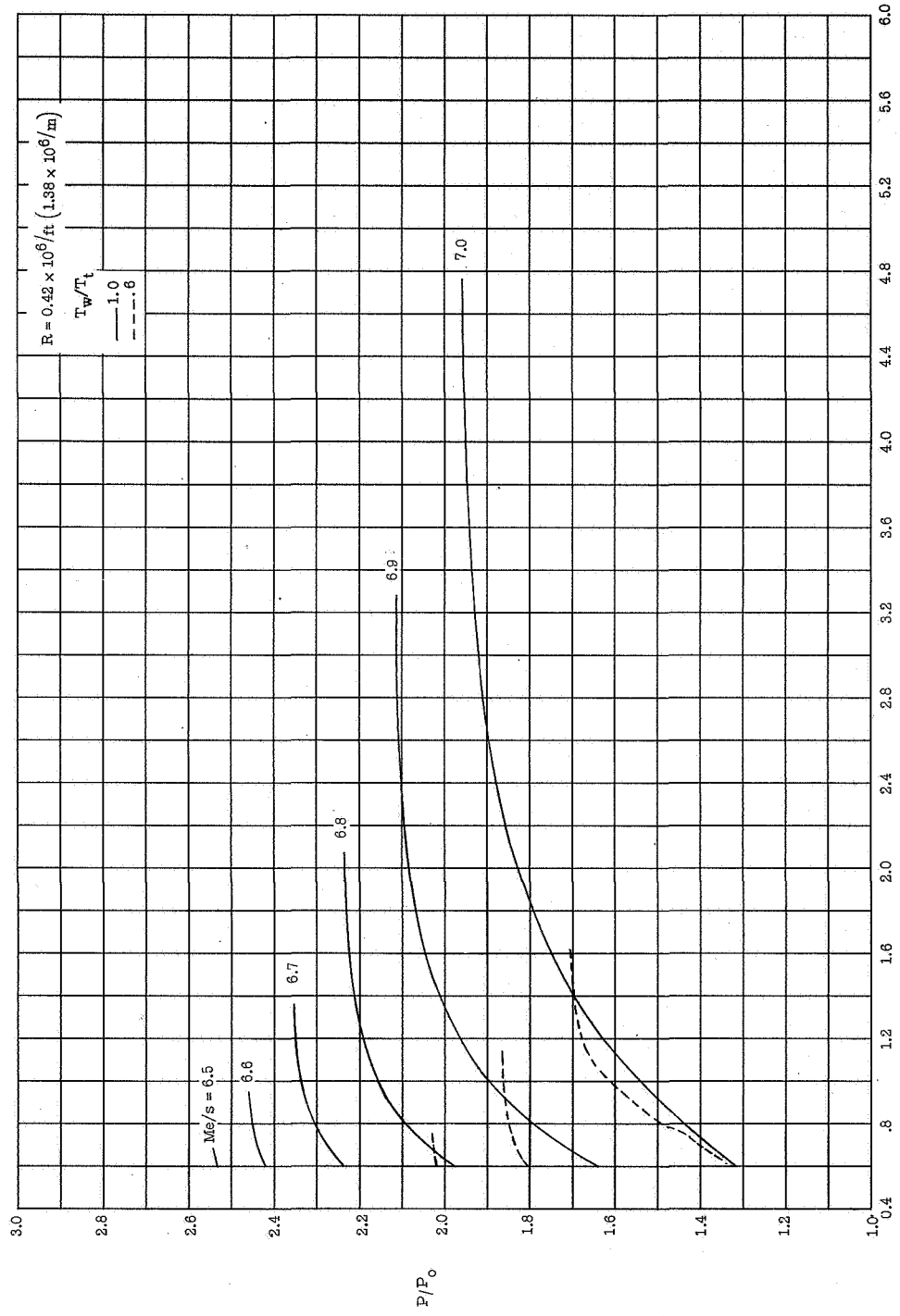

(f) R = 0.42×10^6/ft (1.38×10^6/m).

Figure 12.- Continued.

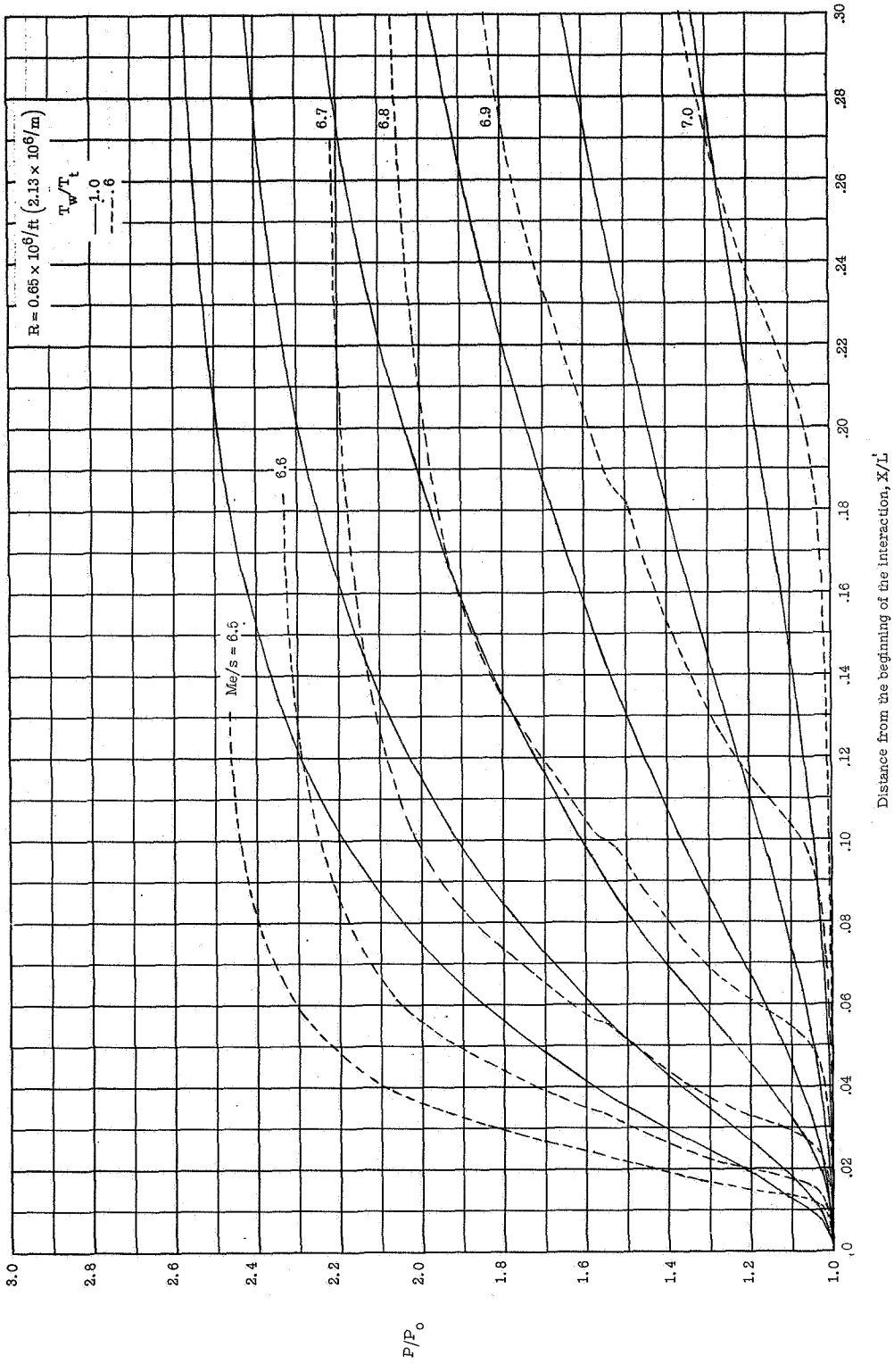

(g) R = 0.65×10^6/ft (2.13×10^6/m).

Figure 12.- Continued.

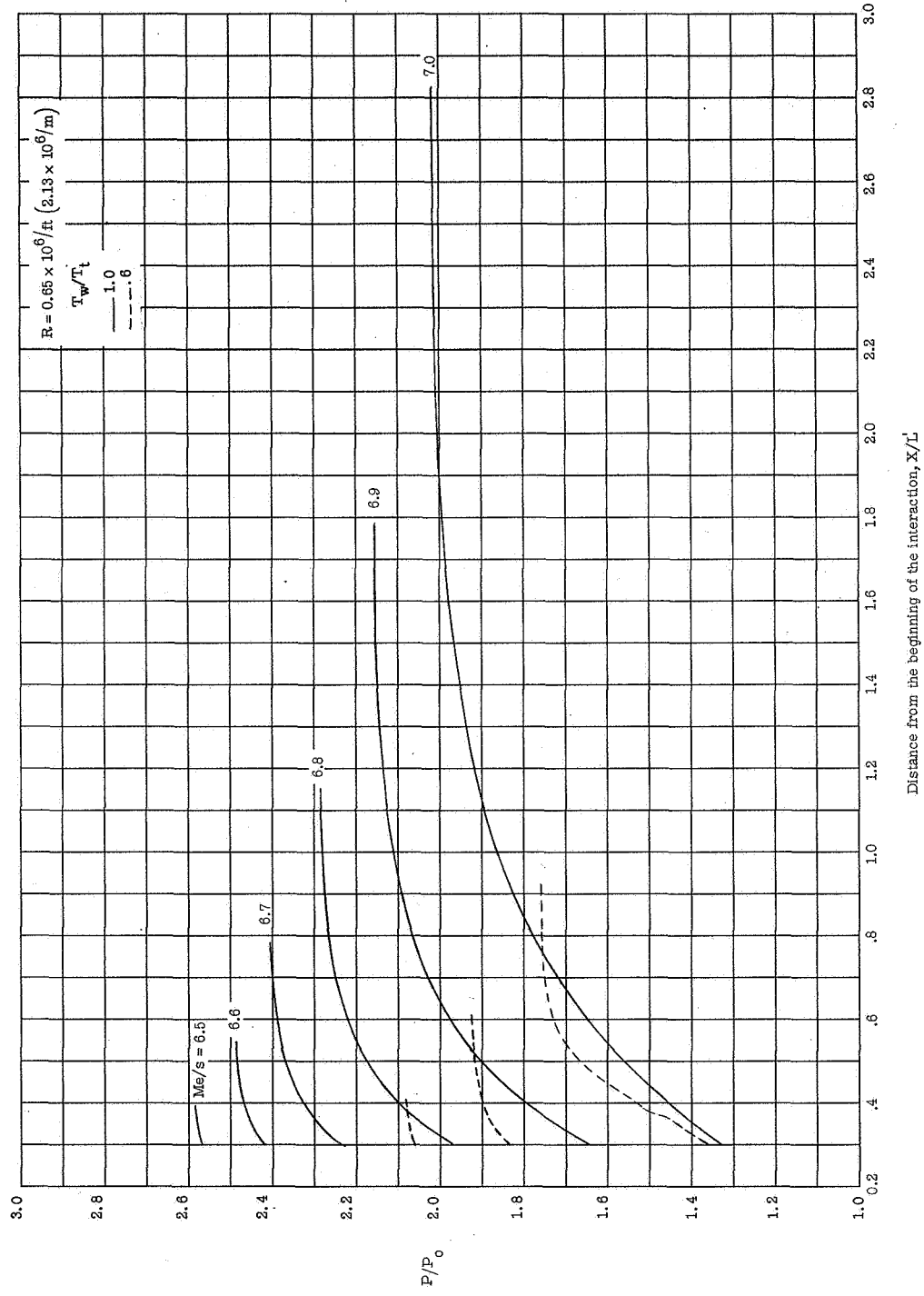

(h) R = 0.65×10^6/ft (2.13×10^6/m).

Figure 12.- Continued.

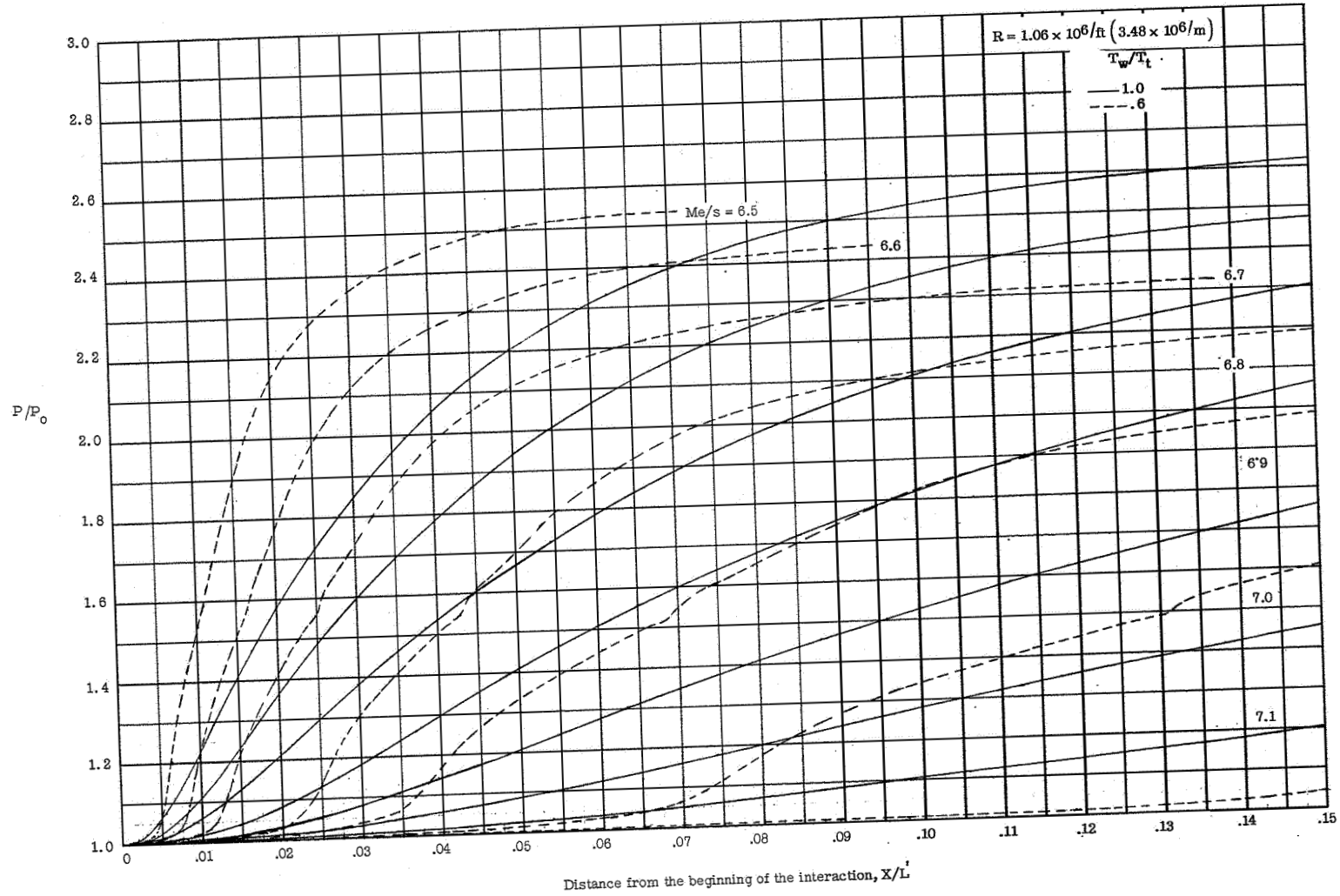

(i) $R = 1.06 \times 10^6/ft\ (3.48 \times 10^6/m)$.

Figure 12.- Continued.

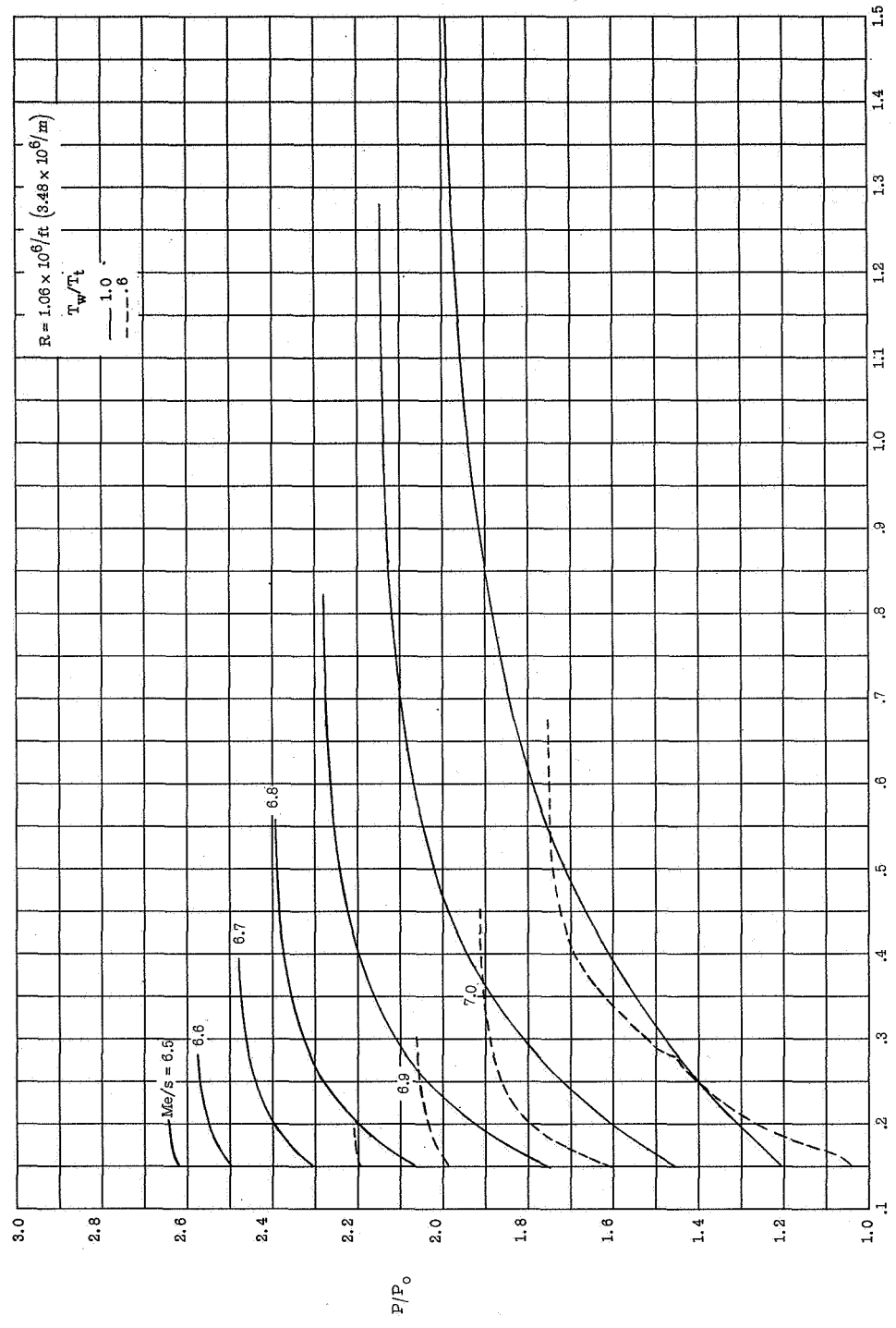

(j) R = 1.06×10^6/ft (3.48×10^6/m).

Figure 12.- Continued.

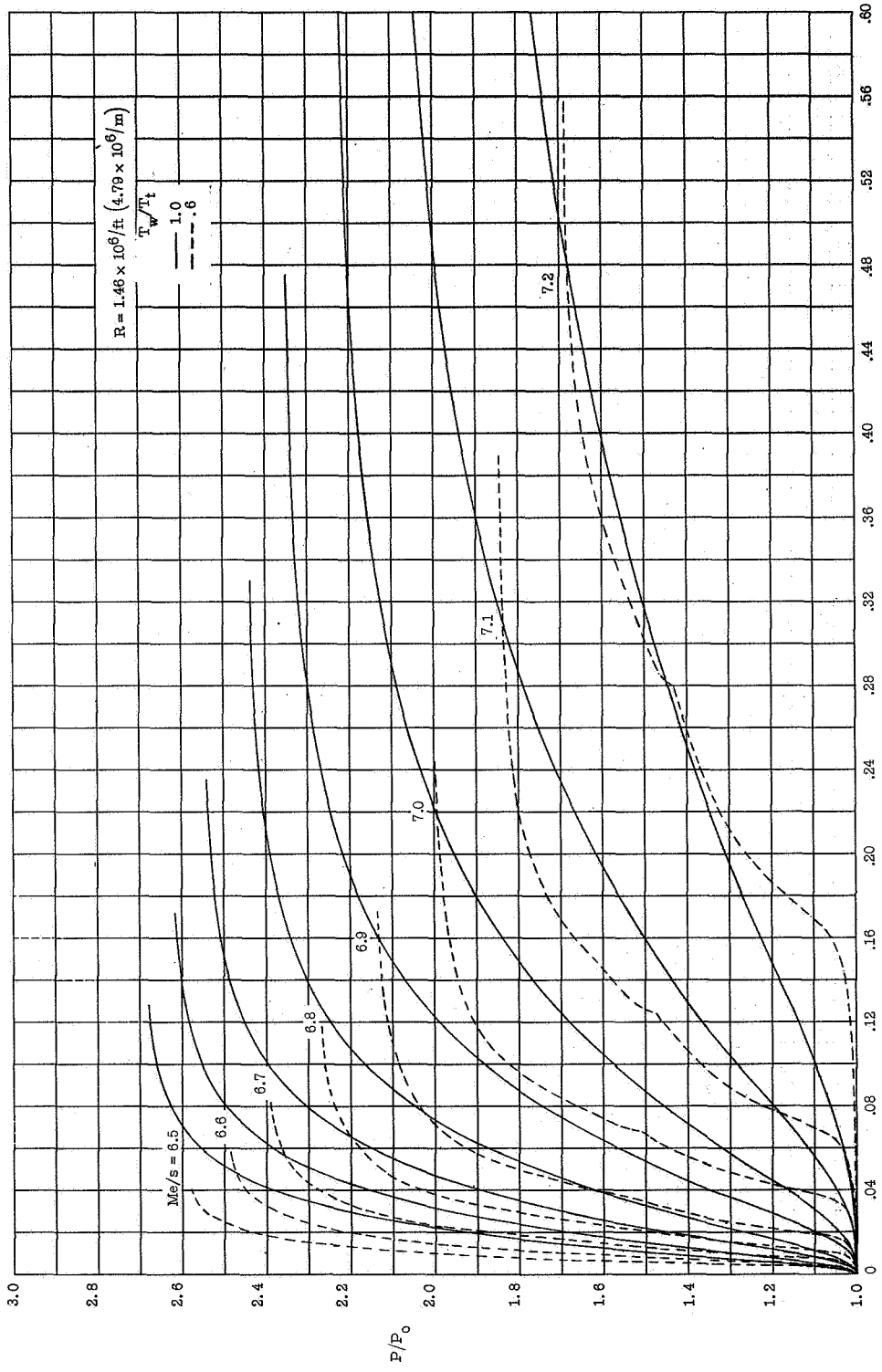

(k) R = 1.46 × 10^6/ft (4.79 × 10^6/m).

Figure 12.- Continued.

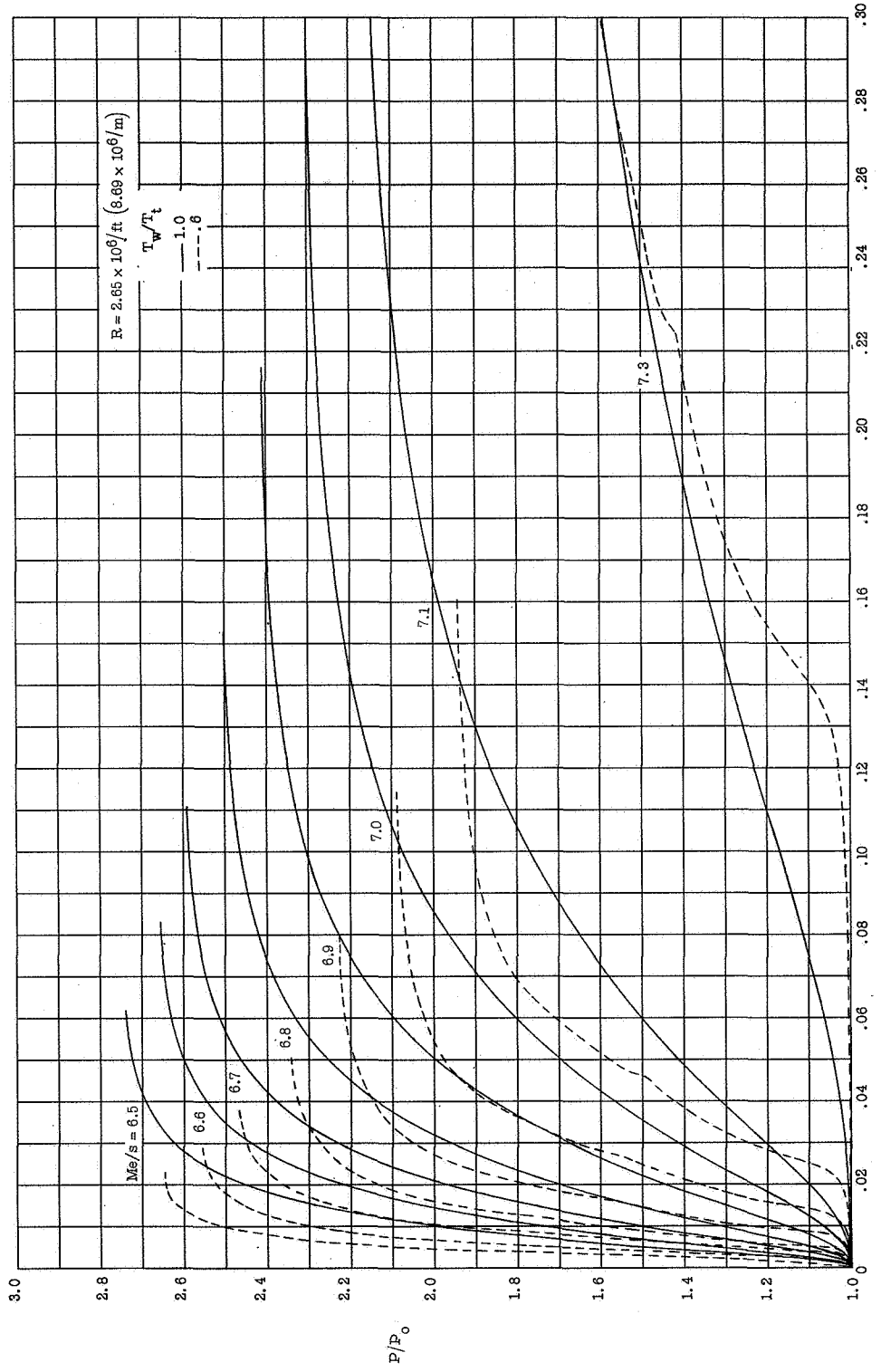

(1) $R = 2.65 \times 10^6/ft\ (8.69 \times 10^6/m)$.

Figure 12.- Continued.

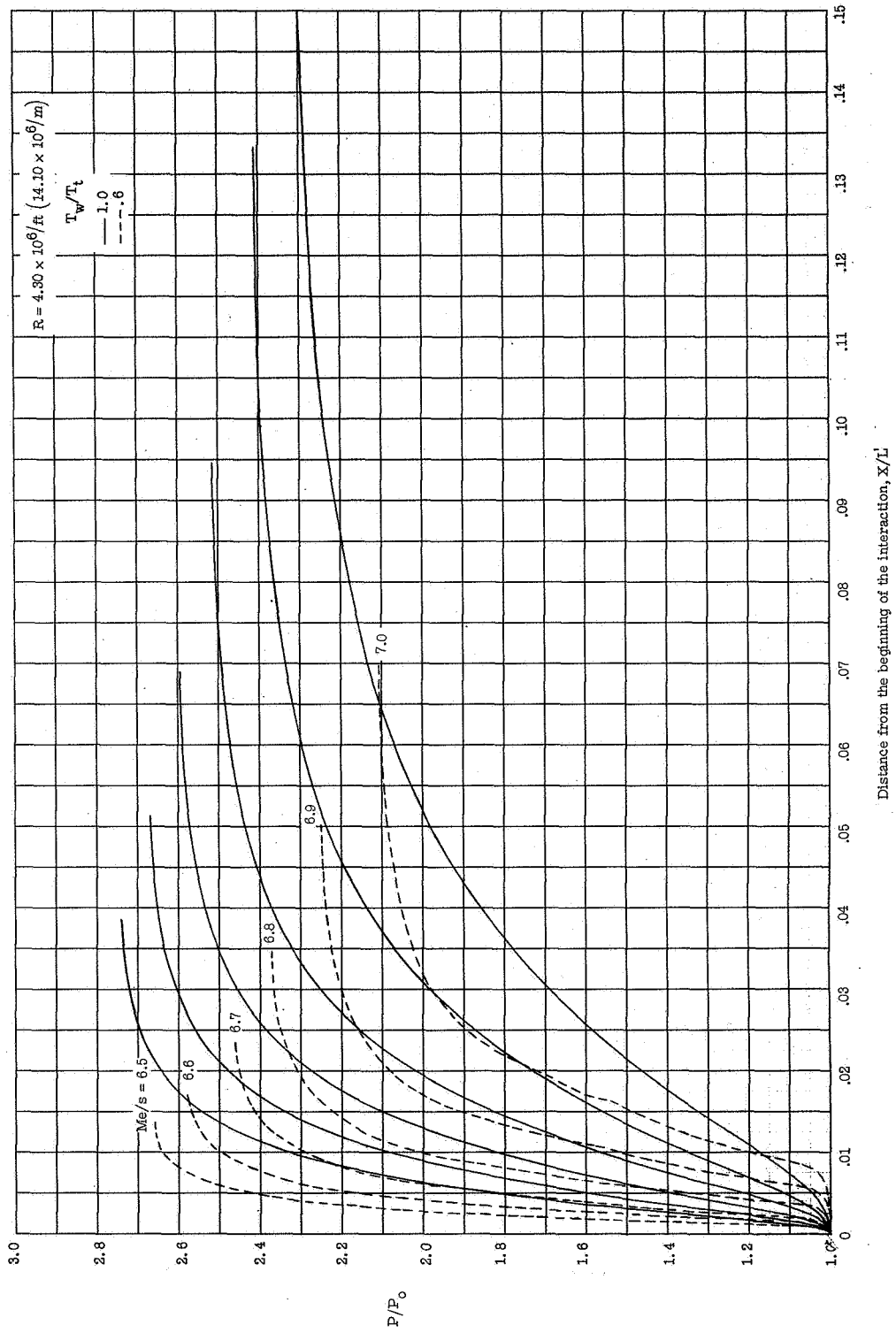

(m) R = 4.30 × 10^6/ft (14.10 × 10^6/m).

Figure 12.- Concluded.

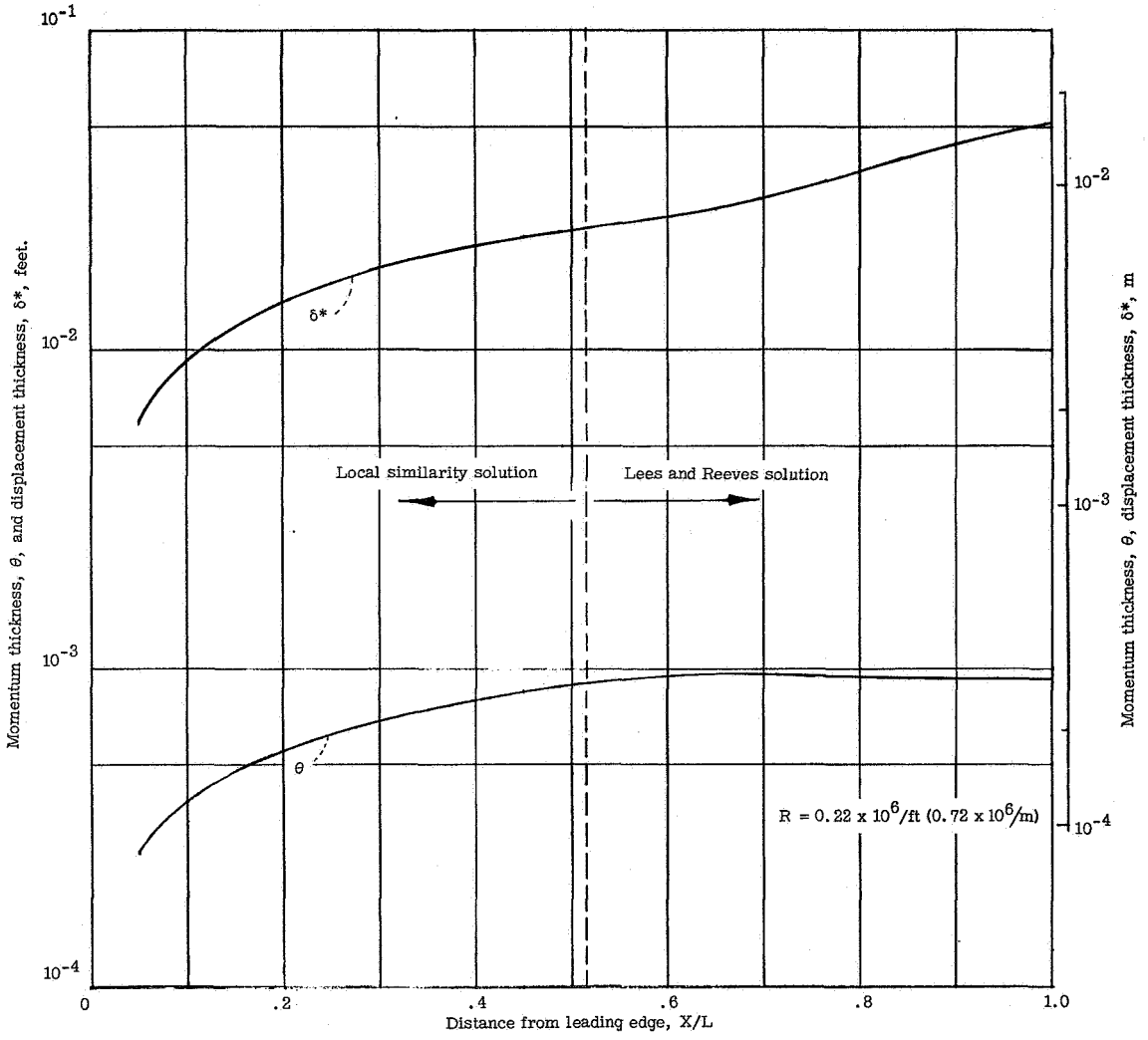

Figure 13.- A comparison of the growth of the momentum thickness and the displacement thickness over a flat plate with flow separation.

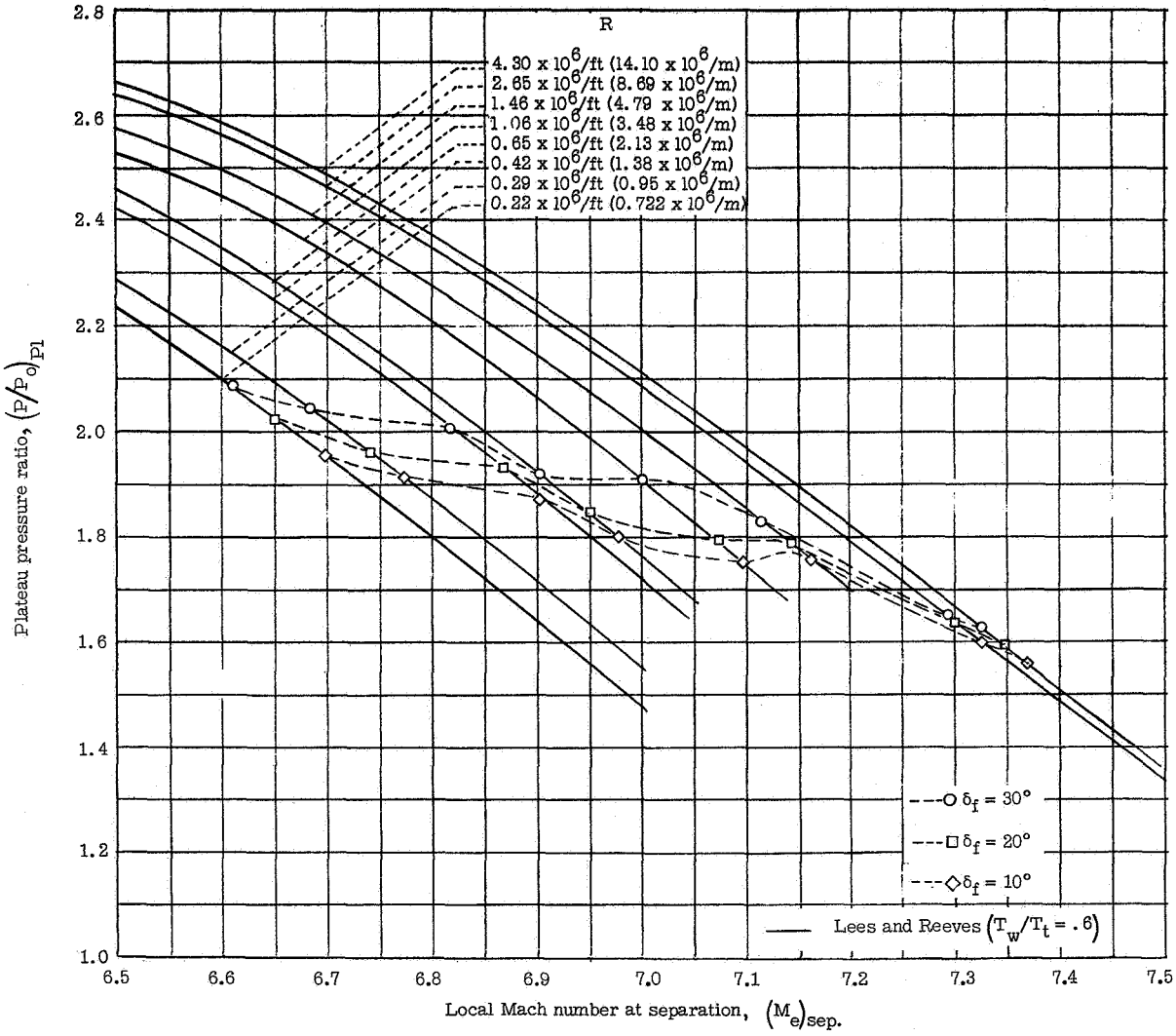

Figure 14.- The effect of Reynolds number and flap angle on the theoretical prediction of plateau pressure for cool walls.

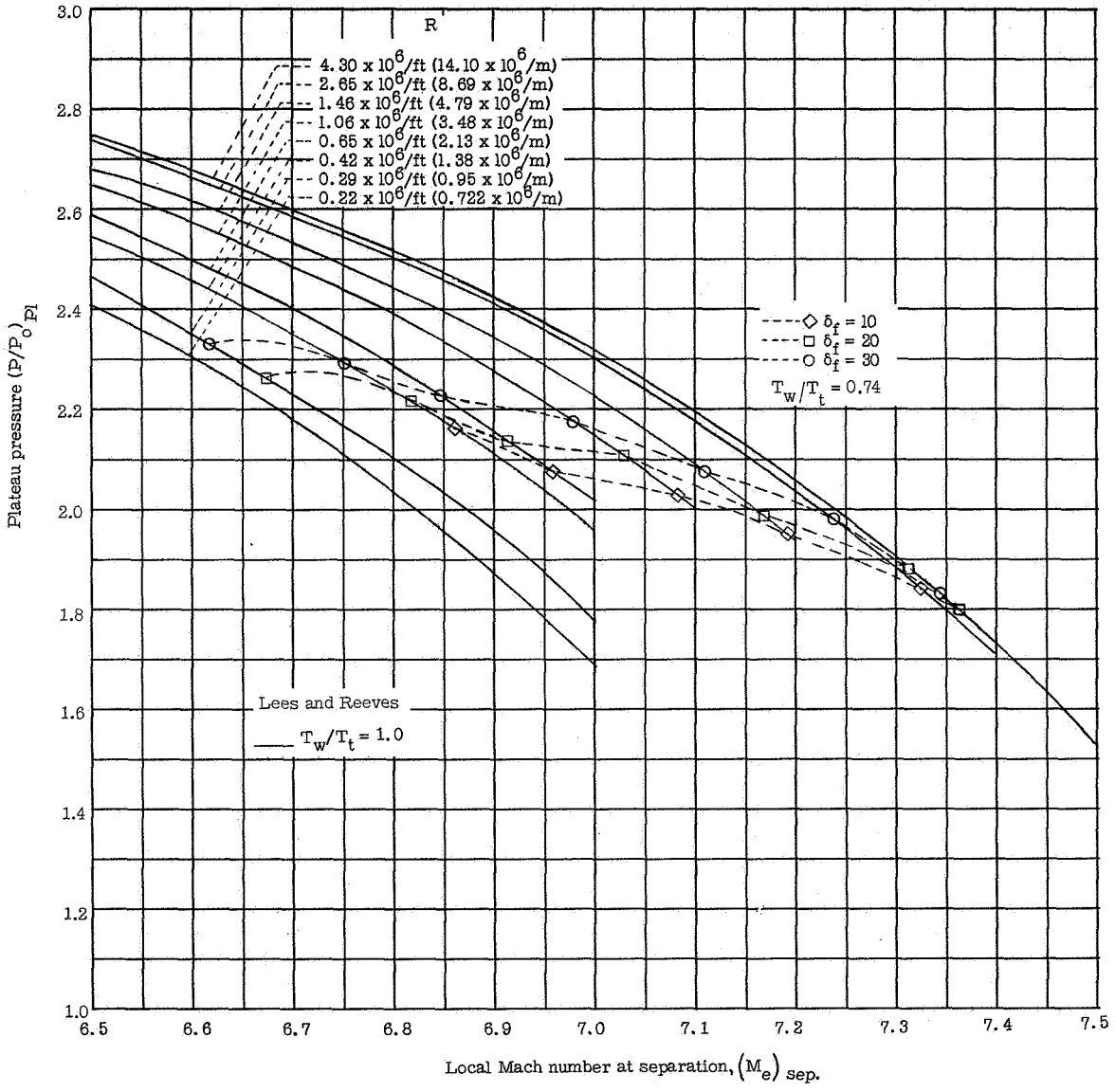

Figure 15.- The effect of Reynolds number and flap angle on the theoretical prediction of plateau pressure for adiabatic walls.

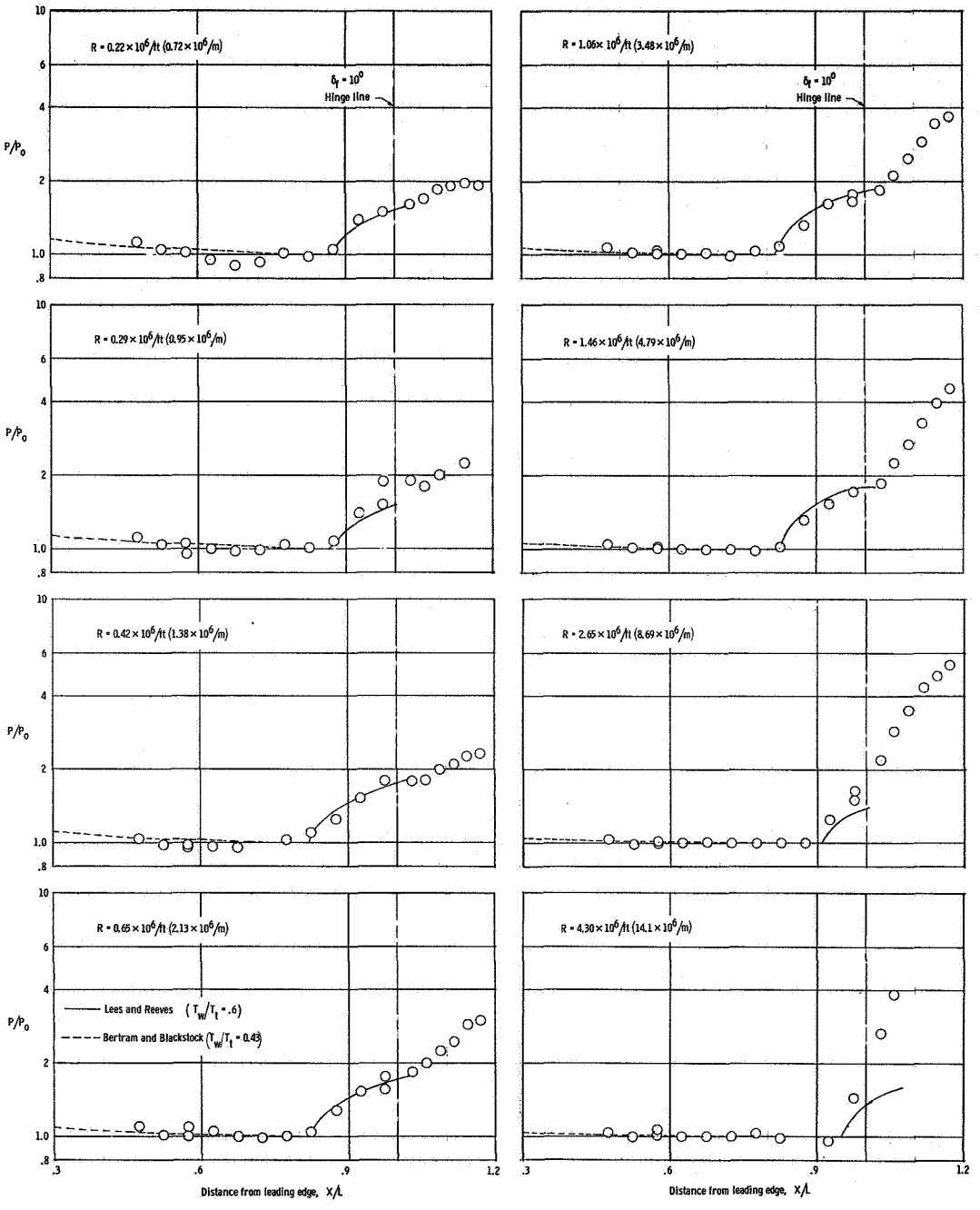

(a) $\delta_f = 10^\circ$.

Figure 16.- The effect of Reynolds number on the plateau pressure distribution at $T_w/T_t = 0.43$ for three flap angles, with and without side plates.

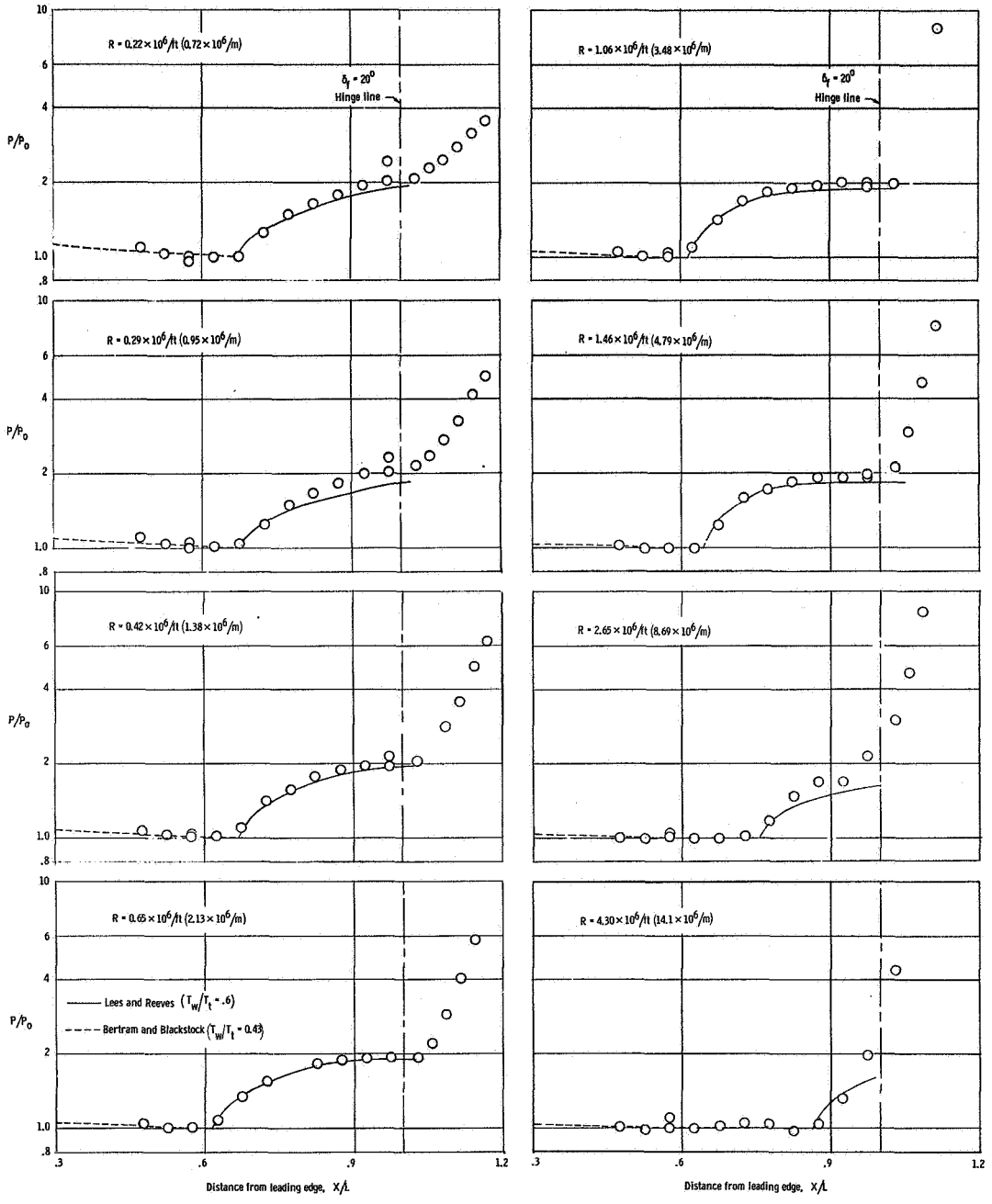

(b) $\delta_f = 20^\circ$.

Figure 16.- Continued.

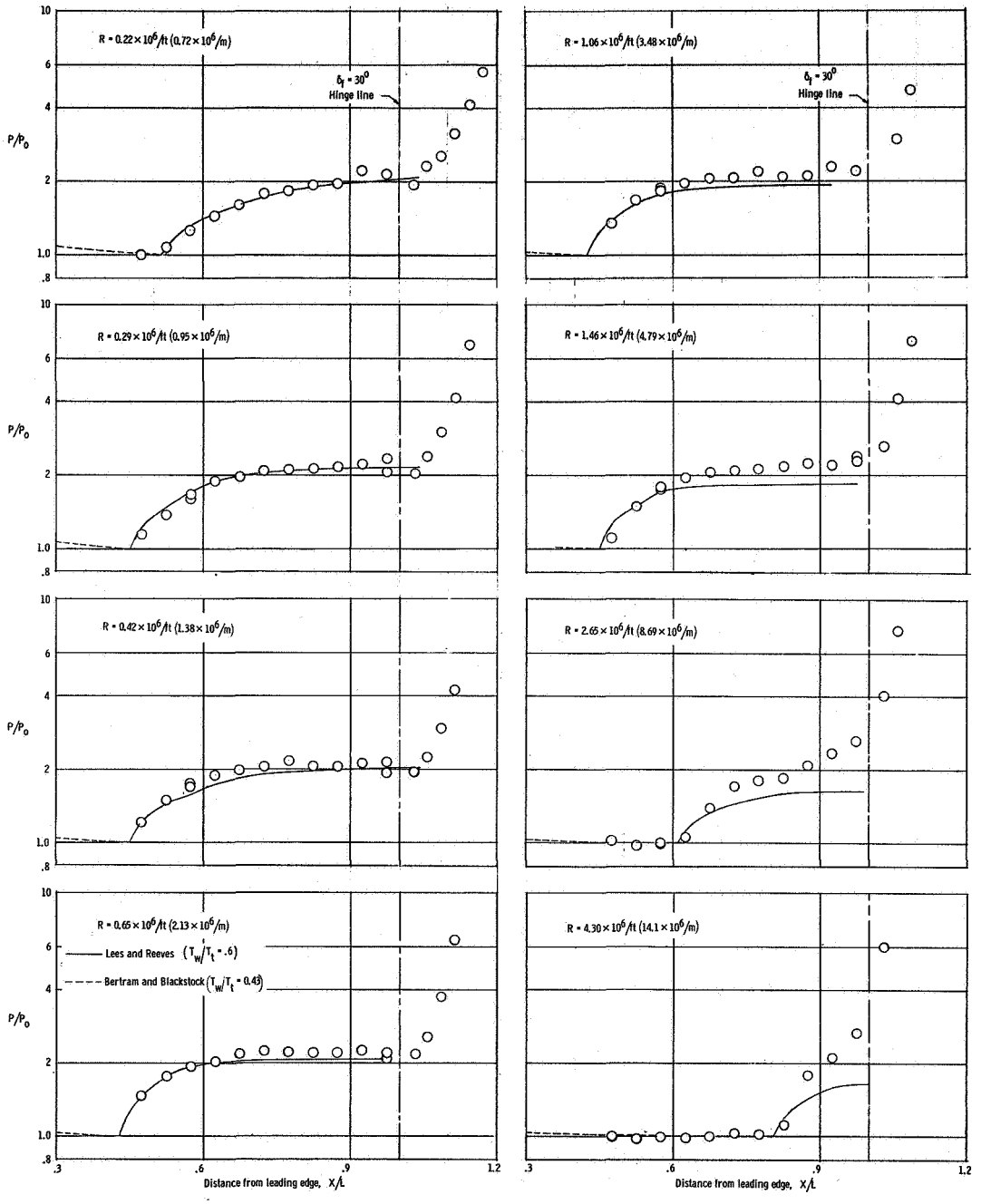

(c) $\delta_f = 30^\circ$.

Figure 16.- Continued.

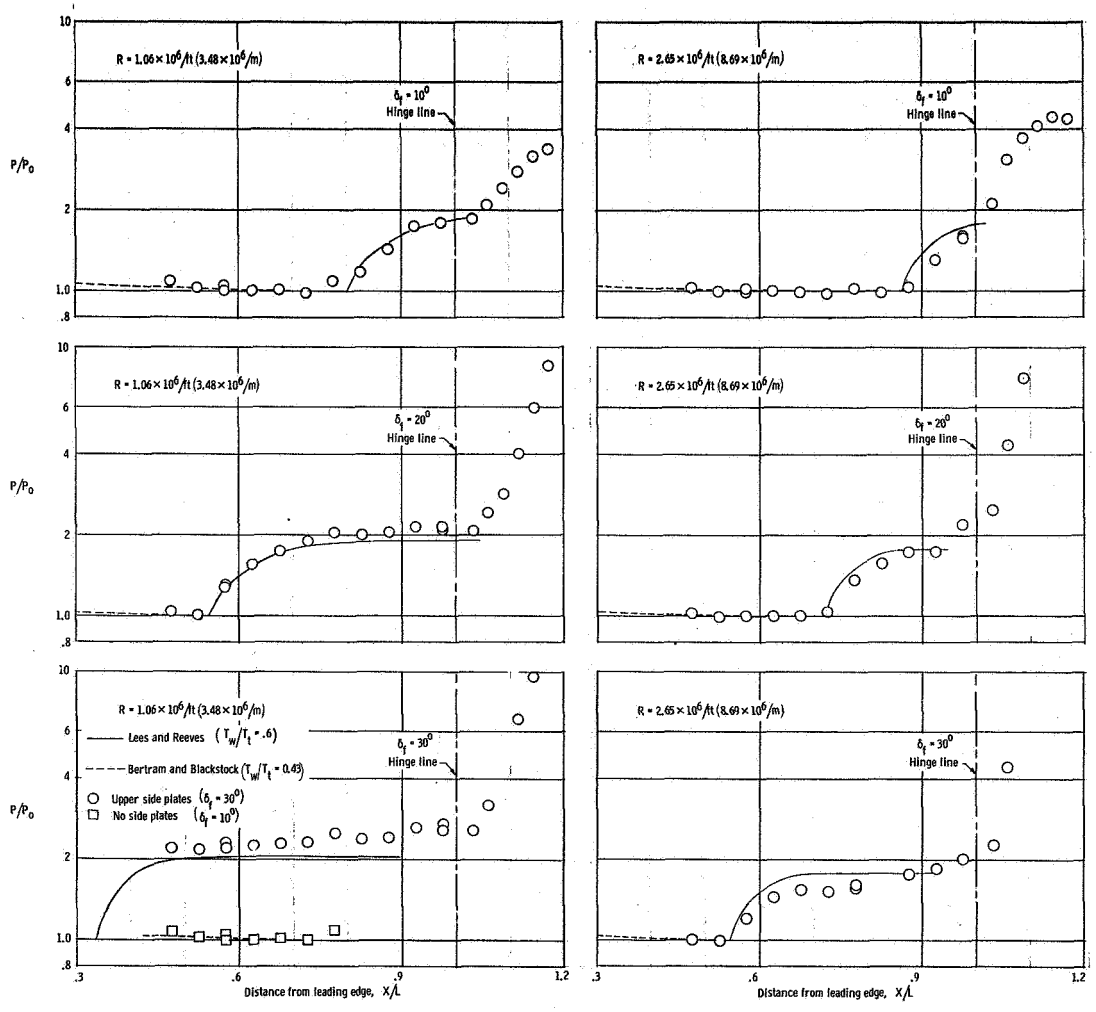

(d) Side plates.

Figure 16.- Concluded.

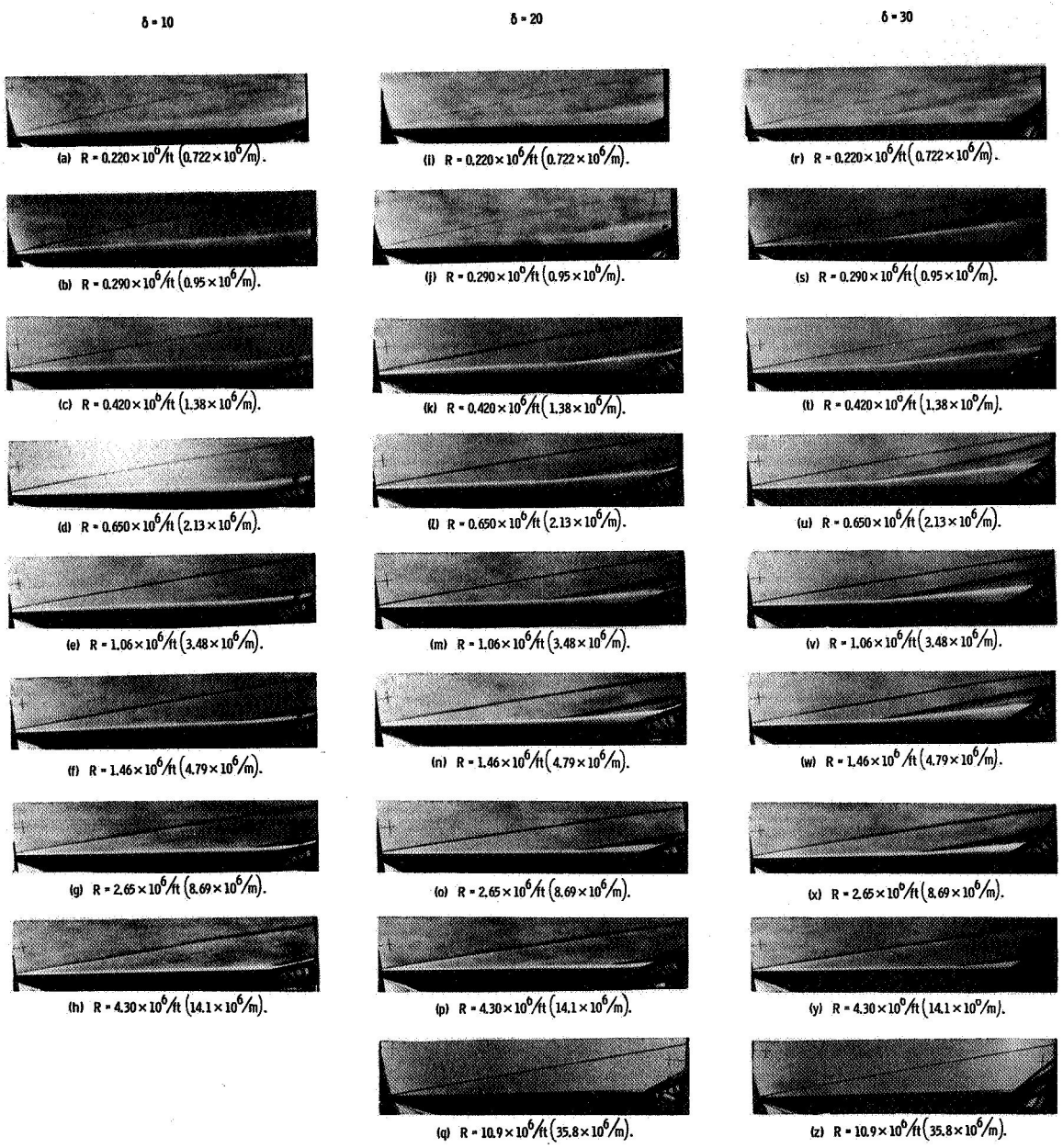

Figure 17.- Schlieren photographs of the flow separation model at $T_w/T_t = 0.43$ for three flap angles and various unit Reynolds numbers.

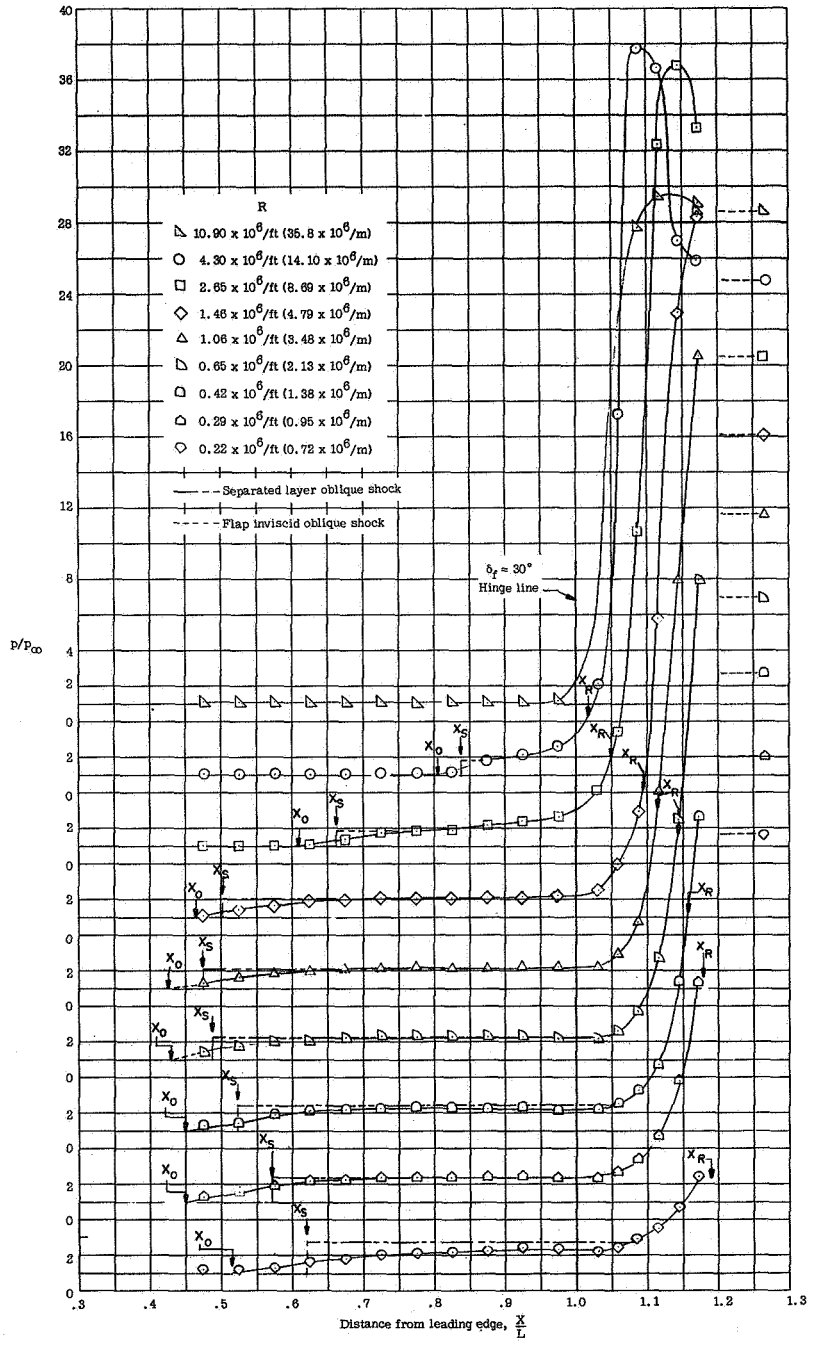

(a) $\delta_f = 30^o$.

Figure 18.- The effect of Reynolds number on the plateau and flap pressures at a $T_w/T_t = 0.43$ for three flap angles, with and without side plates.

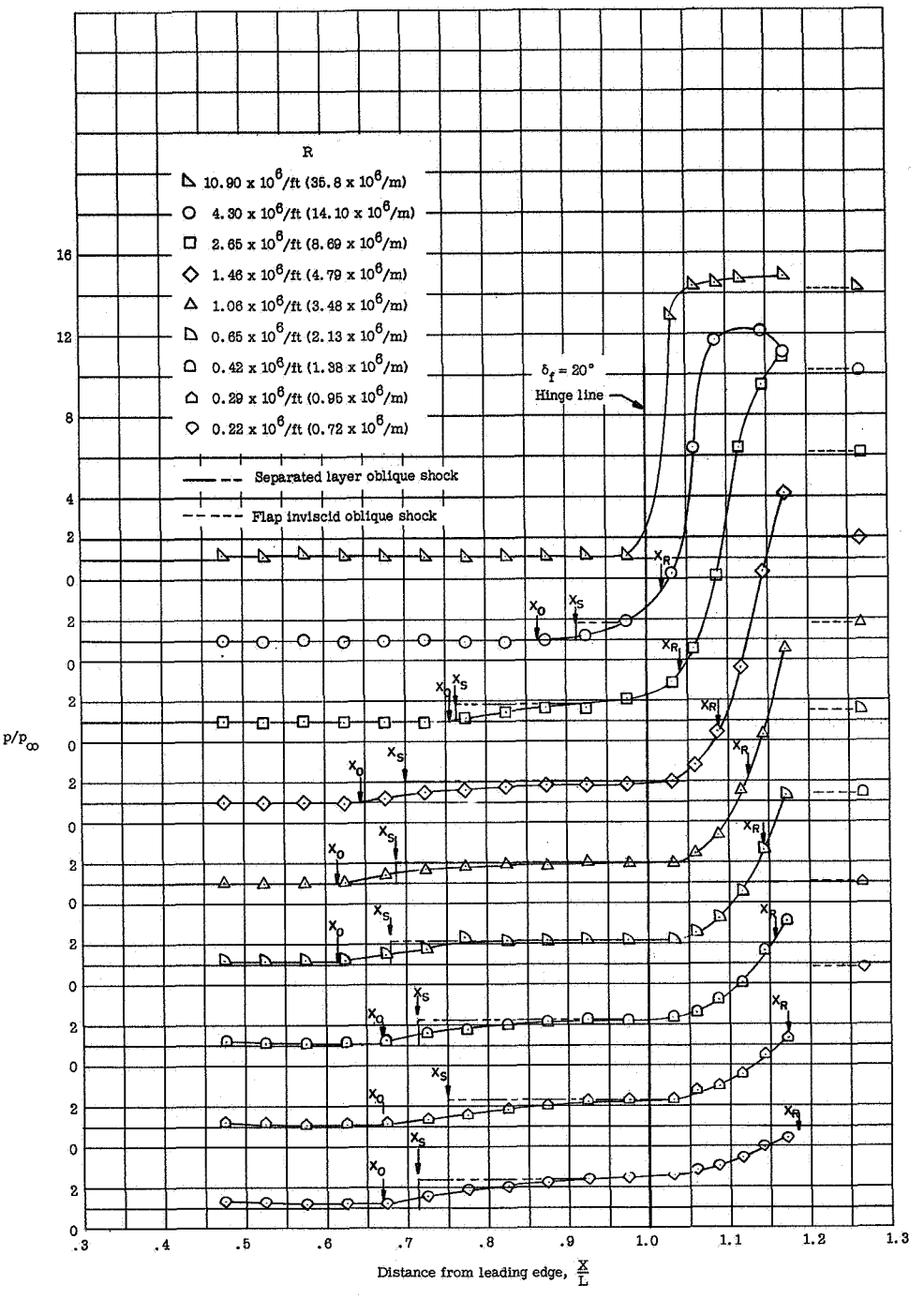

(b) $\delta_f = 20^\circ$.

Figure 18.- Continued.

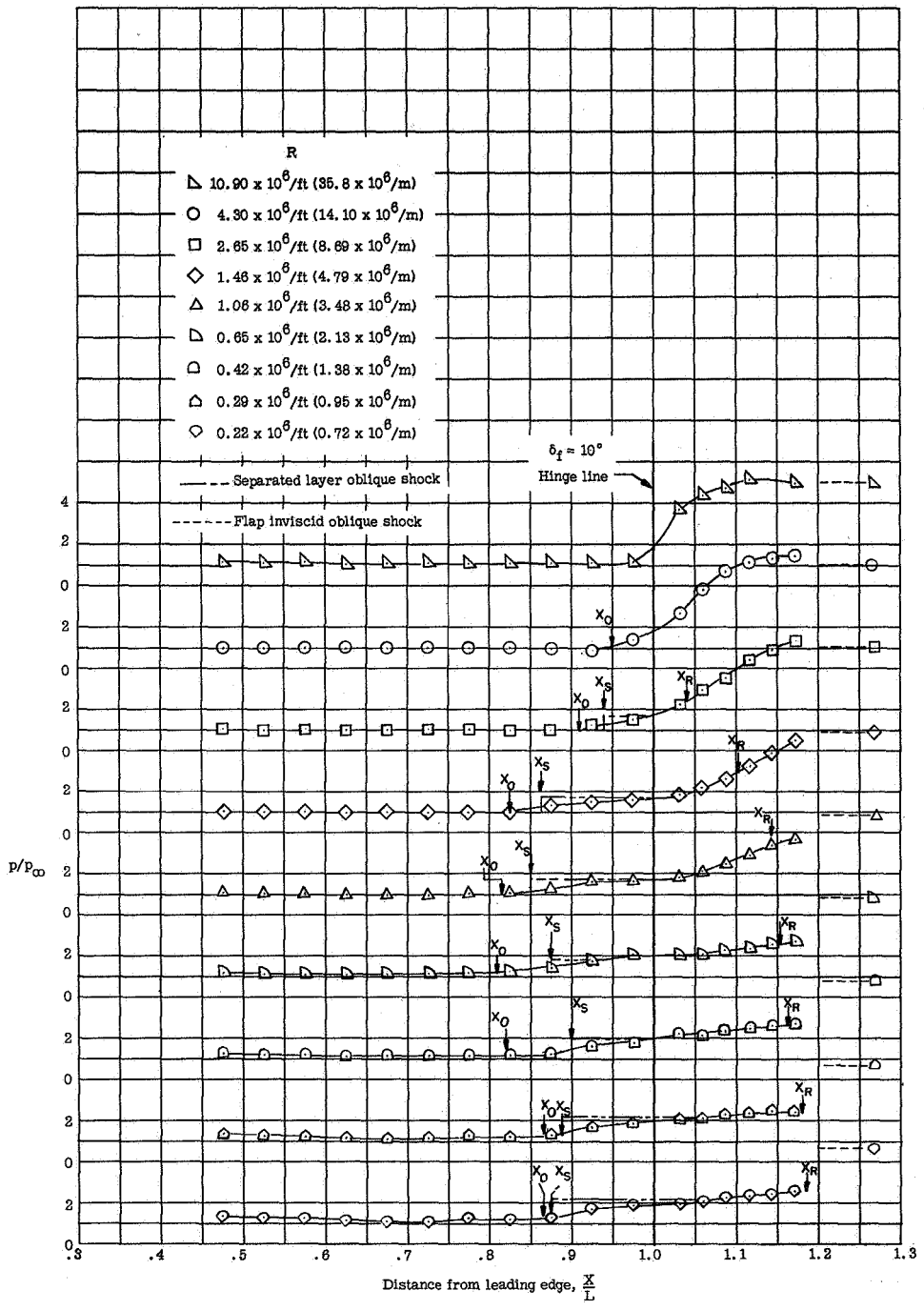

(c) $\delta_f = 10^\circ$.

Figure 18.- Continued.

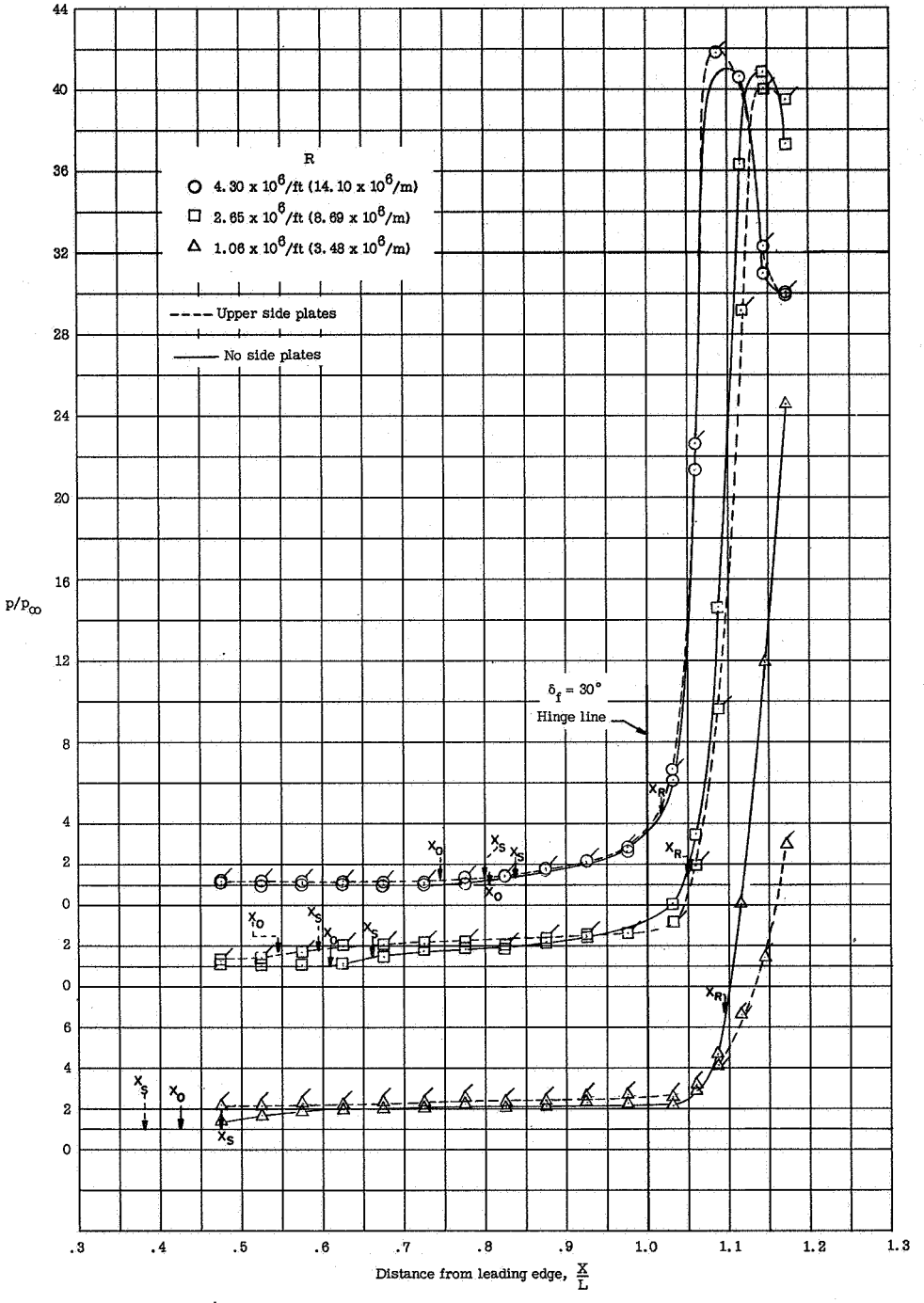

(d) Side plates.

Figure 18.- Continued.

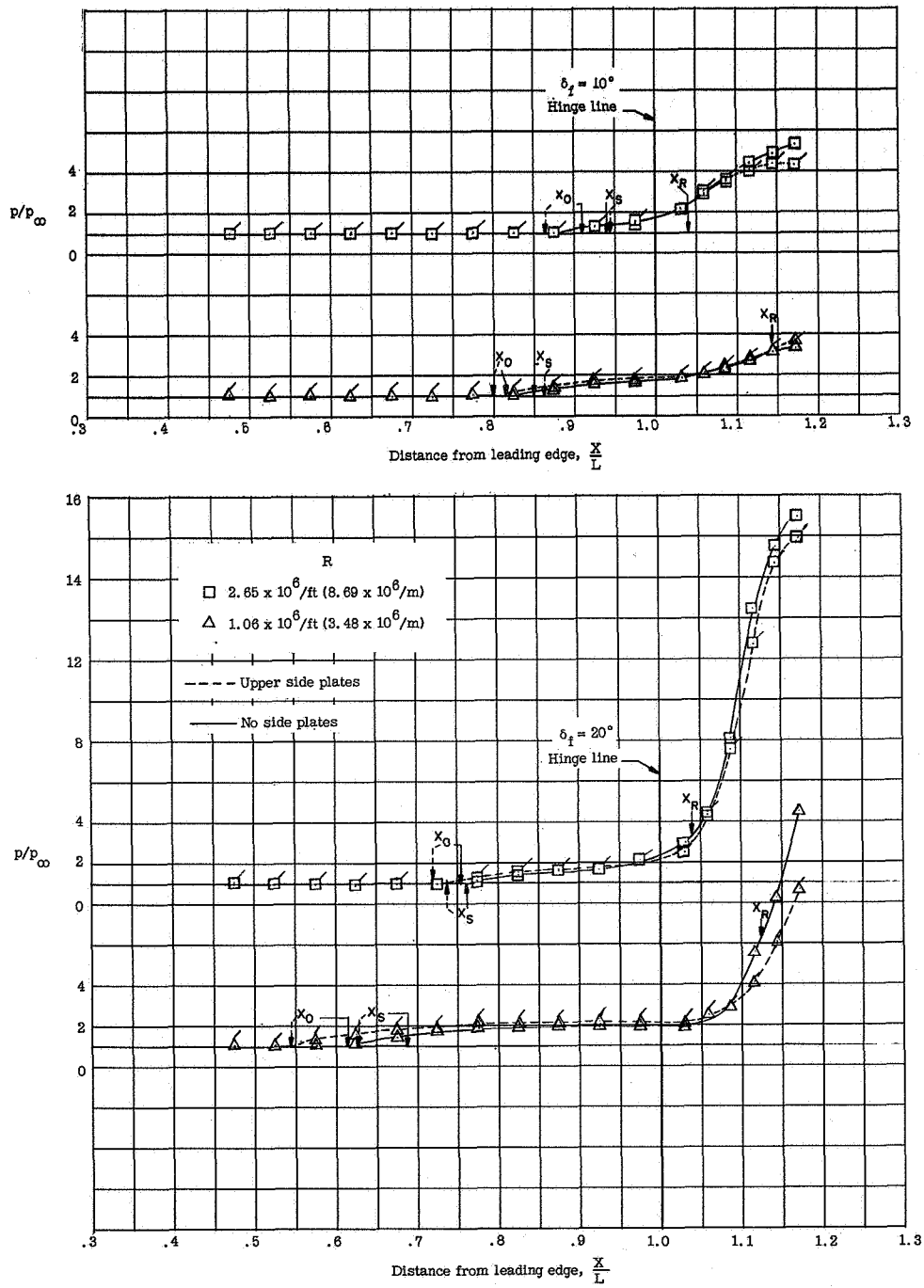

(e) Side plates.

Figure 18.- Concluded.

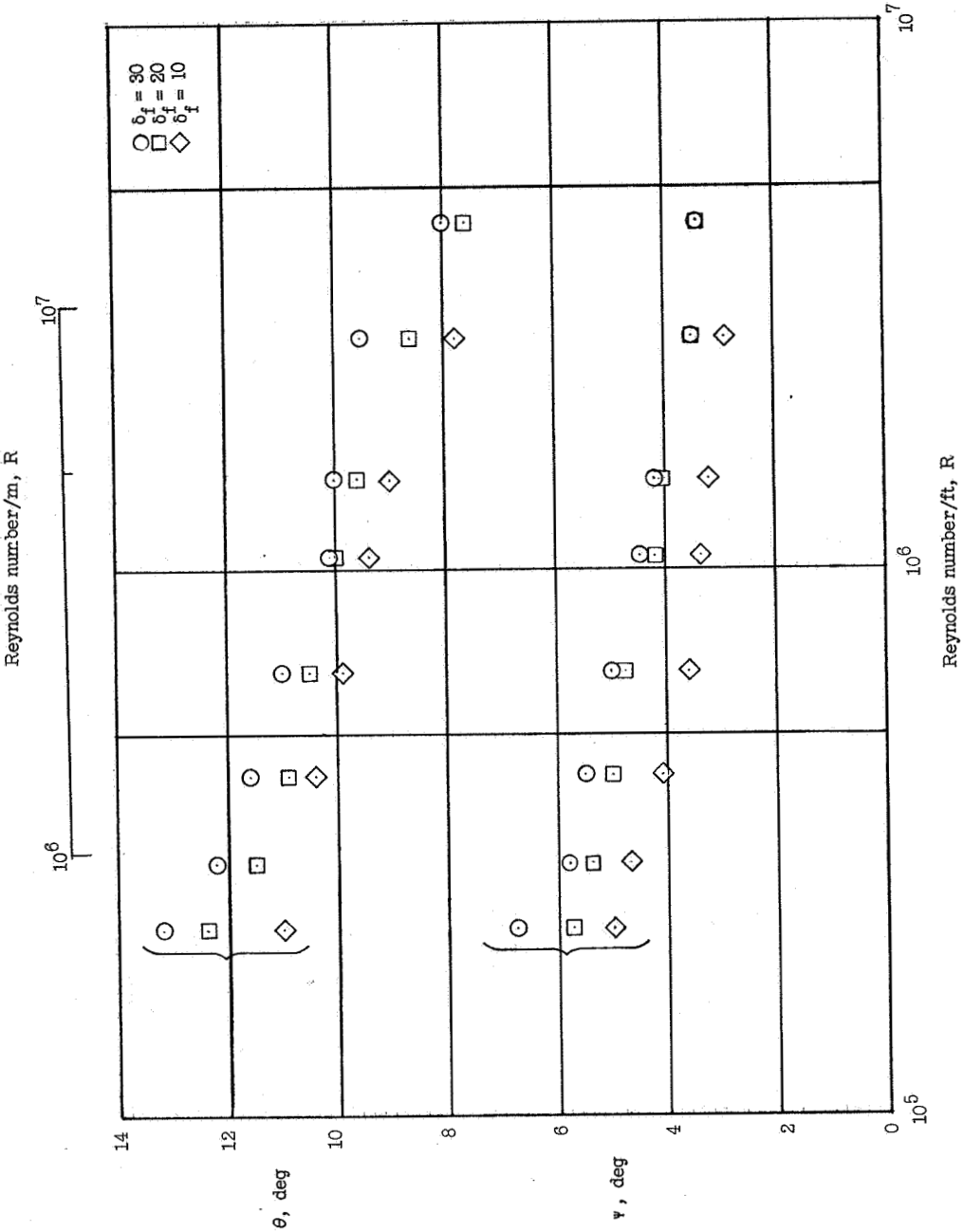

Figure 19.- The effect of Reynolds number and flap angle on the separation point flow deflection angle and the separation shock wave angle for $T_w/T_t = 0.43$.

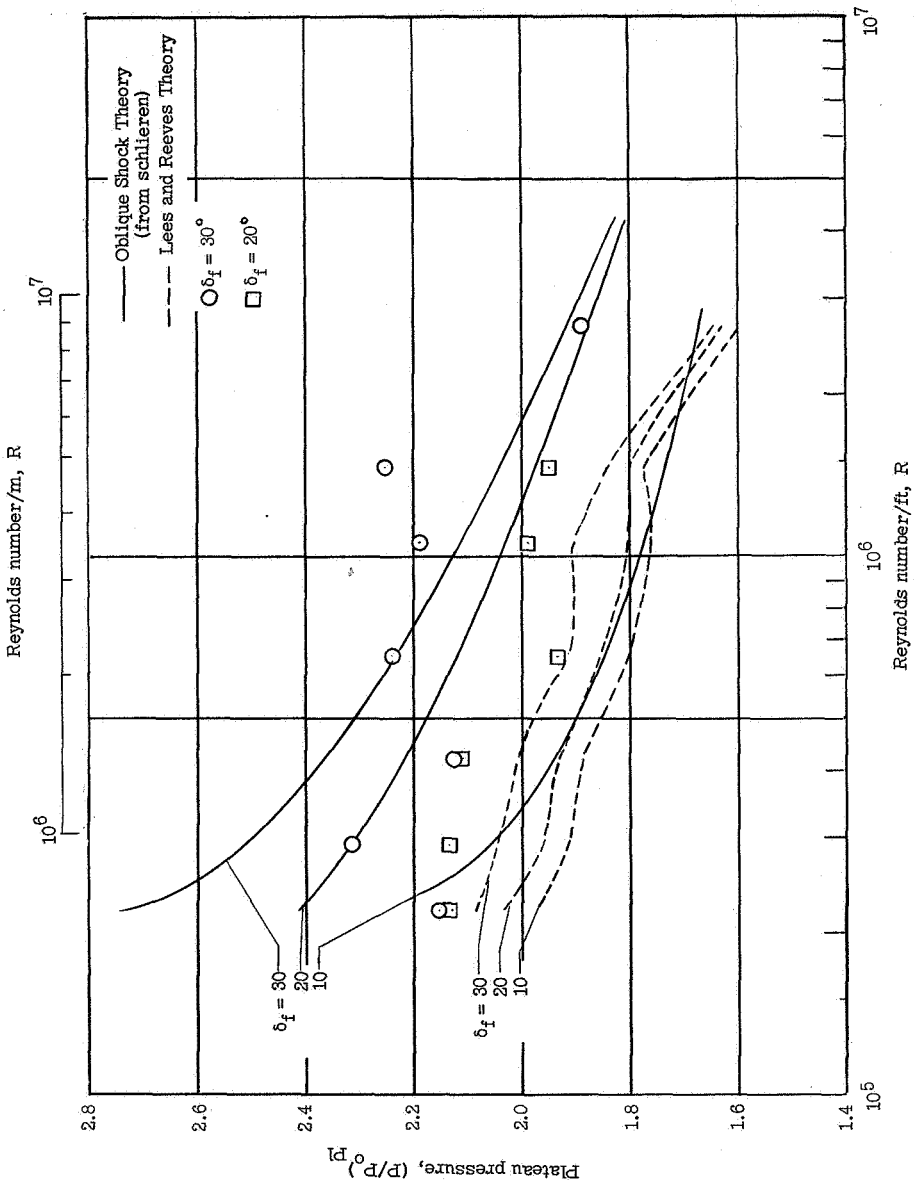

Figure 20.- The effect of Reynolds number and flap angle on three means of determining plateau pressure at $T_w/T_t = 0.43$.

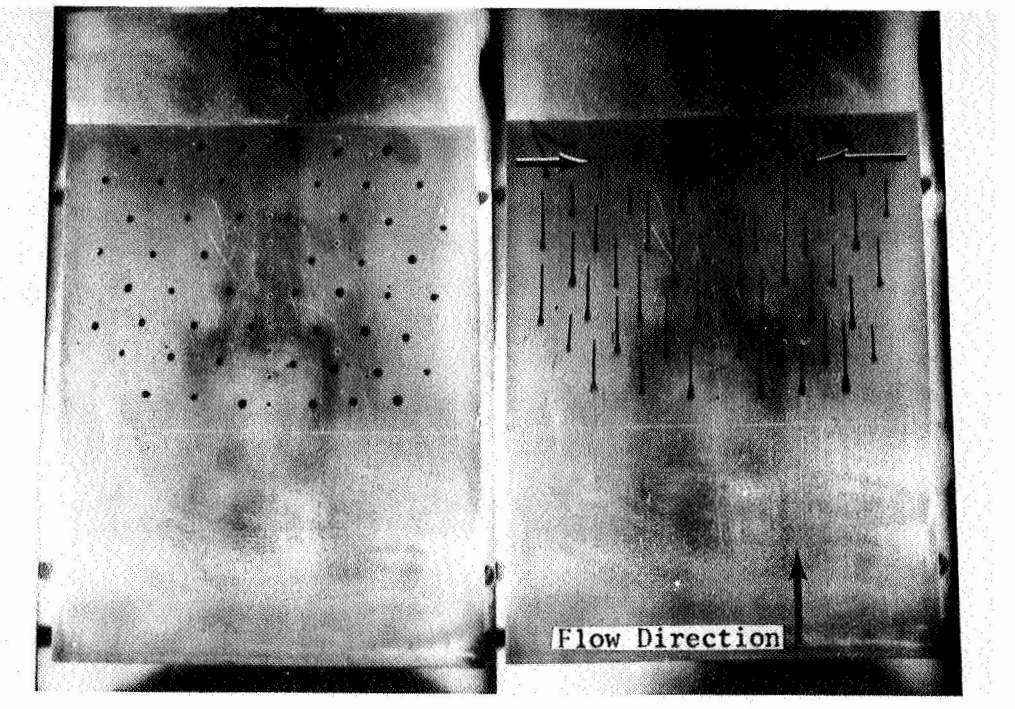

Figure 21.- Photographs of oil-flow patterns before and after tests at a Reynolds number of 4.3×10^6 per foot and a flap angle of 20°.

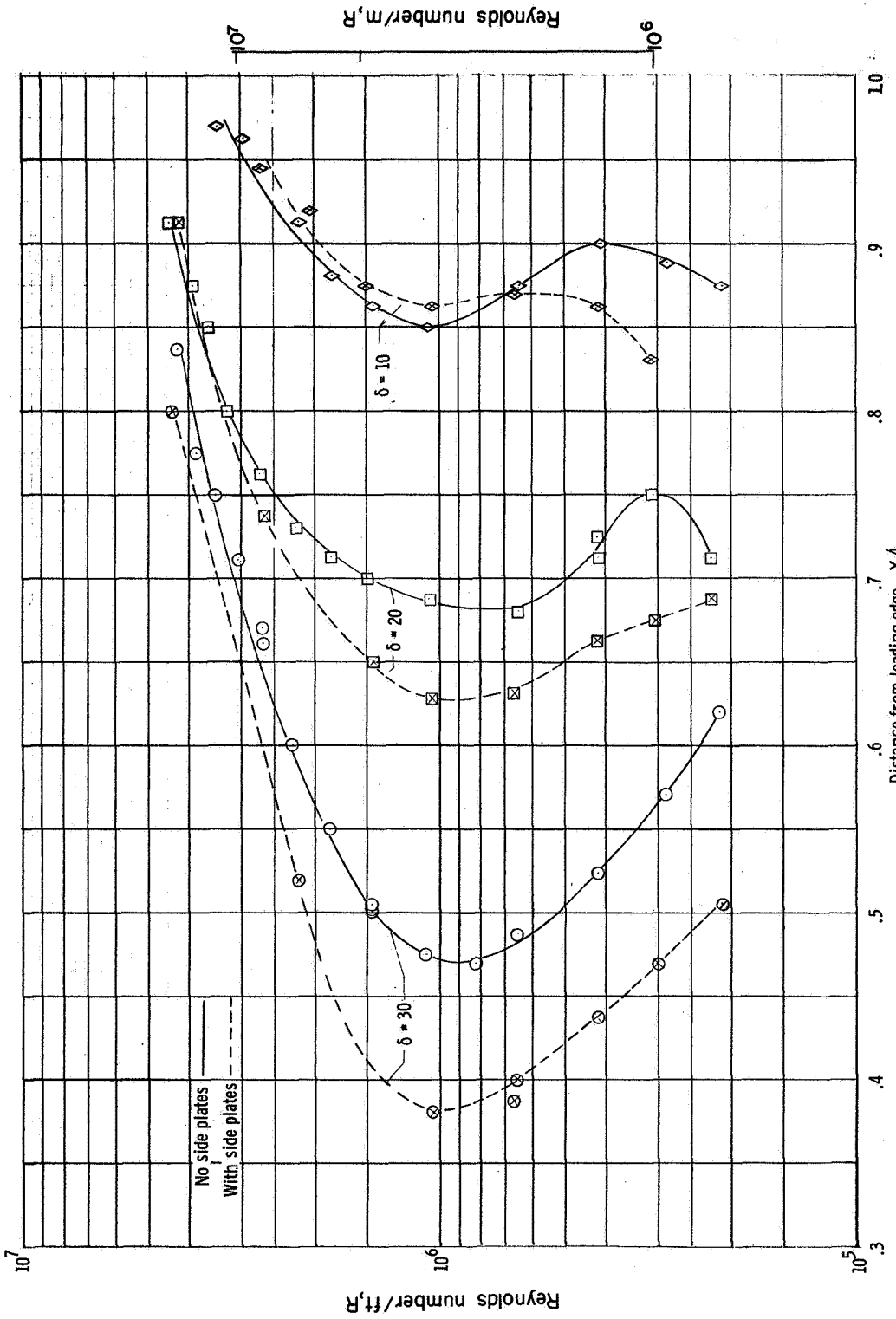

Figure 22.- Location of the separation point for various free-stream unit Reynolds numbers.

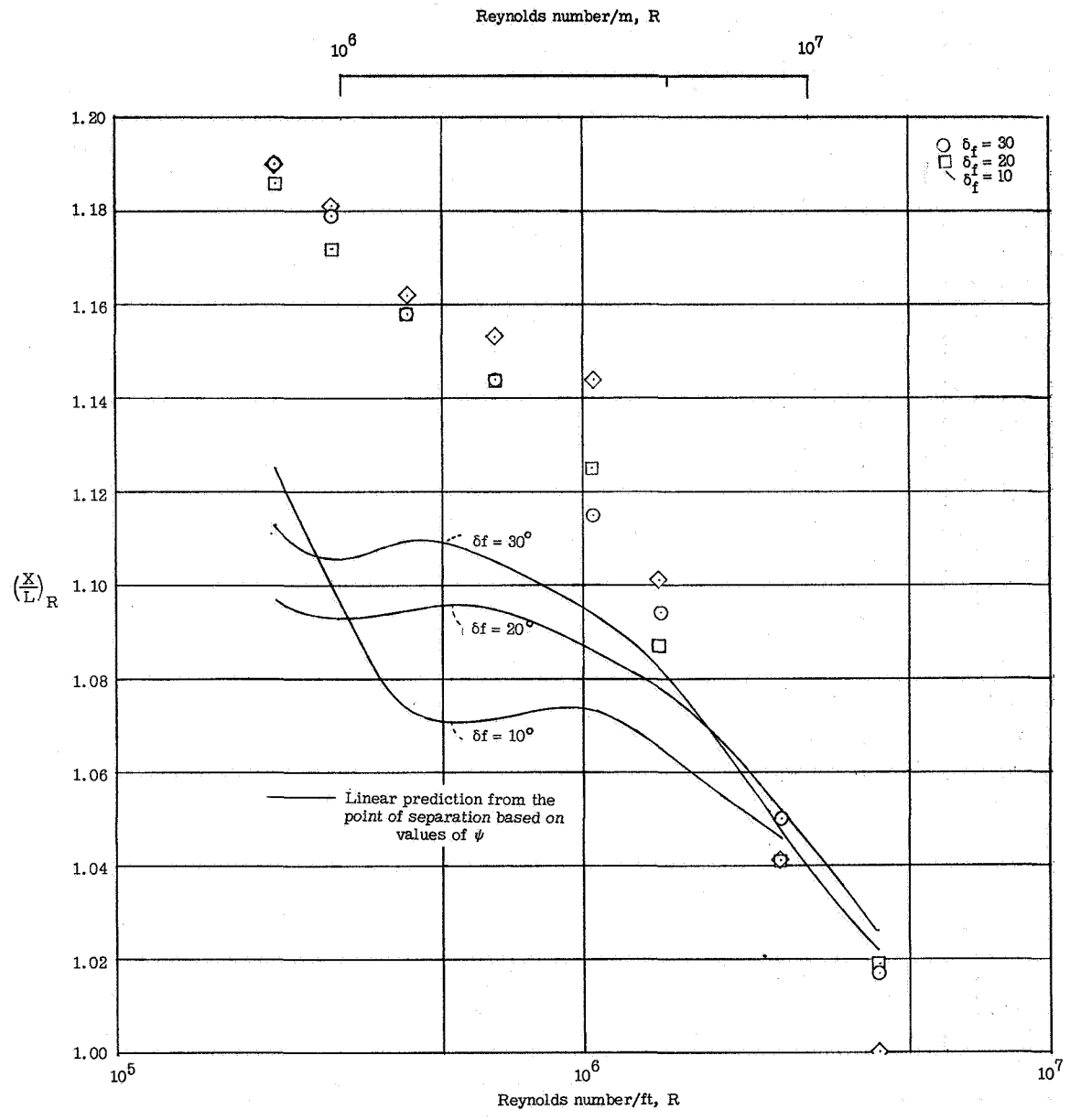

Figure 23.- The effect of Reynolds number and flap angle on the point of reattachment on the flap for $T_w/T_t = 0.43$.

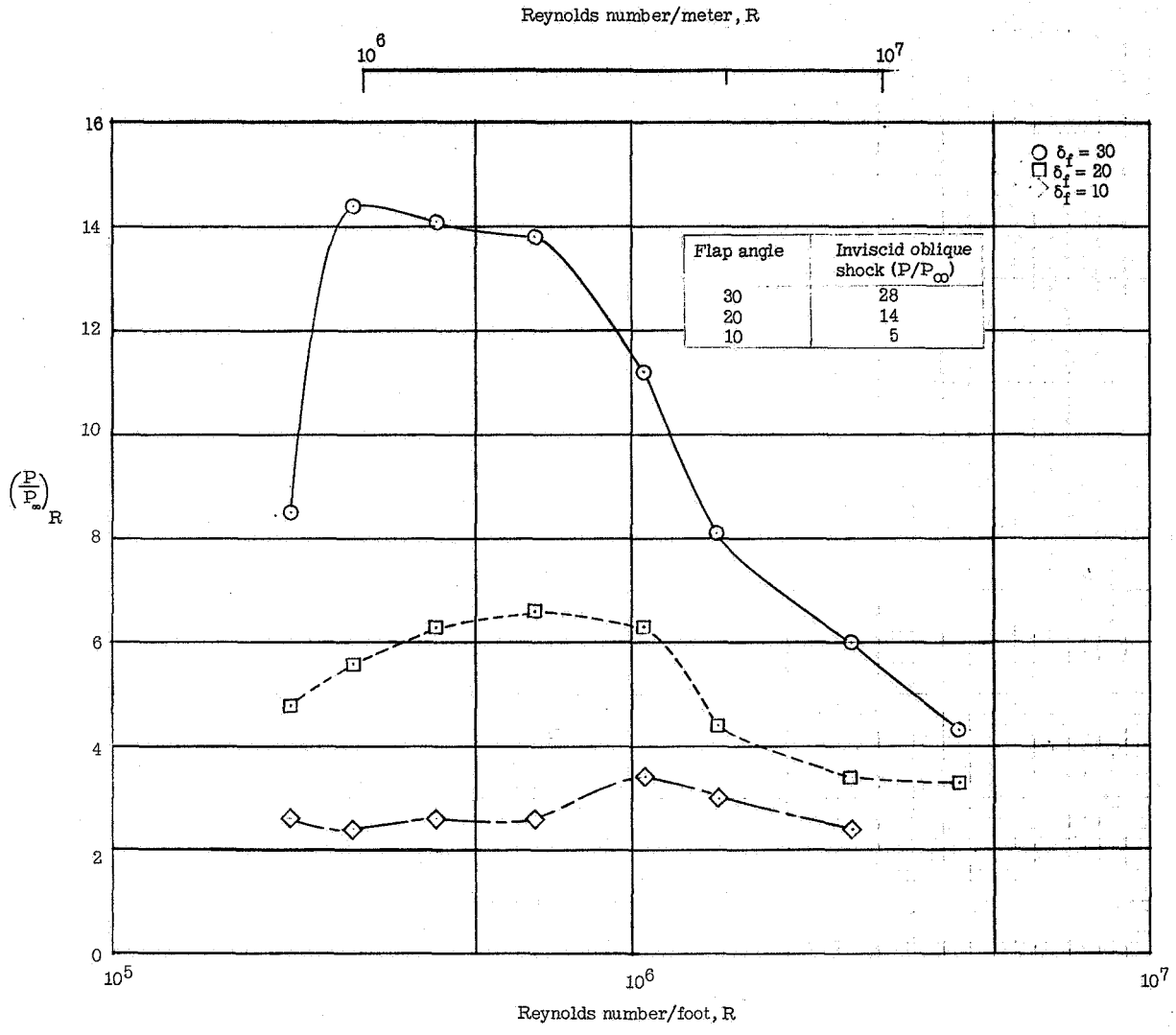

Figure 24.- The effect of Reynolds number and flap angle of the pressure at the reattachment point on the flap for a $T_w/T_t = 0.43$.

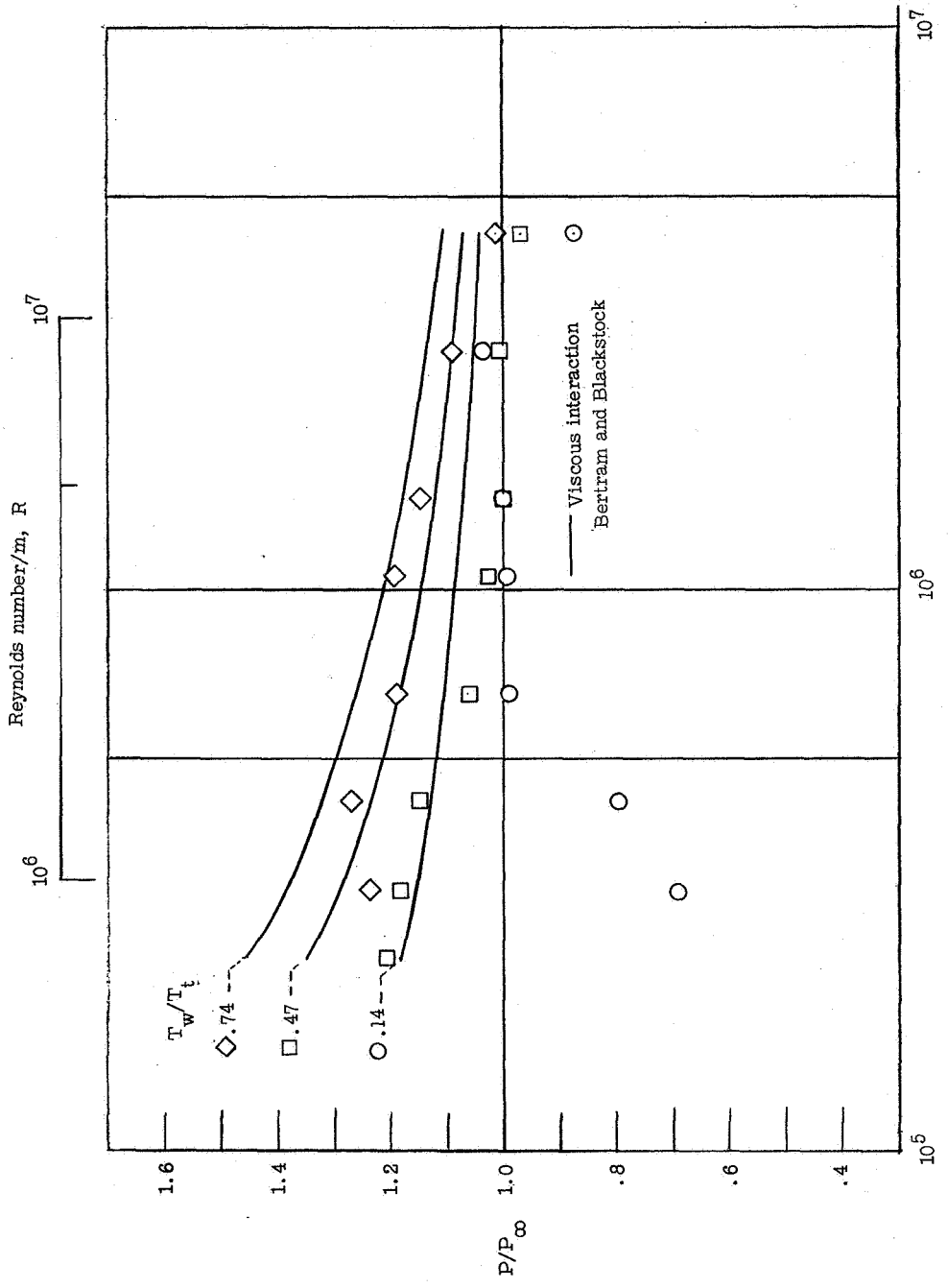

Figure 25.- The effect of wall temperature and Reynolds number on the induced flat-plate pressure 5 inches from the leading edge.

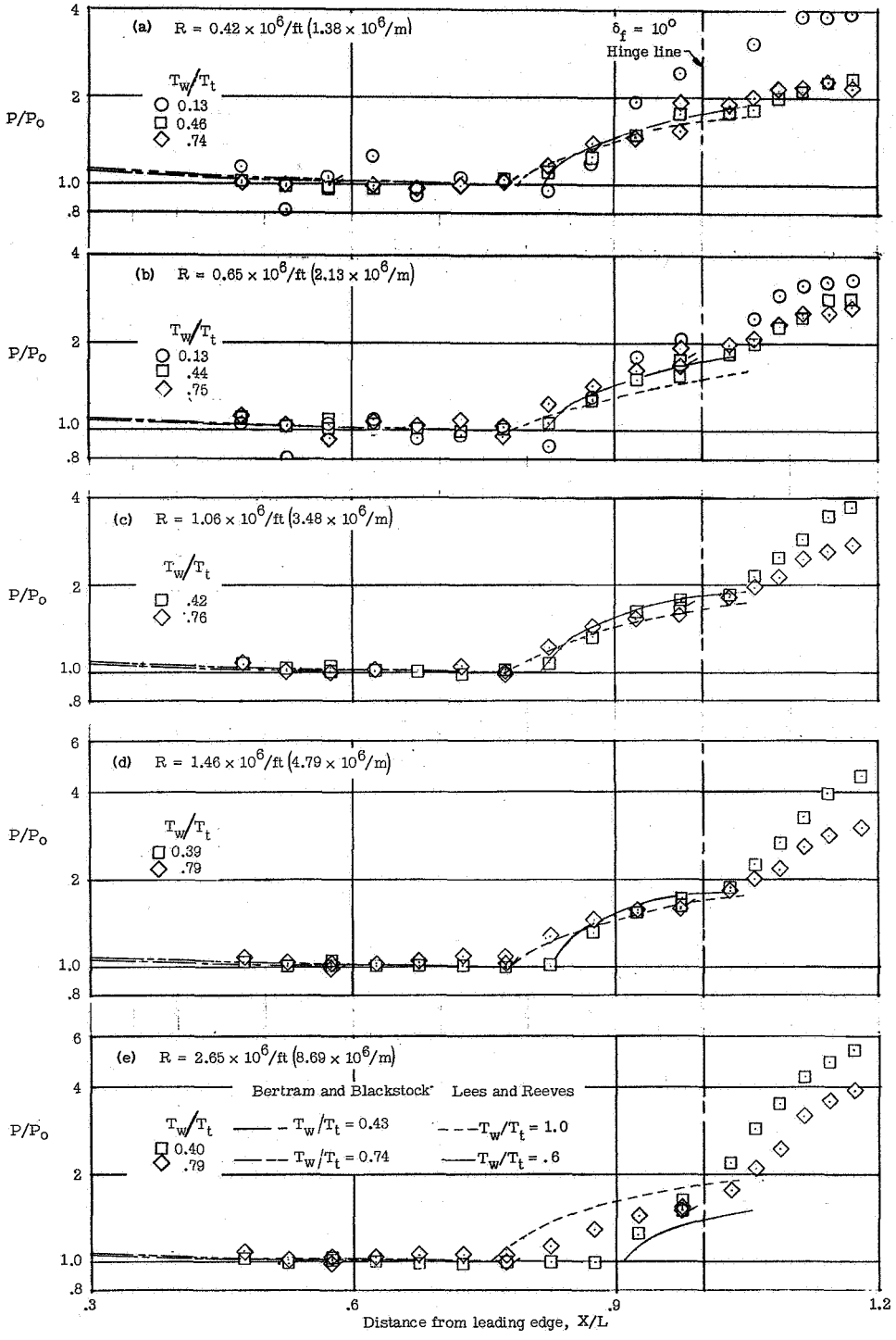

Figure 26.- The effect of wall temperature and Reynolds number on the pressure distribution at a flap angle of 10°.

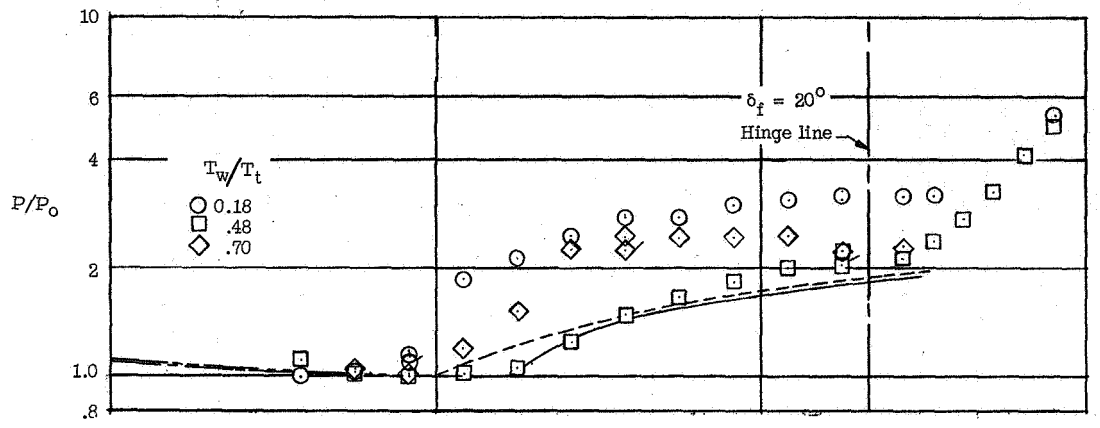

(a) R = 0.29 × 10^6/ft (0.95 × 10^6/m).

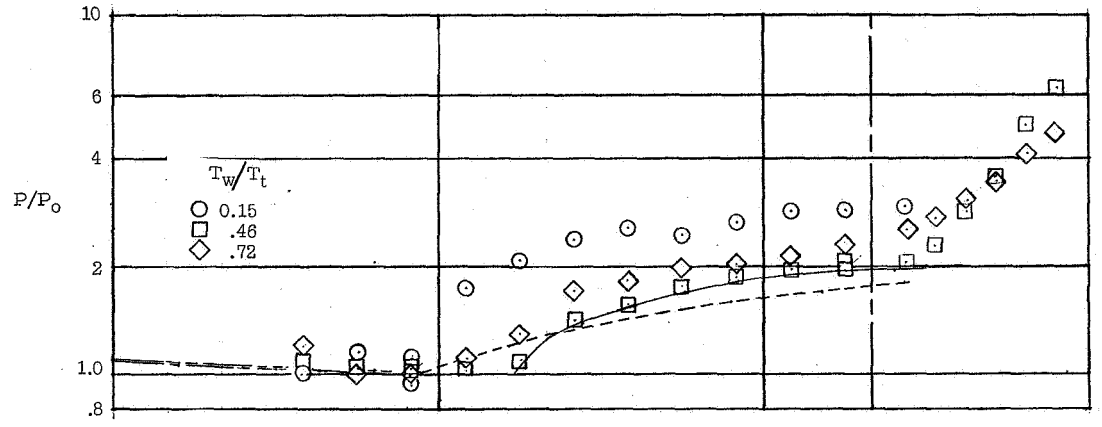

(b) R = 0.42 × 10^6/ft (1.38 × 10^6/m).

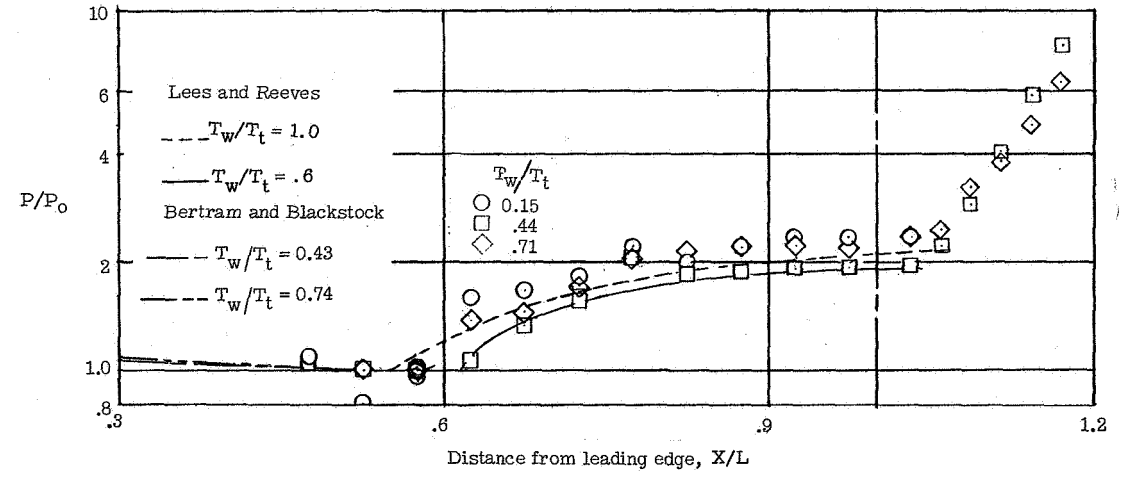

(c) R = 0.65 × 10^6/ft (2.13 × 10^6/m).

Figure 27.- The effect of wall temperature and Reynolds number on the pressure distribution at a flap angle of 20°.

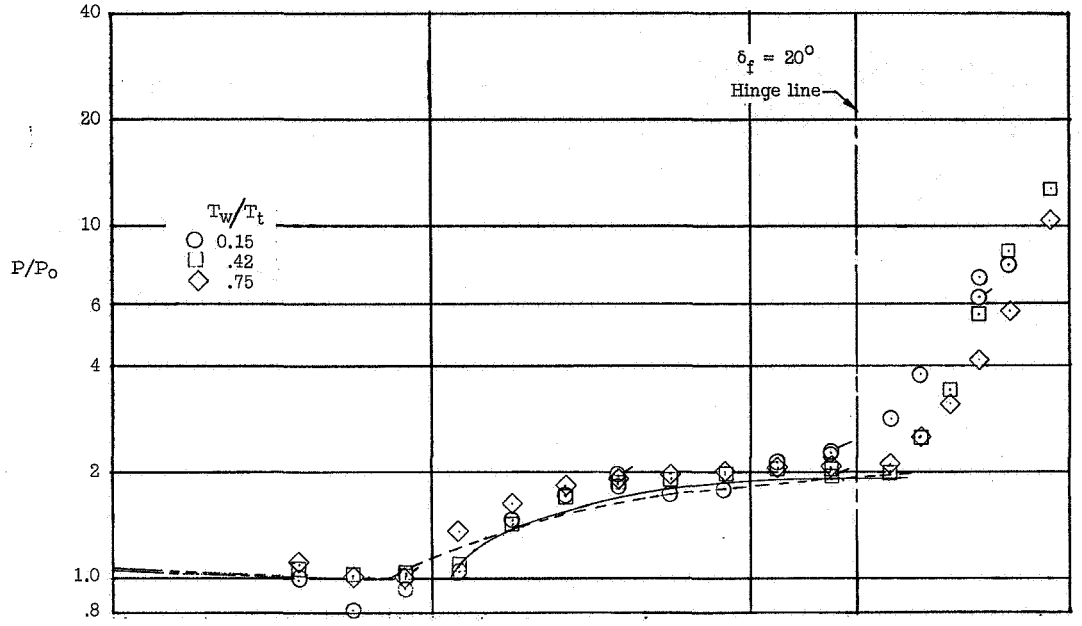

(d) $R = 1.06 \times 10^6/\text{ft}$ $(3.48 \times 10^6/\text{m})$.

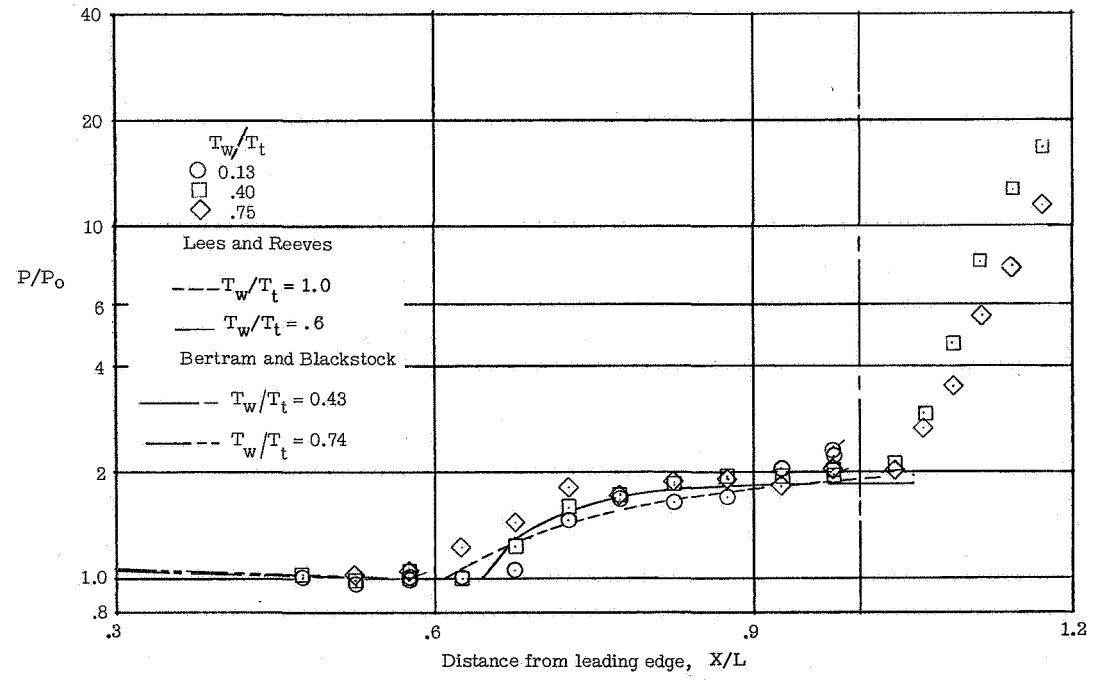

(e) $R = 1.46 \times 10^6/\text{ft}$ $(4.79 \times 10^6/\text{m})$.

Figure 27.- Continued.

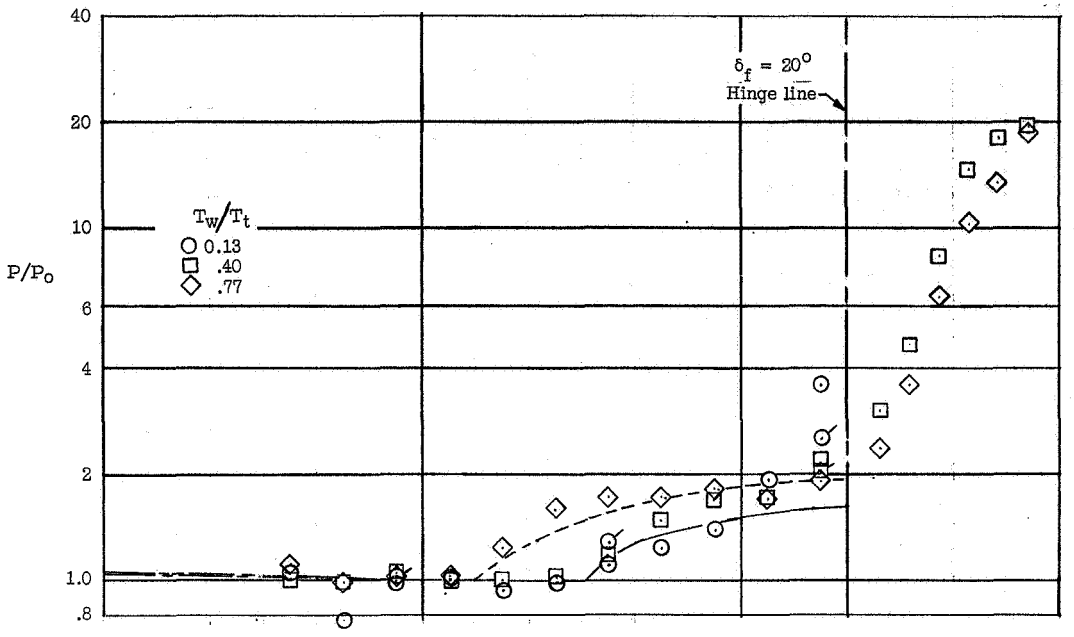

(f) R = 2.65 × 10^6/ft (8.69 × 10^6/m).

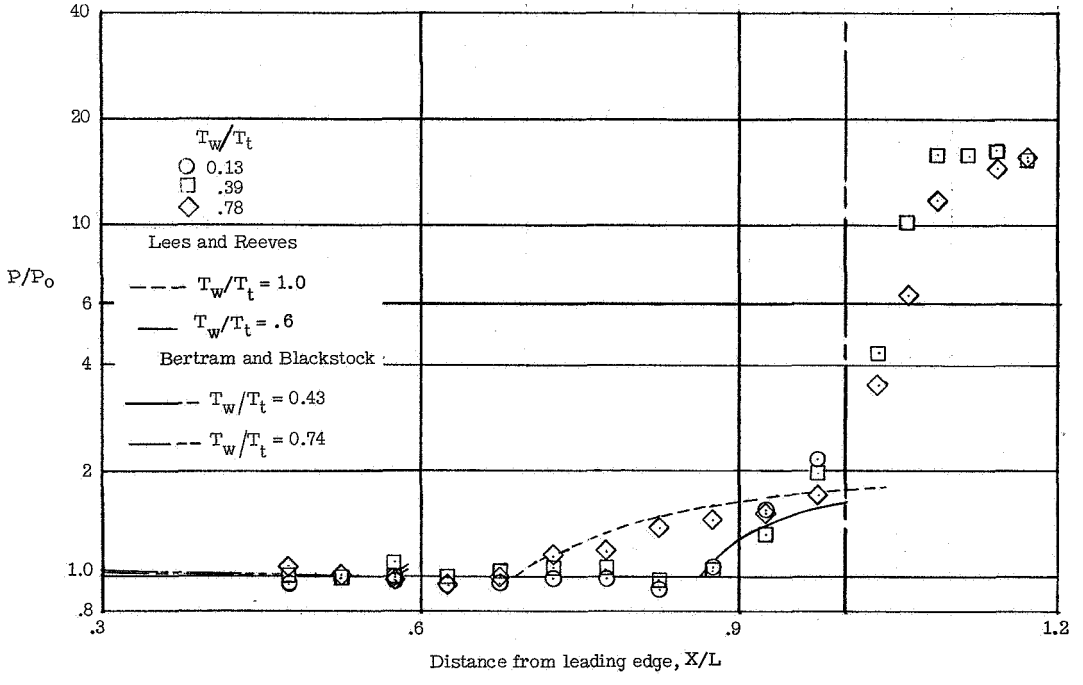

(g) R = 4.3 × 10^6/ft (14.1 × 10^6/m).

Figure 27.- Concluded.

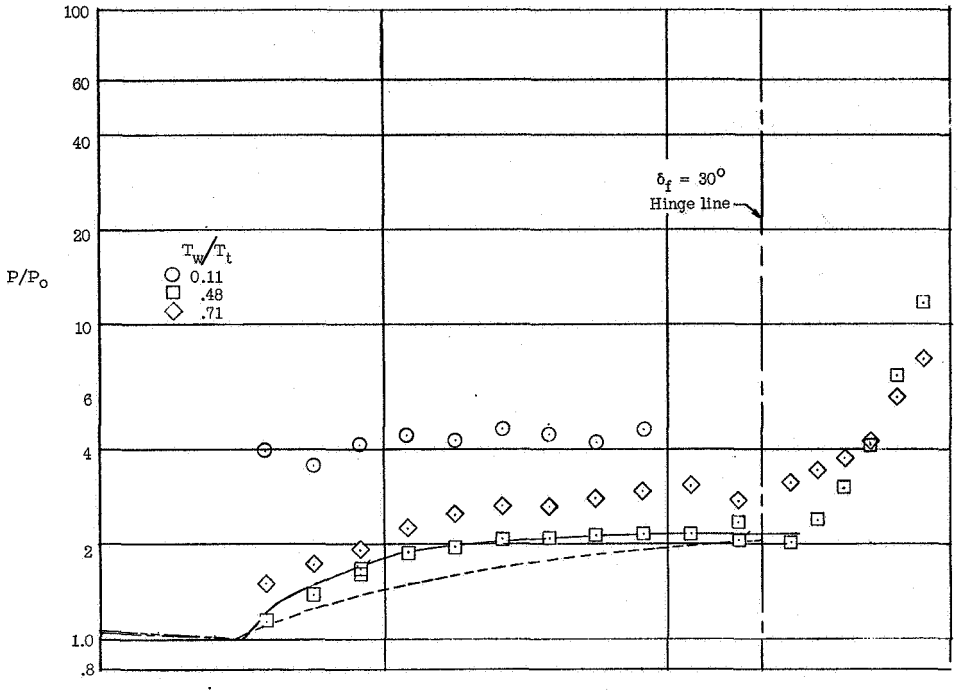

(a) $R = 0.29 \times 10^6/ft \ (0.95 \times 10^6/m)$.

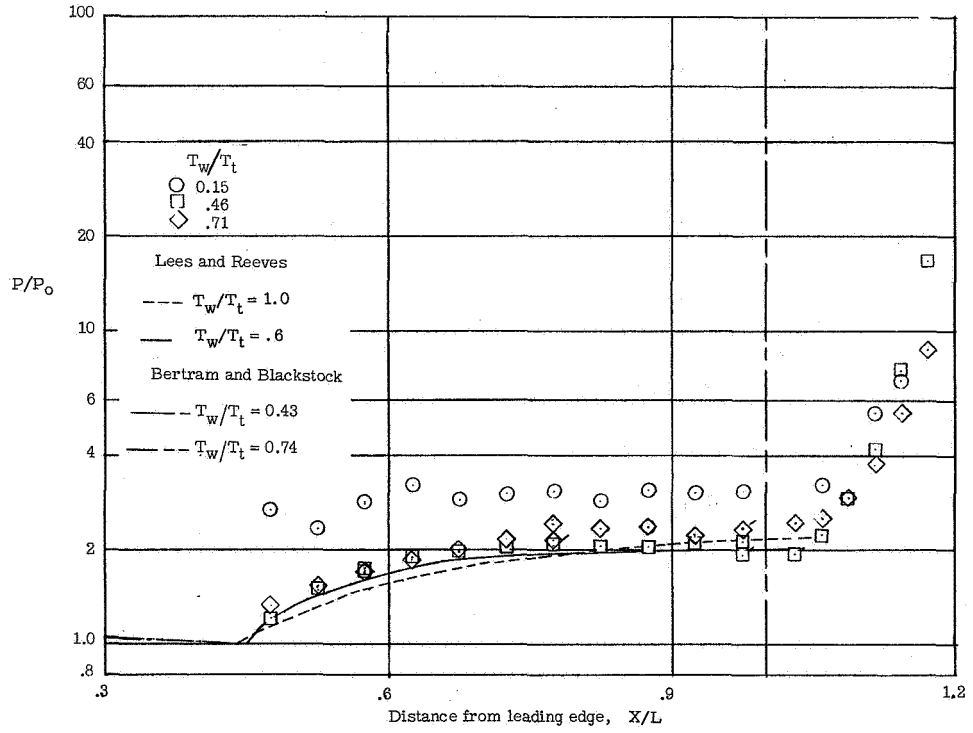

(b) $R = 0.42 \times 10^6/ft \ (1.38 \times 10^6/m)$.

Figure 28.- The effect of wall temperature and Reynolds number on pressure distribution at a flap angle of 30°.

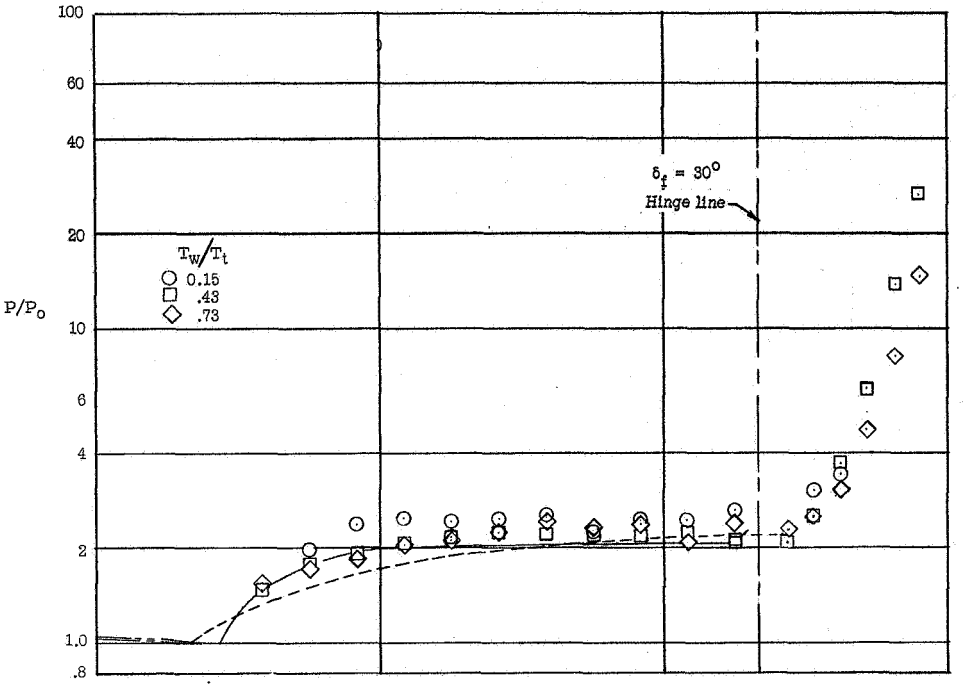

(c) R = 0.65 × 10^6/ft (2.13 × 10^6/m).

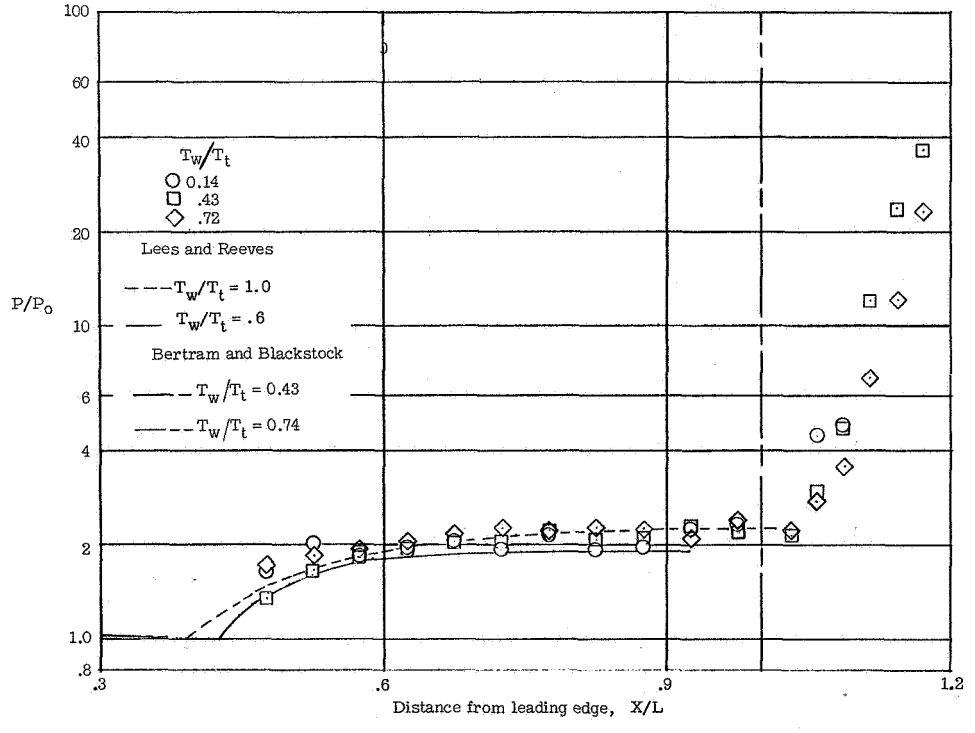

(d) R = 1.06 × 10^6/ft (3.48 × 10^6/m).

Figure 28.- Continued.

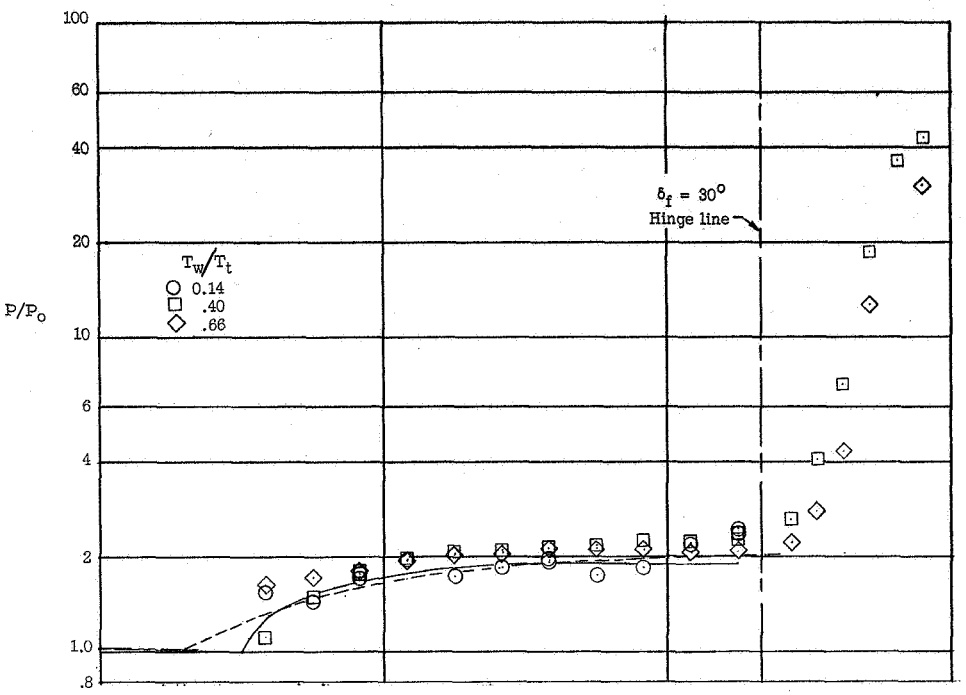

(e) R = 1.46×10^6/ft (4.79×10^6/m).

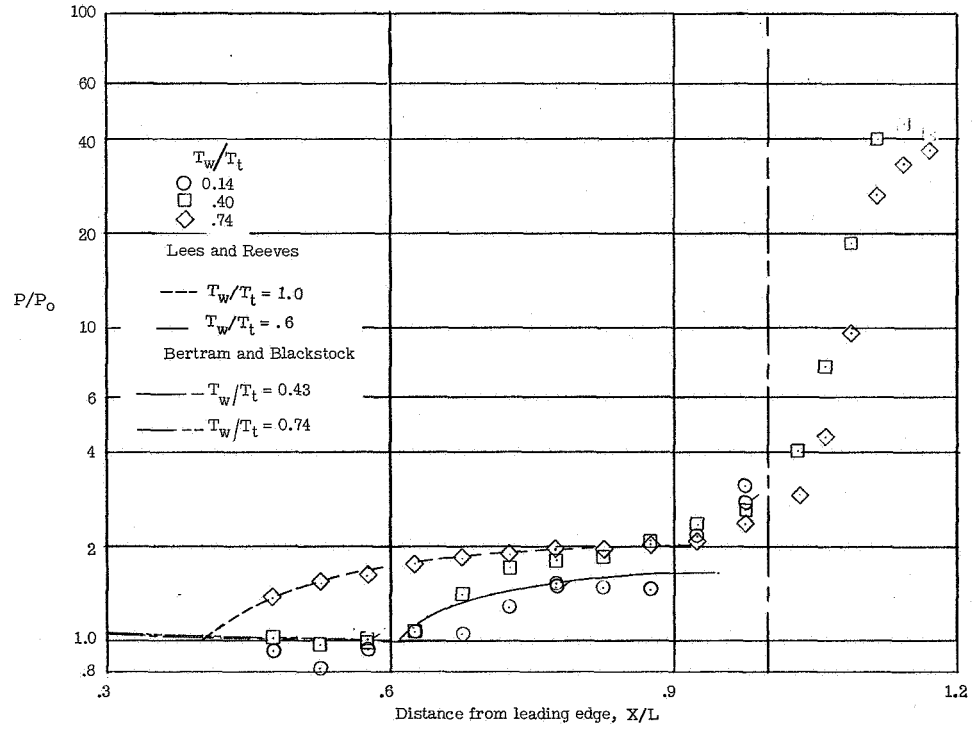

(f) R = 2.65×10^6/ft (8.69×10^6/m).

Figure 28.- Continued.

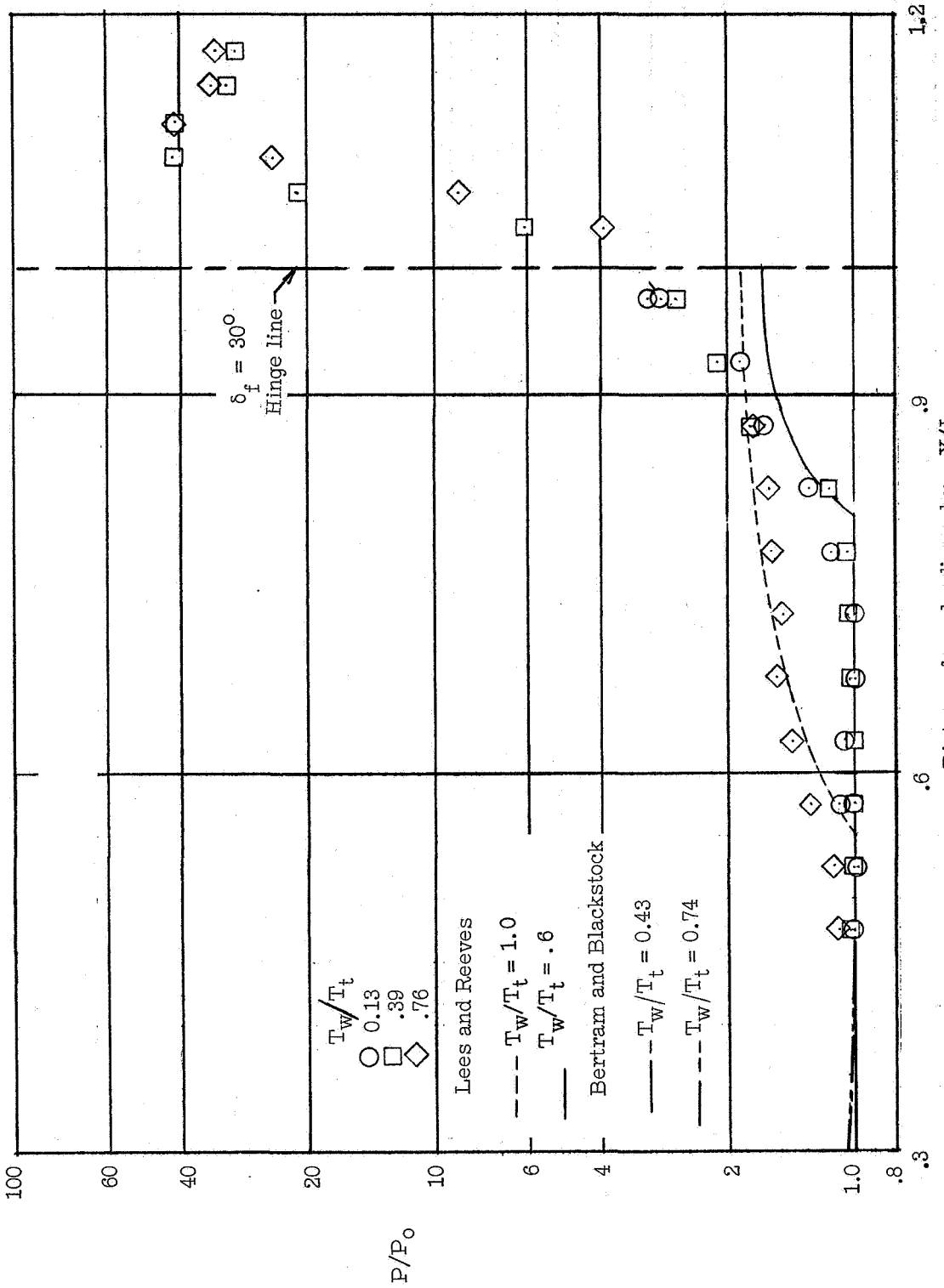

(g) R = 4.3×10^6/ft $(14.1 \times 10^6/m)$.

Figure 28.- Concluded.

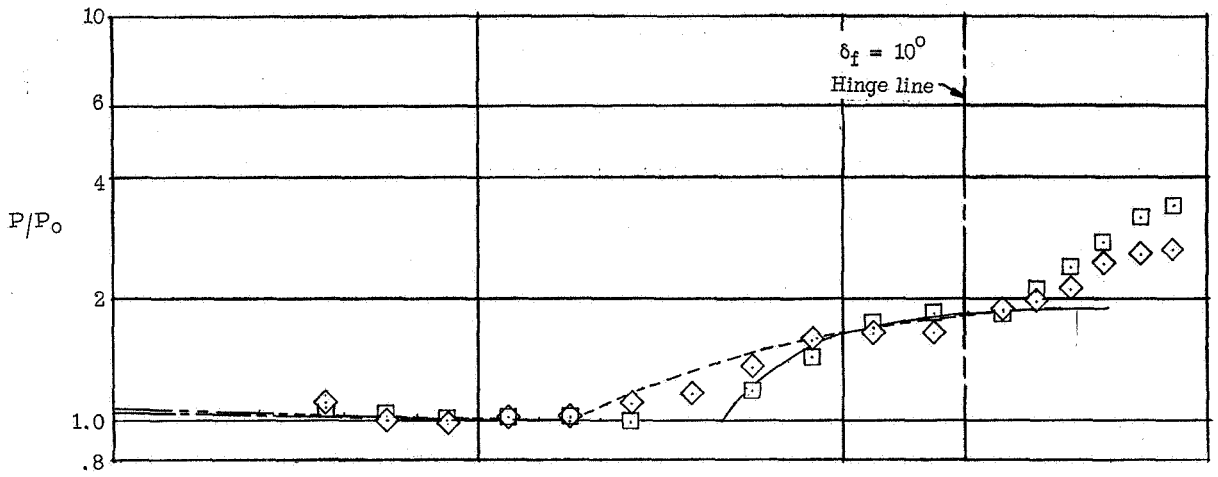

(a) R = 1.06×10^6/ft $(3.48 \times 10^6$/m).

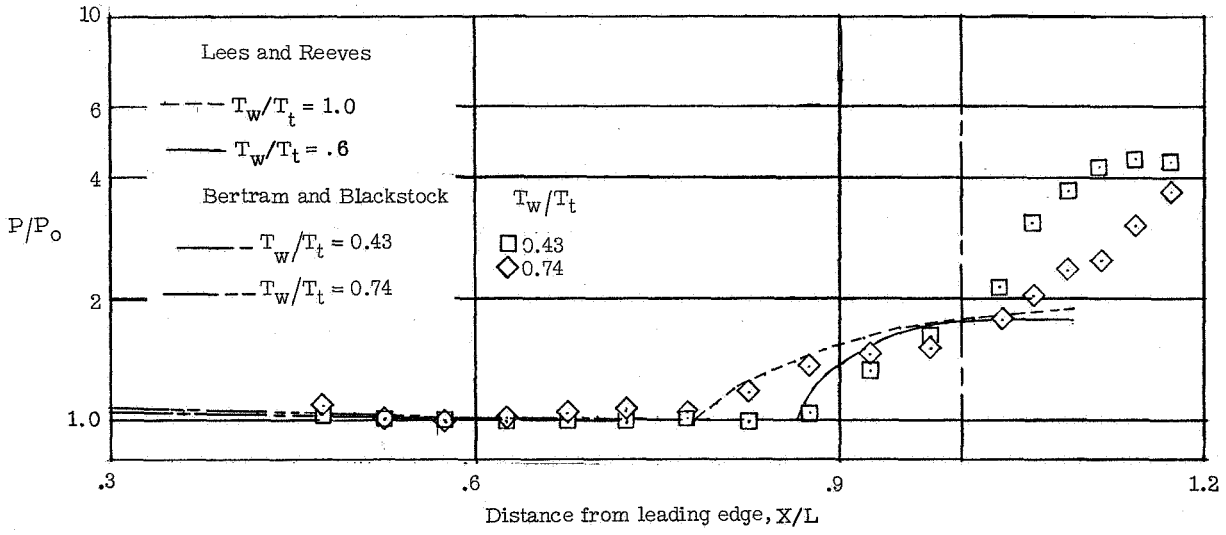

(b) R = 2.65×10^6/ft $(8.69 \times 10^6$/m).

Figure 29.- The effect of wall temperature and Reynolds number on the pressure distribution at a flap angle of 10°. Side plates attached.

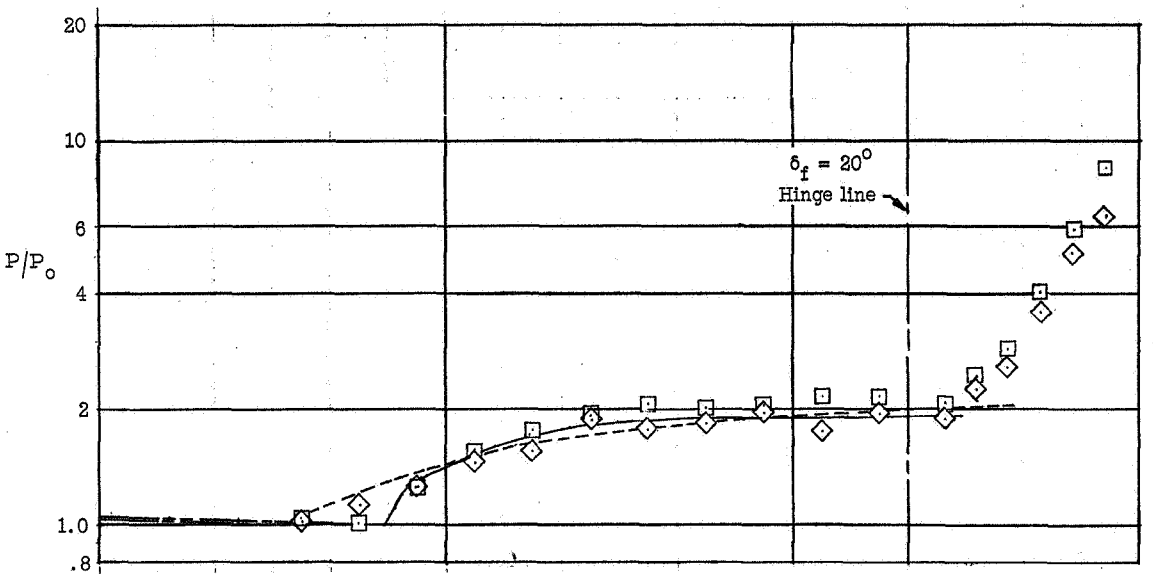

(a) R = 1.06 × 10^6/ft (3.48 × 10^6/m).

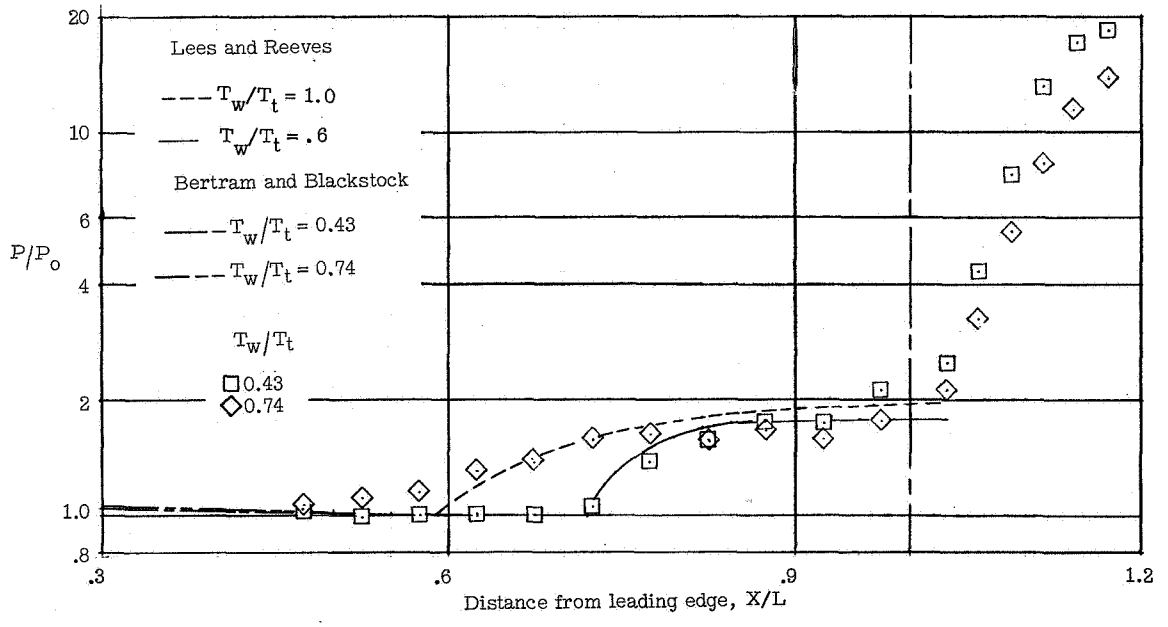

(b) R = 2.65 × 10^6/ft (8.69 × 10^6/m).

Figure 30.- The effect of wall temperature, Reynolds number, and side plates on the pressure distribution at a flap angle of 20°.

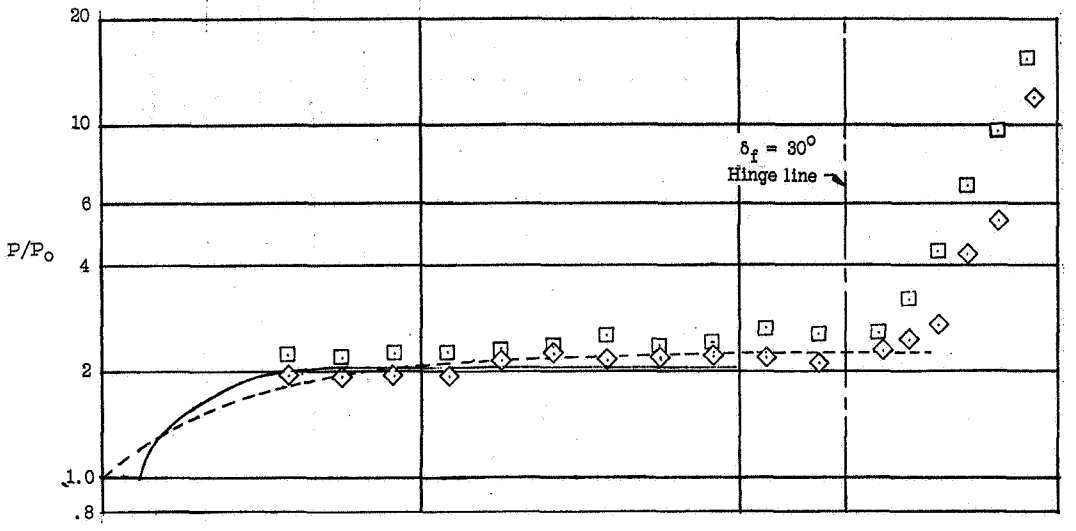

(a) $R = 1.06 \times 10^6/ft \left(3.48 \times 10^6/m\right)$.

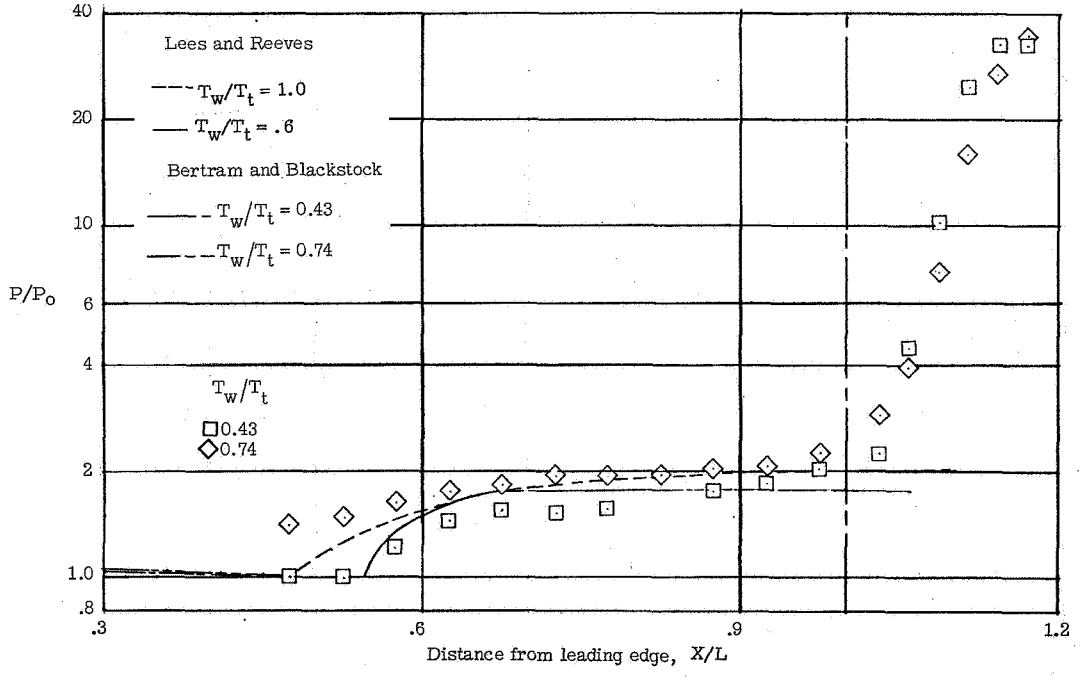

(b) $R = 2.65 \times 10^6/ft \left(8.69 \times 10^6/m\right)$.

Figure 31.- The effect of wall temperature, Reynolds number, and side plates on the pressure distribution at a flap angle of 30°.

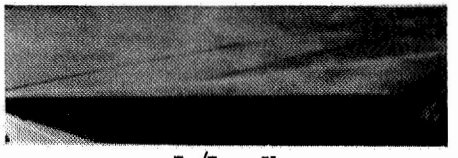

T_w/T_t = .51

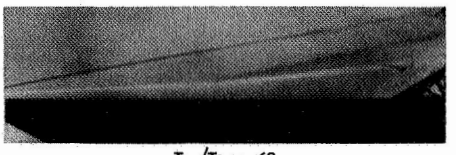

T_w/T_t = .68

(a) R = 0.220×10^6/ft (0.722×10^6/m), δ = 30.

T_w/T_t = .15

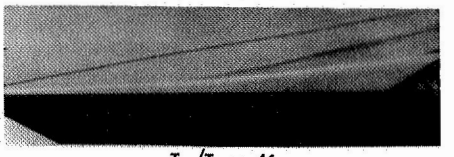

T_w/T_t = .46

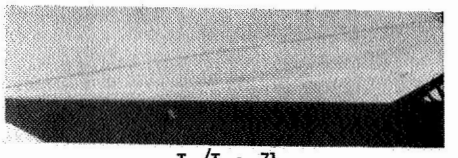

T_w/T_t = .71

(c) R = 0.420×10^6/ft (1.38×10^6/m), δ = 30.

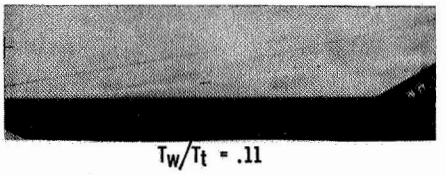

T_w/T_t = .11

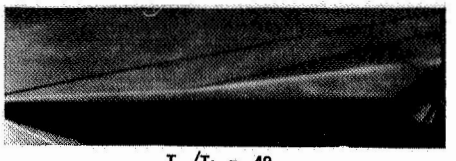

T_w/T_t = .48

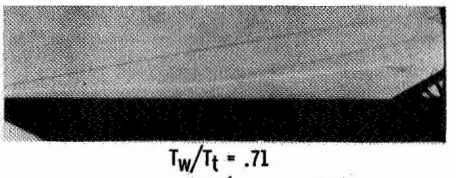

T_w/T_t = .71

(b) R = 0.290×10^6/ft (0.950×10^6/m), δ = 30.

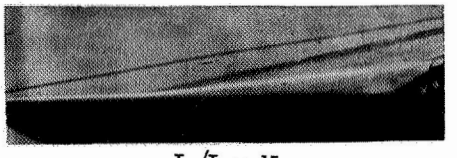

T_w/T_t = .15

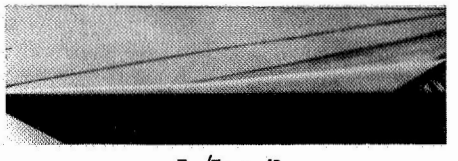

T_w/T_t = .43

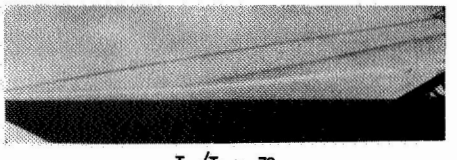

T_w/T_t = .73

(d) R = 0.65×10^6/ft (2.13×10^6/m), δ = 30.

Figure 32.- Schlieren photographs showing wall temperature effects various Reynolds numbers and flap angles.

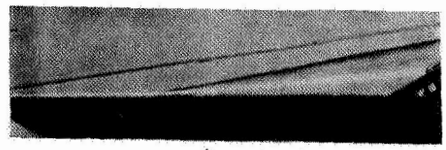

T_w/T_t = .14

T_w/T_t = .43

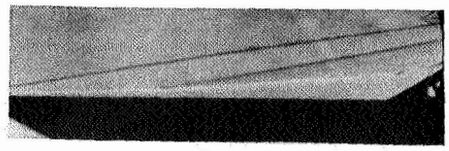

T_w/T_t = .72

(a) R = 1.06×10^6/ft (3.48×10^6/m), δ = 30.

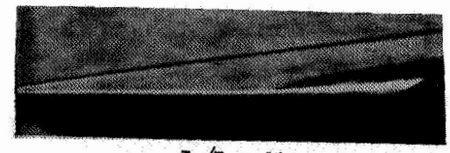

T_w/T_t = .14

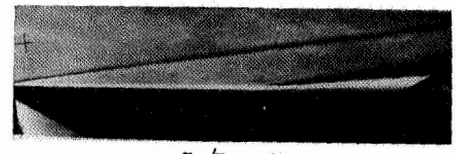

T_w/T_t = .40

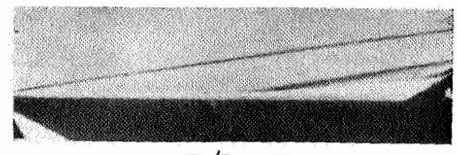

T_w/T_t = .74

(c) R = 2.65×10^6/ft (8.69×10^6/m), δ = 30.

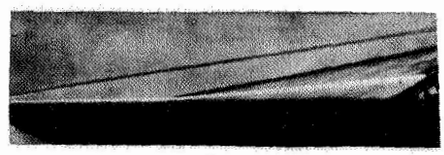

T_w/T_t = .14

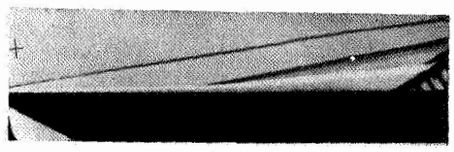

T_w/T_t = .40

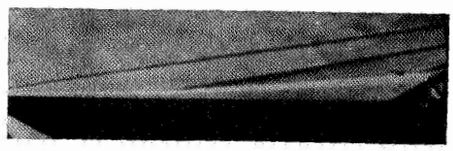

T_w/T_t = .66

(b) R = 1.46×10^6/ft (4.79×10^6/m), δ = 30.

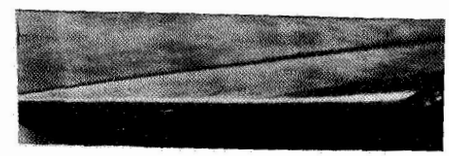

T_w/T_t = .13

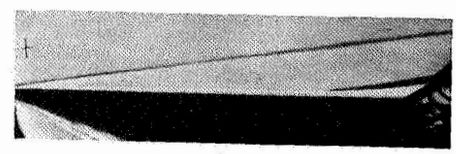

T_w/T_t = .39

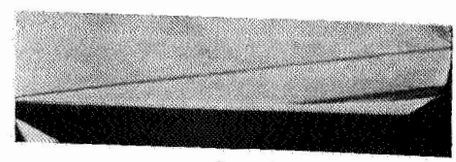

T_w/T_t = .76

(d) R = 4.30×10^6/ft (14.1×10^6/m), δ = 30.

Figure 32.- Continued.

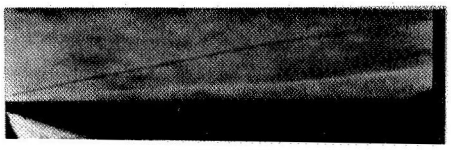

T_w/T_t = .51

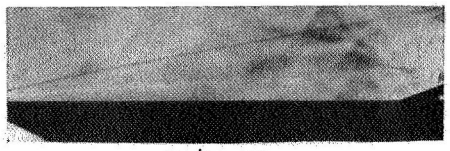

T_w/T_t = .70

(a) R = 0.220×10^6/ft (0.722×10^6/m), δ = 20

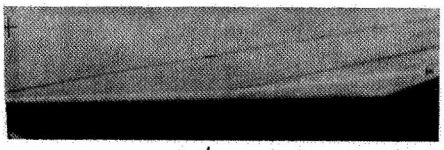

T_w/T_t = .15

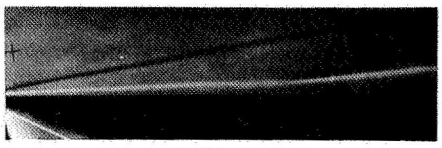

T_w/T_t = .46

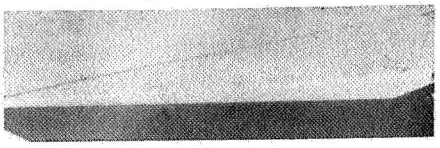

T_w/T_t = .72

(c) R = 0.420×10^6/ft (1.38×10^6/m), δ = 20.

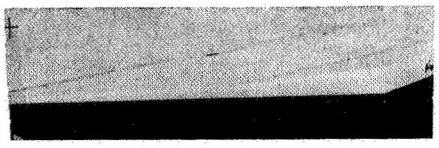

T_w/T_t = .18

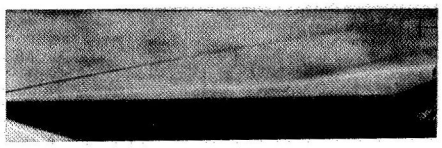

T_w/T_t = .48

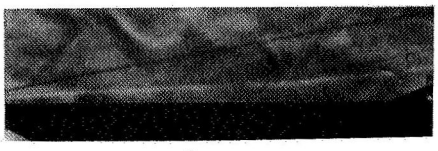

T_w/T_t = .70

(b) R = 0.290×10^6/ft (0.950×10^6/m), δ = 20.

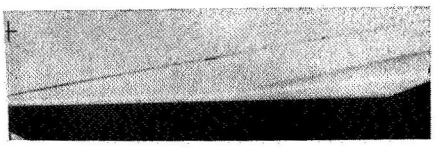

T_w/T_t = .15

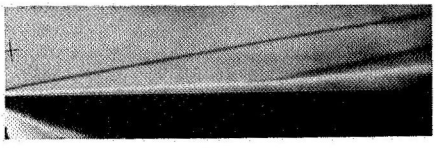

T_w/T_t = .44

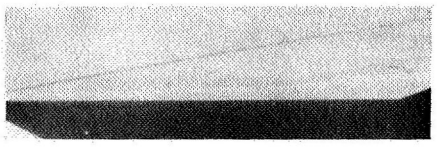

T_w/T_t = .71

(d) R = 0.650×10^6/ft (2.13×10^6/m), δ = 20.

Figure 32.- Continued.

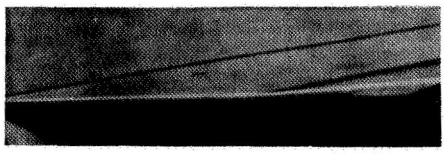

T_w/T_t = .15

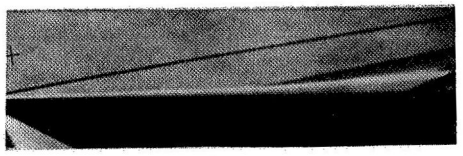

T_w/T_t = .42

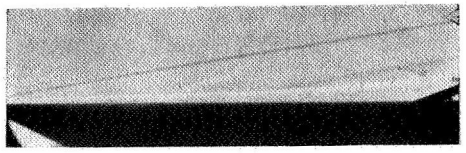

T_w/T_t = .75

(a) R = 1.06×10^6/ft (3.48×10^6/m), δ = 20.

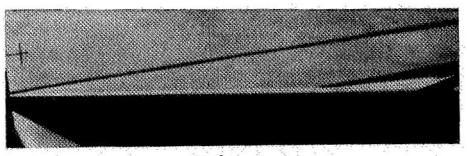

T_w/T_t = .13

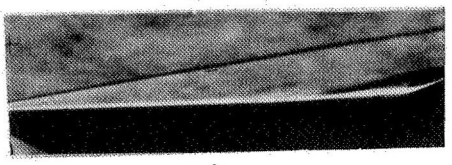

T_w/T_t = .40

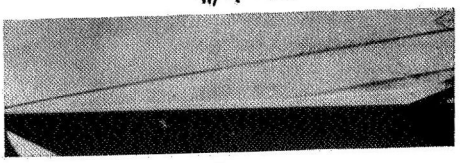

T_w/T_t = .77

(c) R = 2.65×10^6/ft (8.69×10^6/m), δ = 20.

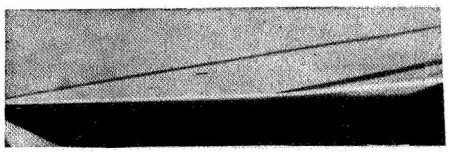

T_w/T_t = .13

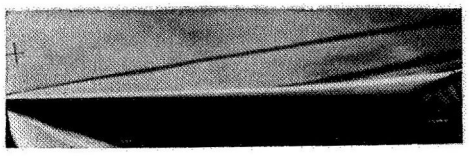

T_w/T_t = .40

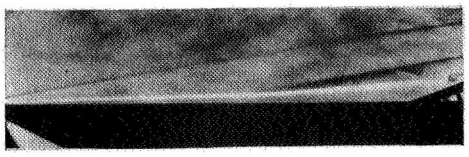

T_w/T_t = .75

(b) R = 1.46×10^6/ft (4.79×10^6/m), δ = 20.

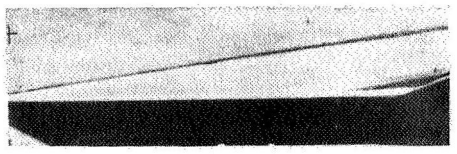

T_w/T_t = .13

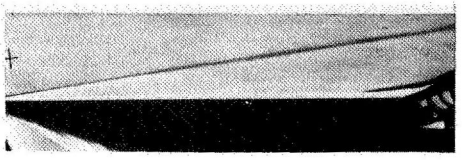

T_w/T_t = .39

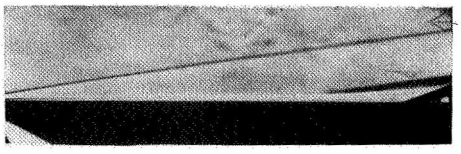

T_w/T_t = .78

(d) R = 4.30×10^6/ft (14.1×10^6/m), δ = 20.

Figure 32.- Concluded.

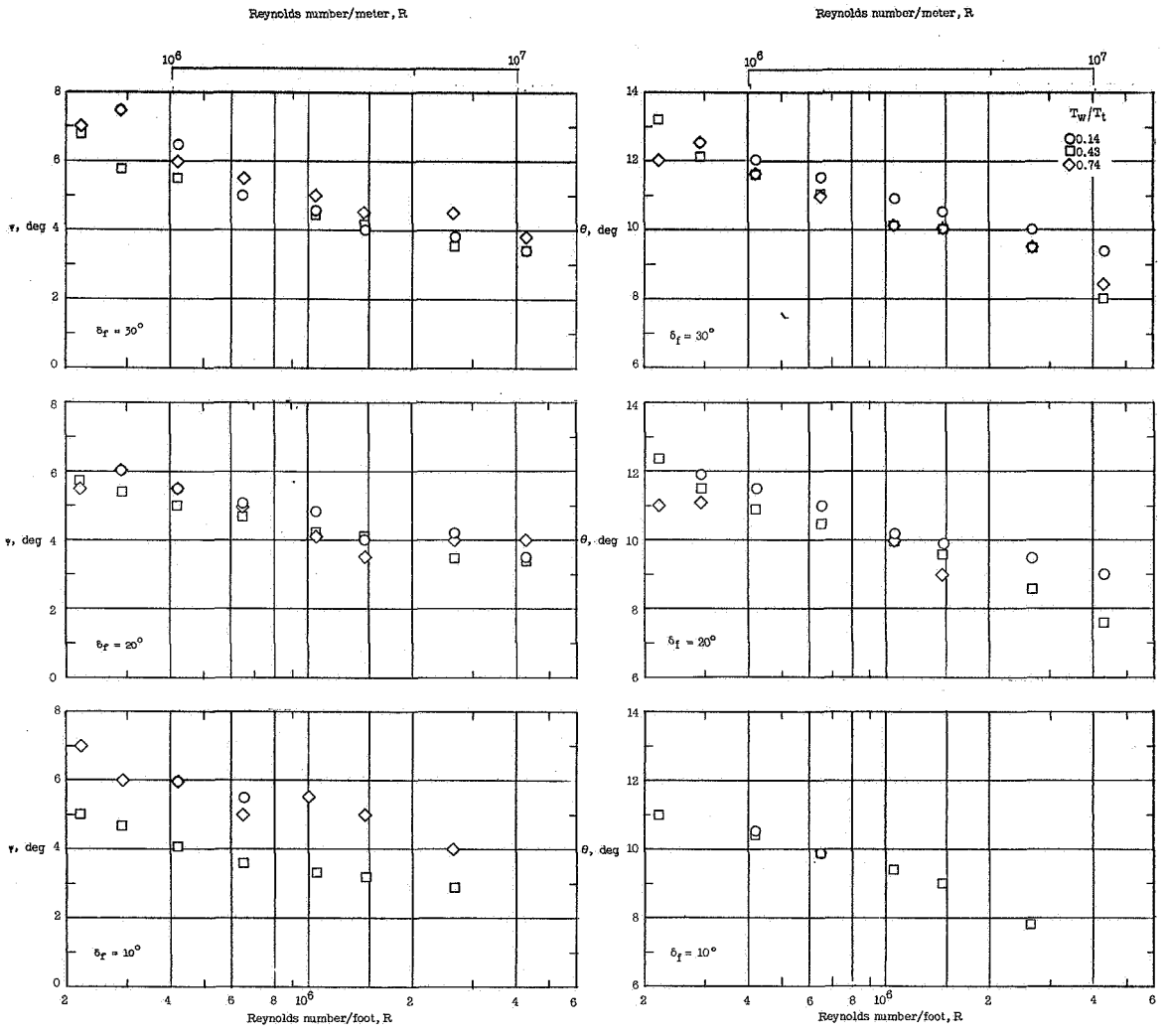

Figure 33.- The effect of Reynolds number, wall temperature, and flap angle on the separation point flow-deflection angle and the separation shock-wave angle.

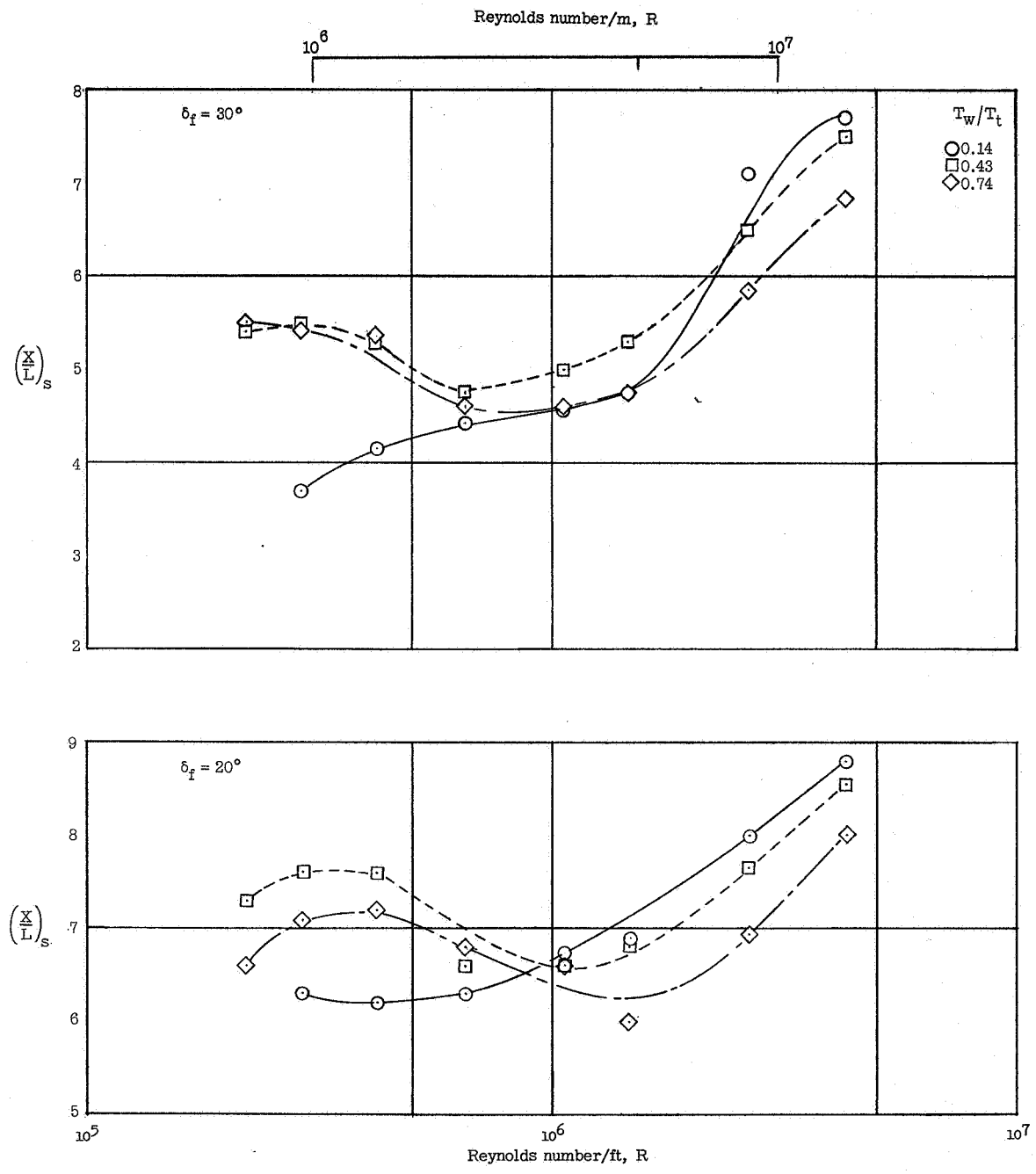

Figure 34.- The effect of Reynolds number, wall temperature, and flap angle on the location of the separation point on the plate surface.

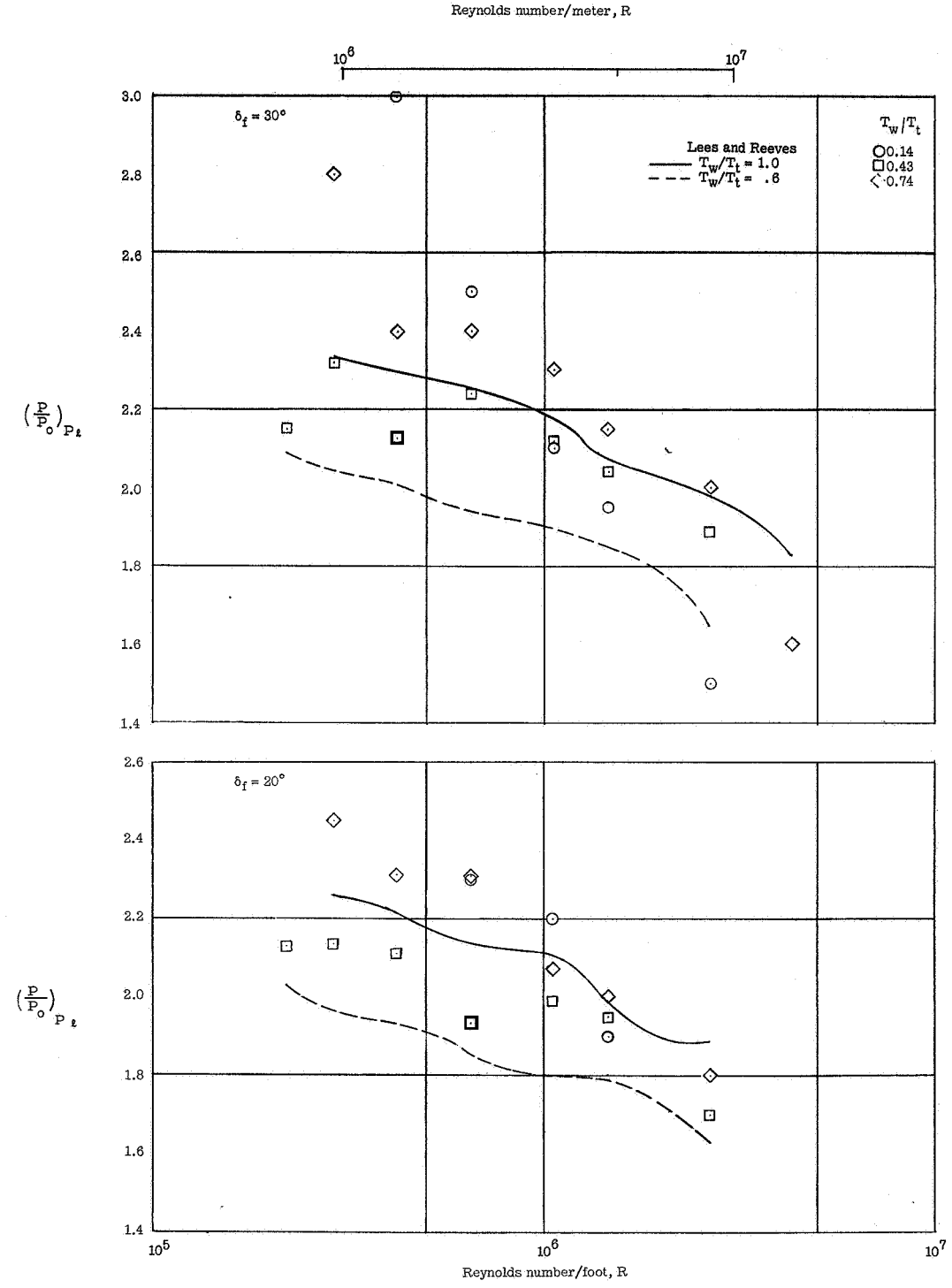

Figure 35.- The effect of Reynolds number, wall temperature, and flap angle on the value of plateau pressure.

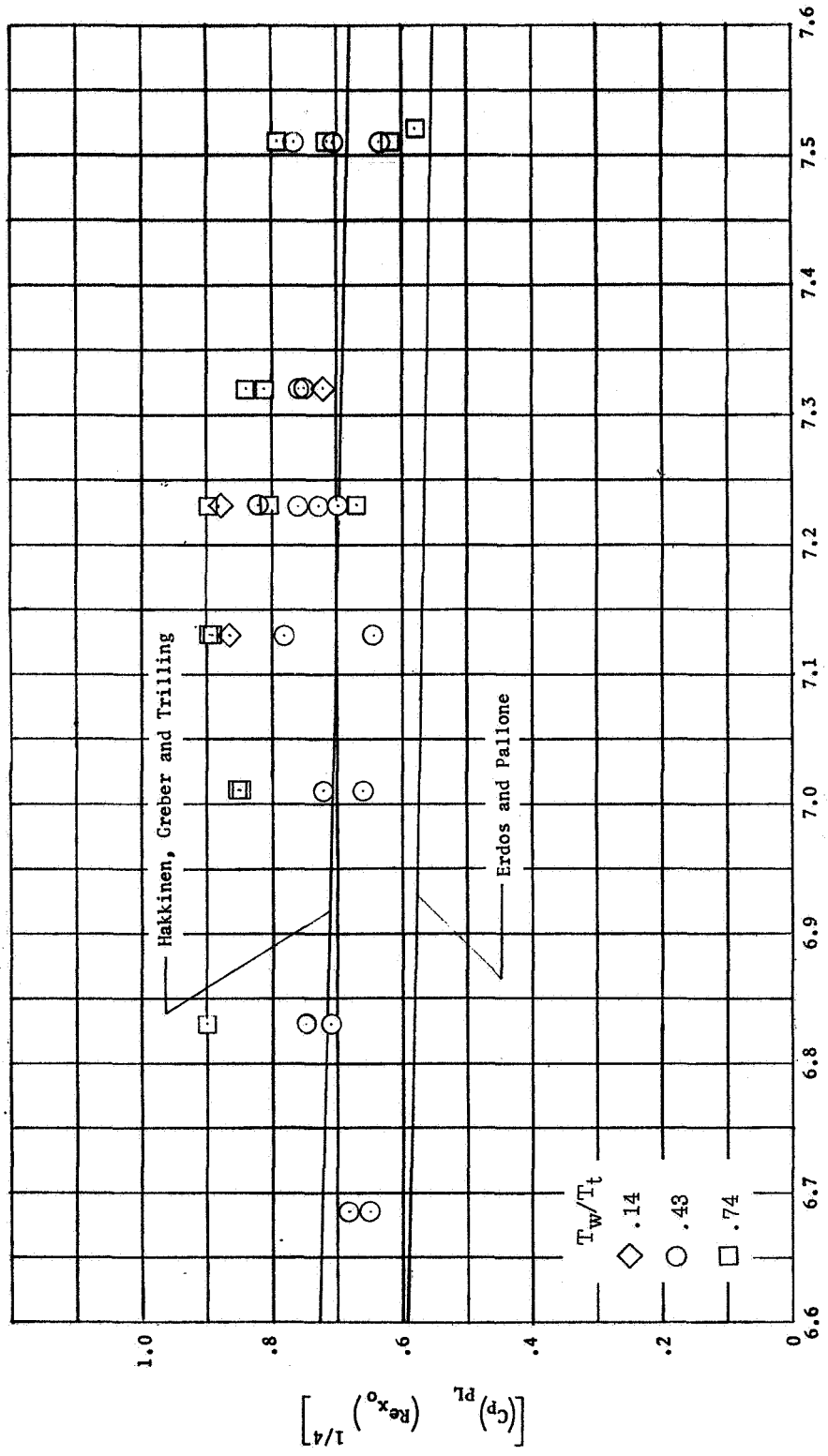

Figure 36.- The effect of wall temperature on the plateau pressure correlation.

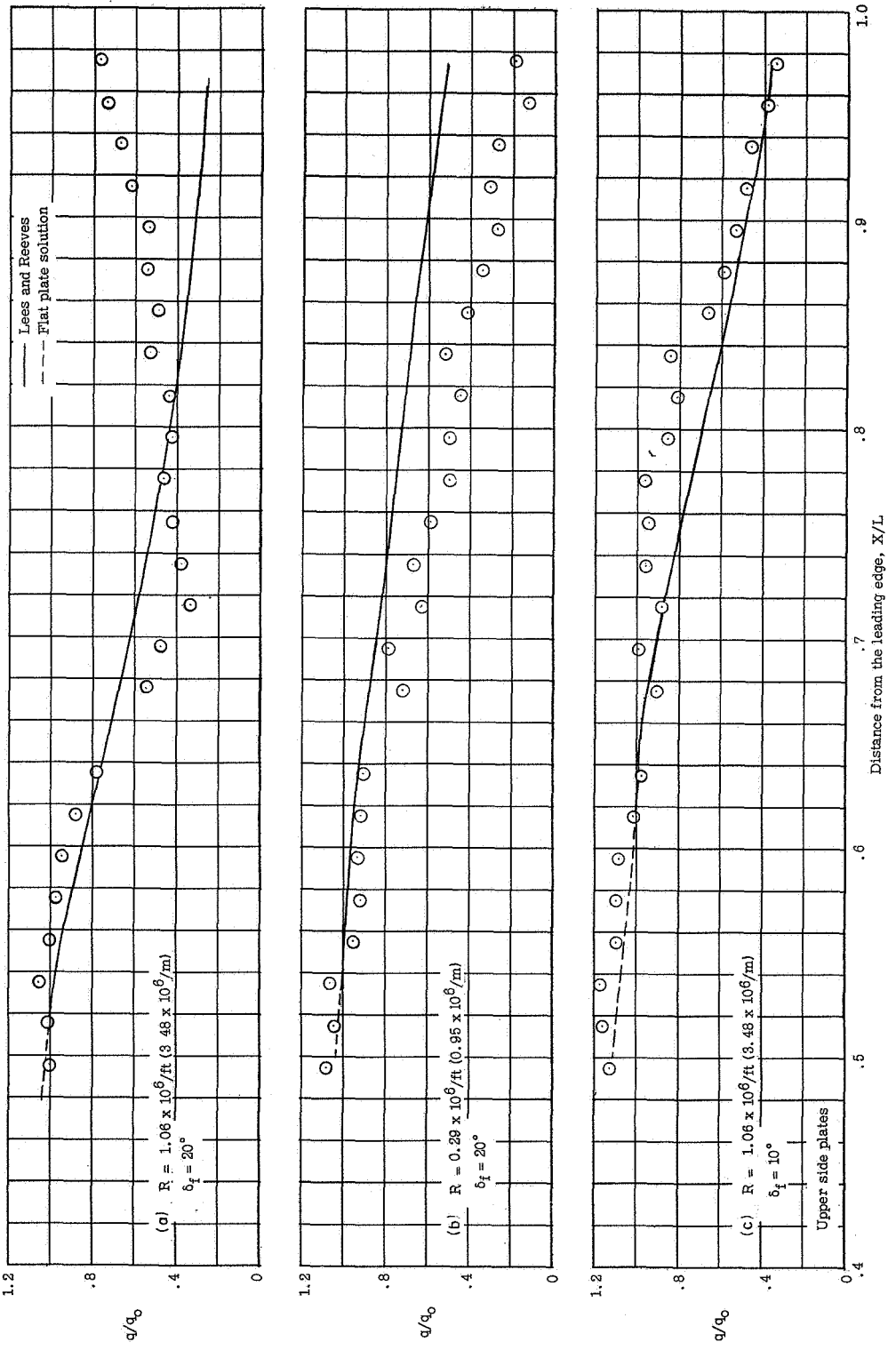

Figure 37.- Three typical heat-transfer runs.

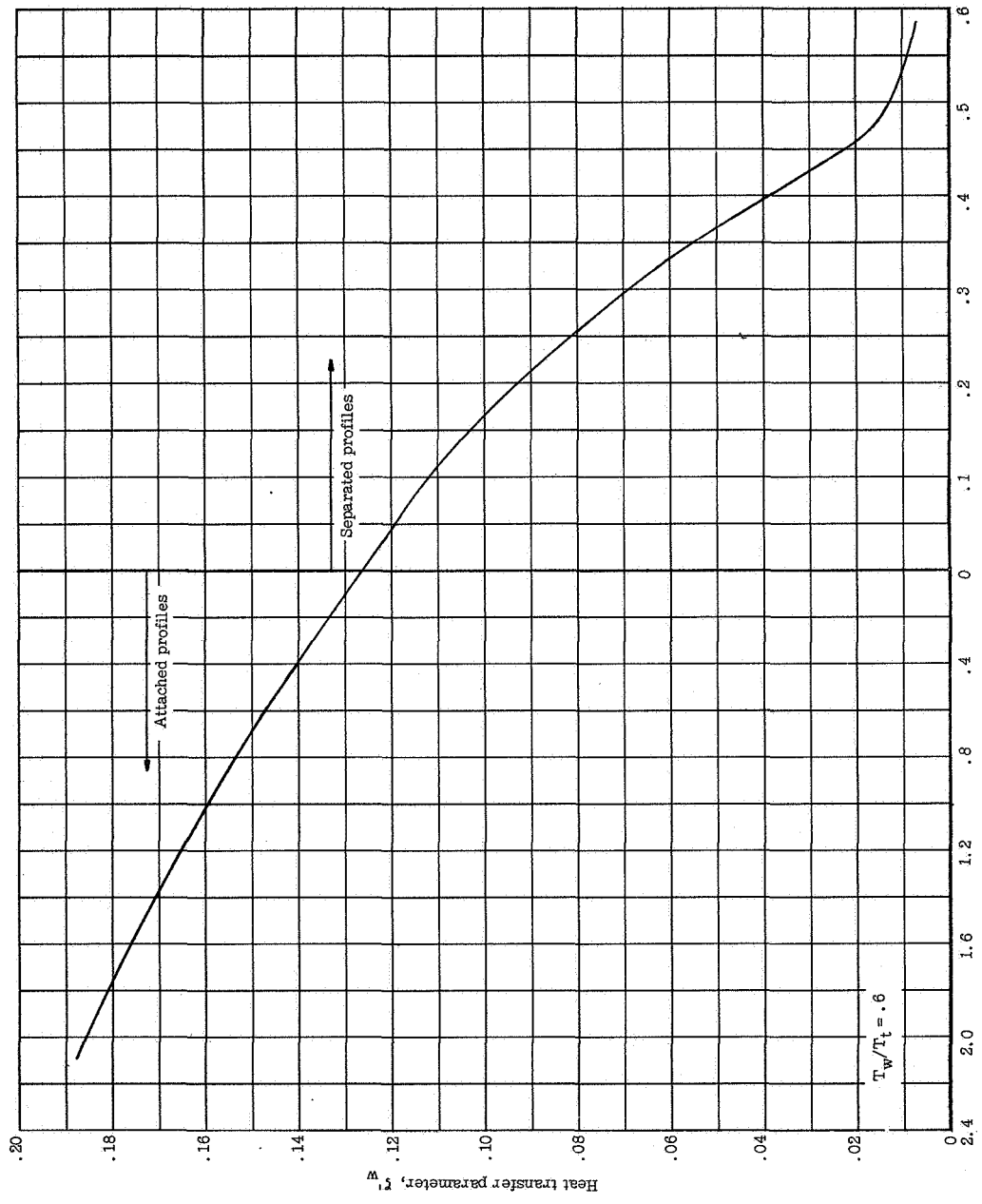

Figure 38.- The heat transfer parameter from similar solutions as a function of the Lees and Reeves' parameter.

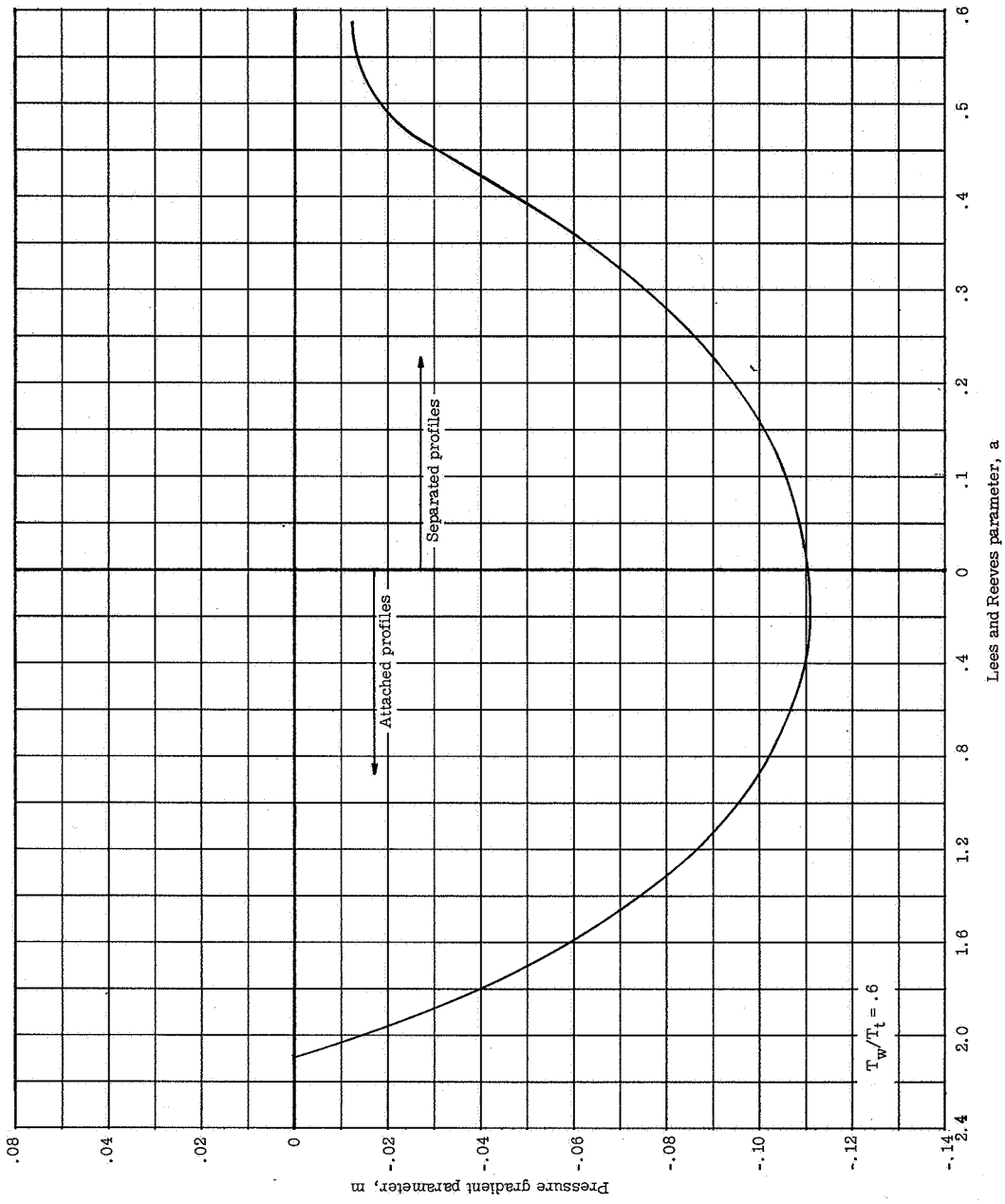

Figure 39.- The pressure gradient parameter from similar solutions as a function of the Lees and Reeves' parameter.

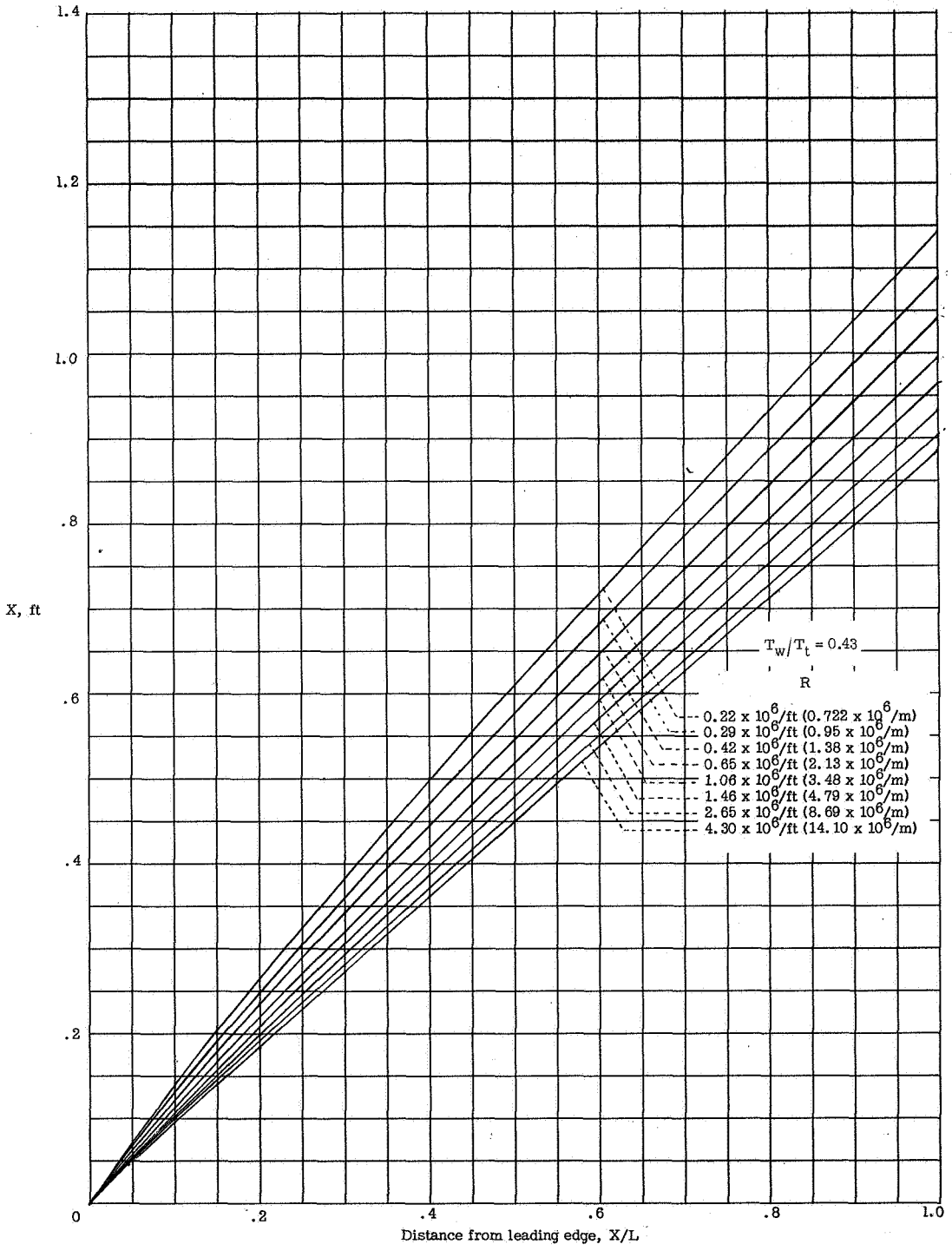

Figure 40.- The x coordinate in the transformed plane for a flat plate solution at various Reynolds numbers.